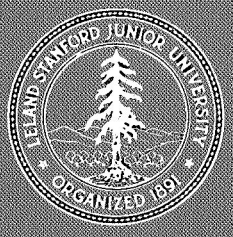

STANFORD UNIVERSITY
ENGINEERING IN MEDICINE AND BIOLOGY

ON THE DETERMINATION OF THE ELASTIC PROPERTIES OF BLOOD VESSELS FROM THEIR WAVE TRANSMISSION CHARACTERISTICS

PH. D. DISSERTATION

BY

MICHAEL K. WELLS

BIOMECHANICS LABORATORY

DEPARTMENT OF AERONAUTICS AND ASTRONAUTICS

APRIL 1969

This work was carried out at the Ames Research Center of NASA with the support of NASA Grant NGR 05-020-223 and with the aid of an NIH Predoctoral Fellowship. The initial phase of the investigation was financed by the National Science Foundation under Grant No. GK 47. The material from SUDAAR No. 362 has been included here for the sake of completeness.

SUDAAR NO. 368

Department of Aeronautics and Astronautics
Stanford University
Stanford, California

ON THE DETERMINATION OF THE ELASTIC PROPERTIES OF BLOOD VESSELS FROM THEIR WAVE TRANSMISSION CHARACTERISTICS

by

Michael K. Wells

SUDAAR NO. 368
April 1969

This work was carried out at the Ames Research Center of NASA with the support of NASA Grant NGR 05-020-223 and with the aid of an NIH Predoctoral Fellowship. The initial phase of the investigation was financed by the National Science Foundation under Grant No. GK 47. The material from SUDAAR No. 362 has been included here for the sake of completeness.

ACKNOWLEDGMENT

I am deeply indebted to my adviser, Professor Max Anliker, for his guidance and encouragement both before and during the course of this investigation. I also wish to thank members of the Biomechanics Group at Stanford University for their helpful discussions and suggestions pertinent to the experimental phases of the research, Mr. Leonard Chan whose technical assistance in the laboratory proved invaluable and Professors I-Dee Chang and Leo Sapirstein for reading the preliminary manuscript. Above all, I am grateful to my wife, Phyllis, for her patience and understanding.

This work was carried out at the Ames Research Center of NASA with the support of NASA Grant NGR 05-020-223 and with the aid of an NIH Predoctoral Fellowship. The initial phase of the investigation was financed by the National Science Foundation under Grant No. GK 47.

ABSTRACT

The wave transmission characteristics of blood vessels serve as measures of their mechanical properties including the elastic and viscoelastic behavior of the vessel walls. To aid in the proper assessment of these characteristics, various theoretical and experimental aspects of dispersion and attenuation of waves propagating in blood vessels are investigated. In order to determine the individual effects of a mean blood flow and anisotropy of the vessel wall on the speed and mode shapes of waves in blood vessels, the theoretical study of Anliker and Maxwell is extended. The vessel is taken as perfectly elastic and the fluid inviscid and incompressible. Motions of the wall are considered small and the linearized equations of Flügge for pre-stressed, thin walled, circular cylindrical shells are used to describe the equilibrium of the blood vessel. Under these conditions three distinct types of waves (I, II and III) are possible which at high frequencies are associated essentially with radial, circumferential or axial motions of the vessel respectively. In addition, we consider both axisymmetric and nonaxisymmetric wall displacements.

In the presence of a mean flow the speed of axisymmetric pressure waves (type I) in the larger vessels is given approximately by the wave speed at zero mean flow plus the average stream velocity in the direction of the propagating wave for signals with frequencies less than about 100 Hz. For nonaxisymmetric type I waves the increase in signal speed is generally about half the mean flow velocity. The propagation characteristics of torsion and

axial waves (II and III) are not significantly affected by the addition of a net flow. It appears that the proper interpretation of experimental data regarding the transmission of pressure waves requires information describing the blood flow during the time the data were obtained.

Effects of anisotropy of the vessel wall are studied by considering the vessel as an orthotropic elastic shell with different Young's moduli and Poisson's ratios in the axial and circumferential directions. The results of a parametric analysis show that the dimensionless phase velocity and mode shapes of non-axisymmetric waves of all three types are not strongly influenced by variations in anisotropy except near the cut-off frequencies. On the other hand, dispersion of each type of axisymmetric wave is affected by anisotropy. For instance, the speed of pressure waves depends primarily on the value of the circumferential Young's modulus, torsion waves on the shear modulus and the velocity of axial waves on the value of the longitudinal Young's modulus.

Experimentally, the mechanical behavior of the abdominal venae cavae of anesthetized dogs has been studied by measuring the speed, attenuation and changes in wave form of various types of induced pressure signals. The speed of large amplitude pressure waves normally ranged from about 100 to 700 cm/sec and was found to depend strongly on the signal amplitude, transmural pressure and physiological state of the animal. The propagation of these signals is shown to be affected by reflection interference and pronounced nonlinear phenomena. For pressure signals exceeding a few mm Hg the speed increases with amplitude and the wave front steepens during propagation as in the early phases of the

formation of a shock wave. By inducing distension waves in the form of finite trains of sine waves with amplitudes less than 20 mm H_2O the dispersion and attenuation were determined without requiring Fourier transform computations. These small amplitude waves traveled with phase velocities between 100 and 400 cm/sec and exhibited only mild dispersion for frequencies from 20 to 100 Hz. Attenuation of these signals is attributed primarily to viscoelastic damping in the vessel wall and appears to follow an exponential decay pattern which is independent of frequency. The logarithmic decrement ranged from about 1 to 2.5 for the vena cava. Irrespective of the amplitude and shape of the pressure signals, their speeds varied along the vena cava and also with respiration. In addition the speeds generally increased with rising transmural pressure and a linear relationship between these two quantities was apparent. When the transmural pressure was increased by occluding the vena cava the phase velocity varied at a rate from 1.5 to 2.5 cm/sec/mm H_2O.

TABLE OF CONTENTS

Table of Contents (Continued)

NOMENCLATURE

a = equilibrium radius of the middle surface of the vessel wall

A = wave amplitude

A_o = wave amplitude at origin

A_{sc}, B_{sc}, C_{sc} = mode amplitudes for circumferential wave number s, phase velocity c (isotropic shell)

$\tilde{A}_{sc}$, $\tilde{B}_{sc}$, $\tilde{C}_{sc}$ = mode amplitudes for circumferential wave number s, phase velocity c (orthotropic shell)

c = axial phase velocity

c_I, c_{II}, c_{III} = axial phase velocity of type I, II and III waves, respectively

$c_p = [E/\rho_w(1 - \nu^2)]^{1/2}$ = normalizing phase velocity (isotropic shell)

$\bar{c} = c/c_p$ = dimensionless phase velocity (isotropic shell)

$c_p^* = [E_x/\rho_w(1 - \nu_x\nu_\beta)]^{1/2}$ = normalizing phase velocity (orthotropic shell)

$\tilde{c} = c/c_p^*$ dimensionless phase velocity (orthotropic shell)

$\tilde{c}_I$, $\tilde{c}_{II}$, $\tilde{c}_{III}$ = dimensionless axial phase velocity of type I, II and III waves, respectively

D_{sc} = constant related to initial conditions of fluid

$e^2 = h^2/12a^2$ = dimensionless parameter

$\vec{e}_x$ = unit vector in axial direction

E = Young's modulus of vessel wall (isotropic shell)

E_x = Young's modulus of vessel wall in axial direction (orthotropic shell)

E_β = Young's modulus of vessel wall in circumferential direction (orthotropic shell)

G = elastic shear modulus

$\tilde{g}$ = $G(1 - \nu_x \nu_\beta)/E_x$ = dimensionless elastic shear modulus (orthotropic shell)

h = thickness of vessel wall

i = $\sqrt{-1}$

$I_s(\xi)$ = modified Bessel function of the first kind, argument ξ

k = logarithmic decrement

L_{ij} = differential operators (isotropic shell)

$\tilde{L}_{ij}$ = differential operators (orthotropic shell)

m_f = radial apparent mass of fluid contained in vessel

$\vec{n}$ = unit normal vector of vessel wall

p_e = external pressure applied to vessel

p_i = perturbed internal pressure applied to vessel

p_{io} = unperturbed internal pressure

p_v = transmural venous pressure

q_1 = $T_{10}(1 - \nu^2)/Eh$ = dimensionless axial stress resultant (isotropic shell)

$\tilde{q}_1$ = $T_{10}(1 - \nu_x \nu_\beta)/E_x h$ = dimensionless axial stress resultant (orthotropic shell)

q_2 = $a\Delta p(1 - \nu^2)/Eh$ = dimensionless stress resultant (isotropic shell)

$\tilde{q}_2$ = $a\Delta p(1 - \nu_x \nu_\beta)/E_x h$ = dimensionless circumferential stress resultant (orthotropic shell)

r = coordinate in radial direction

s = circumferential wave number

t = time

T_{10} = initial axial tension of vessel

u, v, w = displacements of middle surface of vessel wall in axial, circumferential and radial directions, respectively

U = velocity of mean flow in axial direction

$\overline{U}$ = U/c_p = dimensionless velocity of mean flow in axial direction

$\vec{v}$ = perturbation fluid velocity

v_x = perturbation fluid velocity in axial direction

$\vec{V}$ = total fluid velocity

x = coordinate in axial direction

α = x/a dimensionless axial coordinate

β = coordinate in circumferential direction

γ = $\gamma_1 = \gamma_2$ for initially unstressed vessel

γ_1 = E_β/E_x = ratio of Young's moduli in circumferential and axial directions

γ_2 = ν_β/ν_x = ratio of Poisson's constants in circumferential and axial directions

$\gamma_{x\beta}$ = shear strain

Δp = $p_{io} - p_e$ = transmural pressure

Δx = distance between pressure transducers

ϵ_x = strain in axial direction

ϵ_β = strain in circumferential direction

λ = wavelength of disturbance

μ_f = $(1 - \nu^2)a^2 m_f/Eh$ = fluid inertia parameter (isotropic shell)

$\tilde{\mu}_f$ = $(1 - \nu_x \nu_\beta)a^2 n_f/E_x h$ = fluid inertia parameter (orthotropic shell)

μ_w = $(1 - \nu^2)a^2(\rho_w h)/Eh$ = wall inertia parameter (isotropic shell)

$\tilde{\mu}_w$ = $(1 - \nu_x \nu_\beta) a^2 (\rho_w h)/E_x h$ = wall inertia parameter (orthotropic shell)

ν = Poisson's ratio (isotropic shell)

ν_x = Poisson's ratio for axial direction (orthotropic shell)

ν_β = Poisson's ratio for circumferential direction (orthotropic shell)

ξ = $\omega a/c$ = dimensionless parameter

ρ_f = density of fluid

ρ_w = density of vessel wall

$\bar{\rho}$ = ρ_f/ρ_w = dimensionless density ratio (isotropic shell)

$\tilde{\rho}$ = ρ_f/ρ_w = dimensionless density ratio (orthotropic shell)

σ_x = stress in axial direction

σ_β = stress in circumferential direction

$\tau_{x\beta}$ = shear stress

Φ = fluid velocity potential

ω = circular frequency

$\bar{\omega}$ = $\omega a/c_p$ = dimensionless circular frequency (isotropic shell)

$\tilde{\omega}$ = $\omega a/c_p^*$ = dimensionless circular frequency (orthotropic shell)

∇ = gradient operator

∇^2 = Laplacian operator

GENERAL INTRODUCTION

Methods for determining the mechanical properties of arteries and veins and their relationship to blood flow under normal and pathological conditions have been subject to intensive study for many years. Recent books and review articles[1-7] trace historically many of the experimental and analytical advances in hemodynamics and contain extensive bibliographies. In addition, these publications detail much of the current knowledge in the field of cardiovascular dynamics gained from both the physical and biological sciences. A significant research effort has been directed toward evaluating the elastic and viscoelastic properties of blood vessels from their wave transmission characteristics and it is the purpose of this paper to provide additional information for elucidating this relationship.

The work presented here is part of a systematic theoretical[8,9,10] and experimental[11,12,13] investigation of the wave transmission characteristics of blood vessels aimed at the development of a noninvasive, nontraumatic method for measuring the elastic properties of arteries and veins. Such a technique would have applications with respect to space flight. Not only could it provide essentially continuous measurements of the distensibility of individual blood vessels of astronauts, but one would also be able to detect possible deconditioning of the cardiovascular system resulting from prolonged exposure to weightlessness. Clinically, the propagation characteristics of various arteries and veins could be measured routinely as an index of aging and could perhaps allow for the

early diagnosis of the onset of atherosclerosis.

Two distinct investigations are described in this paper. The first section is an attempt to extend the theory of Anliker and Maxwell[8] for the dispersion of waves in blood vessels to include somewhat more general conditions. In Chapter I the effects of a mean flow on the wave transmission characteristics of blood vessels are studied while nonisotropic behavior of the vessel wall is considered in Chapter II. In both analyses the vessel is taken as perfectly elastic and the fluid incompressible and inviscid and the effects of the medium surrounding the vessel are neglected. With these assumptions the system is rendered free of all energy dissipation mechanisms. The theory is applicable to wave propagation in arteries and veins and the value of the vessel wall thickness to radius ratio used for computational purposes, although typical for large arteries, was chosen primarily to facilitate comparison with the results of Reference 8.

The second section deals with some experimental aspects of wave propagation in blood vessels and is presented in Chapters III and IV. Studies were devoted exclusively to the transmission of large and small pressure waves in the abdominal vena cava of anesthetized dogs and the results described represent an effort of more than three years duration. In addition to measuring the dispersion and attenuation of sinusoidal pressure waves, the effect of variations in transmural pressure on the signal velocities was determined. These experimental findings are intended to supplement similar investigations of the transmission characteristics of arteries[11,12] and serve as a basis for current and future studies of control mechanisms of the circulatory system.

I. THEORETICAL STUDY OF THE EFFECT OF MEAN FLOW ON THE DISPERSION AND ATTENUATION OF WAVES IN BLOOD VESSELS

Introduction

The wave transmission characteristics of a blood vessel may depend to some degree upon the unperturbed flow existing in the vessel. The extent to which the theoretically computed wave speed of a small disturbance is affected, however, may be influenced not only by the characteristics of the flow but also by the mathematical model chosen to describe the mechanical behavior of the vessel. The derivation of the classical Moens-Korteweg equation, for example, neglects the inertia of the vessel wall and the viscosity of the fluid and requires only a transformation to a coordinate system moving with the fluid in order to account for a mean flow velocity. This results in a simple superposition of the wave speed for the system at rest (no mean flow) with the velocity of the streaming fluid.

The effect of a mean flow of a viscous fluid on wave propagation in a cylindrical tube was investigated theoretically by Morgan and Ferrante[14]. In their analysis, the blood vessel was approximated by a fluid filled circular cylindrical elastic membrane and the results show that the speed of pressure waves propagating in the direction of the flow increases with increasing flow by an amount slightly greater than the average stream velocity. For an inviscid fluid these authors found the increase in wave speed to be somewhat less than the mean flow velocity.

These results indicate that a serious misinterpretation of wave speed

measurements can occur when the effects of a mean flow are neglected irrespective of the flow velocity. In the analysis presented here, the blood vessel is described by a theoretical model which includes the effects of initial axial stretch and transmural pressure and bending rigidity of the vessel wall. On the other hand, however, we assume that the blood behaves like an incompressible inviscid fluid since only at low frequencies does viscosity significantly influence the dispersion[15,16,17] or attenuation[10] of waves in blood vessels and the transmission of all but the highest frequency signals does not seem to be affected by the compressibility of the blood[8]. It is felt that with these features the model represents a more realistic approximation to the actual behavior exhibited by blood vessels and in view of the findings of Morgan and Ferrante[14] the extent to which a mean blood flow influences the velocity and mode shape of propagating waves should be determined. The following analysis, it should be mentioned, is not restricted to the transmission of only axisymmetric waves but also includes those waves associated with nonaxisymmetric displacements of the vessel wall.

Basic Equations

We refer the middle surface of the vessel wall to a set of cylindrical coordinates x, β, r. The signals associated with a disturbance are defined by the displacements u, v, w of an arbitrary point of the middle surface in the axial, circumferential and radial directions respectively. For a given pressure difference and initial axial tension the equilibrium configuration of the middle surface $(u, v, w = 0)$ is a circular cylinder defined by $r = a$.

The fluid is assumed to be incompressible and inviscid and its velocity

is given by

$$\vec{V} = \vec{v} + \vec{U} \tag{1.1}$$

where $\vec{v}$ is the perturbation velocity associated with the disturbance and $\vec{U}$ is the velocity of the streaming flow. In addition, $\vec{v}$ is taken to be irrotational and the effects of gravity are ignored. This enables us to represent the perturbation velocity as the gradient of a scalar potential function Φ

$$\vec{v} = -\nabla\Phi \tag{1.2}$$

In general, variations in blood flow velocity are periodic and occur with each cardiac and respiratory cycle[1,18]. Since the length of time during which we observe the induced propagating disturbance is short compared to the heart and respiratory rates, the mean flow $\vec{U}$ is taken as constant in magnitude ($|\vec{U}| = U = \text{constant}$). Furthermore we will assume that the flow is directed entirely along the longitudinal axis of the vessel.

For an incompressible fluid the continuity equation may be written

$$\nabla \cdot \vec{V} = \nabla \cdot (\vec{v} + \vec{U}) = 0 \tag{1.3}$$

hence for constant $\vec{U}$

$$\nabla \cdot (-\nabla\Phi + \vec{U}) = -\nabla^2\Phi = 0 \tag{1.4}$$

i.e. the velocity potential Φ satisfies Laplace's equation. In the absence of body forces, Euler's equation for an inviscid fluid takes the form

$$\frac{\partial \vec{V}}{\partial t} + \vec{V} \cdot \nabla\vec{V} = -\frac{1}{\rho_f}\nabla p_i \tag{1.5}$$

where p_i denotes the perturbed intraluminal pressure and ρ_f the fluid density.

Making use of the vector identity

$$\vec{V} \cdot \nabla \vec{V} = \frac{1}{2} \nabla (\vec{V} \cdot \vec{V}) - \nabla \times (\nabla \times \vec{V}), \tag{1.6}$$

the condition of irrotationality

$$\nabla \times \vec{v} = 0 \tag{1.7}$$

and the fact that $\vec{U} = U\vec{e}_x$ we can rewrite Euler's equation as

$$\frac{\partial \vec{v}}{\partial t} + \nabla (v_x U) = - \frac{1}{\rho_f} \nabla p_i \tag{1.8}$$

where $v_x = \vec{v} \cdot \vec{e}_x$ and $v^2 << U^2$. Substituting the velocity potential in (1.8) yields

$$\nabla \left(\frac{\partial \Phi}{\partial t} + U \frac{\partial \Phi}{\partial x} - \frac{p_i}{\rho_f} \right) = 0 \tag{1.9}$$

which becomes upon integration

$$p_i = \rho_f \left(\frac{\partial \Phi}{\partial t} + U \frac{\partial \Phi}{\partial x} \right) + p_{io} \tag{1.10}$$

where the integration constant p_{io} denotes the undisturbed intraluminal pressure.

The fluid and wall velocities are related through the kinematic boundary condition which requires that the fluid velocity in the direction of the normal to the wall be equal to the wall velocity in the same direction, hence

$$\vec{V} \cdot \vec{n} = (\dot{u}, \dot{v}, \dot{w}) \cdot \vec{n} \tag{1.11}$$

where $\vec{n}$ is the outward directed unit normal vector of the wall. Linearizing this condition and applying it at the middle surface $r = a$ we obtain

$$\frac{\partial w}{\partial t} = - \left(\frac{\partial \Phi}{\partial r} \right)_{r = a} - U \frac{\partial w}{\partial x}. \tag{1.12}$$

We consider solutions to the continuity equation (1.4) in the form of undamped, propagating sinusoidal waves

$$\Phi_{sc} = D_{sc} I_s(\xi \frac{r}{a}) \exp[i \frac{\omega}{c}(x - ct) + is\beta] \tag{1.13}$$

with $\xi = \frac{\omega a}{c}$. D_{sc} is the amplitude corresponding to an initial set of conditions, s the circumferential wave number, ω the circular frequency of the sine wave, c its wave velocity and I_s the modified Bessel function of the first kind of order s.

For this analysis we assume that the vessel behaves like an isotropically elastic, thin walled, circular cylindrical shell of thickness h. As material constants we use the Young's modulus E and Poisson's ratio ν. An initial axial stretch of the vessel produces an axial tension in the vessel wall denoted here by T_{10}.

The transmural pressure Δp is given by

$$\Delta p = p_{io} - p_e \tag{1.14}$$

where p_e is the external pressure and is assumed to remain constant. We introduce as dimensionless stress resultants in the axial and circumferential directions respectively

$$q_1 = \frac{T_{10}(1 - \nu^2)}{Eh} \tag{1.15}$$

$$q_2 = \frac{a\Delta p(1 - \nu^2)}{Eh} \tag{1.16}$$

and define a dimensionless axial coordinate

$$\alpha = \frac{x}{a}. \tag{1.17}$$

We now make use of the linearized equations for circular cylindrical shells derived by W. Flügge[19]. These differential equations are valid for small displacements u, v, w of the middle surface of the vessel wall about the equilibrium configuration $u = v = w = 0$ and take the form:

$$\begin{aligned}
&L_{11}(u) + L_{12}(v) + L_{13}(w) + (q_1 + \nu q_2)\frac{\partial^2 u}{\partial \alpha^2} + q_2\left(\frac{\partial^2 u}{\partial \beta^2} - \frac{\partial w}{\partial \alpha}\right) \\
&\quad - \mu_w \frac{\partial^2 u}{\partial t^2} = 0 \\
&L_{21}(u) + L_{22}(v) + L_{23}(w) + (q_1 + \nu q_2)\frac{\partial^2 v}{\partial \alpha^2} + q_2\left(\frac{\partial^2 v}{\partial \beta^2} + \frac{\partial w}{\partial \beta}\right) \\
&\quad - \mu_w \frac{\partial^2 v}{\partial t^2} = 0 \\
&L_{31}(u) + L_{32}(v) + L_{33}(w) - (q_1 + \nu q_2)\frac{\partial^2 w}{\partial \alpha^2} - q_2\left(\frac{\partial u}{\partial \alpha} - \frac{\partial v}{\partial \beta} + \frac{\partial^2 w}{\partial \beta^2}\right) \\
&\quad + (\mu_w + \mu_f)\frac{\partial^2 w}{\partial t^2} = 0.
\end{aligned} \tag{1.18}$$

The linear differential operators L_{ij} are given by

$$L_{11} = \frac{\partial^2}{\partial\alpha^2} + \frac{(1-\nu)}{2}\frac{\partial^2}{\partial\beta^2}(1+e^2)$$

$$L_{22} = \frac{\partial^2}{\partial\beta^2} + \frac{(1-\nu)}{2}\frac{\partial^2}{\partial\alpha^2}(1+3e^2)$$

$$L_{33} = 1 + e^2(\nabla^2\nabla^2 + 2\frac{\partial^2}{\partial\beta^2} + 1) \qquad (1.19)$$

$$L_{12} = L_{21} = \frac{(1+\nu)}{2}\frac{\partial^2}{\partial\alpha\partial\beta}$$

$$L_{13} = L_{31} = \nu\frac{\partial}{\partial\alpha} - e^2[\frac{\partial^3}{\partial\alpha^3} - \frac{(1-\nu)}{2}\frac{\partial^3}{\partial\alpha\partial\beta^2}]$$

$$L_{23} = L_{32} = \frac{\partial}{\partial\beta} - e^2(\frac{3-\nu}{2})\frac{\partial^3}{\partial\alpha^2\partial\beta}$$

where we have used the abbreviations

$$e^2 = \frac{h^2}{12a^2} \qquad (1.20)$$

$$\nabla^2 = \frac{\partial^2}{\partial\alpha^2} + \frac{\partial^2}{\partial\beta^2}. \qquad (1.21)$$

μ_w and μ_f represent inertia quantities associated with the vessel wall and fluid:

$$\mu_w = \frac{1-\nu^2}{Eh}a^2(\rho_w h) \qquad (1.22)$$

$$\mu_f = \frac{1-\nu^2}{Eh}a^2 m_f \qquad (1.23)$$

where m_f, the apparent mass of the fluid, is defined by

$$-m_f \frac{\partial^2 w}{\partial t^2} = (p_i - p_{io})_{r = a}. \tag{1.24}$$

Making use of the Euler equation in the form of (1.10) we obtain

$$-m_f \frac{\partial^2 w}{\partial t^2} = \rho_f \left(\frac{\partial \Phi}{\partial t} + U \frac{\partial \Phi}{\partial x}\right)_{r = a}. \tag{1.25}$$

We assume solutions to (1.18) of the form

$$u = A_{sc} \exp[i \frac{\omega}{c}(x - ct) + is\beta]$$

$$v = B_{sc} \exp[i \frac{\omega}{c}(x - ct) + is\beta] \tag{1.26}$$

$$w = C_{sc} \exp[i \frac{\omega}{c}(x - ct) + is\beta + i \frac{\pi}{2}]$$

i.e. a disturbance propagating in the positive x-direction with velocity c.

Combining (1.12), (1.13), (1.25) and (1.26) we find for the apparent mass

$$m_f = \rho_f a \frac{I_s(\xi)}{\xi I'_s(\xi)} \left(1 - \frac{U}{c}\right)^2 \tag{1.27}$$

where

$$I'_s(\xi) = \left[\frac{d}{d(\xi \frac{r}{a})} I_s(\xi \frac{r}{a})\right]_{r = a}.$$

Substitution of equations (1.26) into (1.18) leads to a set of three linear homogeneous equations for the amplitude factors A_{sc}, B_{sc} and C_{sc} which contain ω as a free parameter. The requirement of the existence of a

nontrivial solution for the three coefficients results in a frequency equation which can be characterized by a vanishing determinant.

For purposes of comparison with Reference 8 it is convenient to introduce the following additional dimensionless parameters:

$$c_p^2 = \frac{E}{\rho_w(1-\nu^2)} \qquad \bar{c}^2 = \frac{c^2}{c_p^2} \qquad \bar{\omega}^2 = \frac{\omega^2 a^2}{c_p^2}$$

$$\bar{\rho} = \frac{\rho_f}{\rho_w} \qquad \bar{U}^2 = \frac{U^2}{c_p^2}. \tag{1.28}$$

Then $\xi = \frac{\bar{\omega}}{\bar{c}}$ and the frequency equation can be written as:

$$\begin{vmatrix} \frac{\bar{\omega}^2}{\bar{c}^2}(1+q_1+\nu q_2)+q_2 s^2 & -\frac{1+\nu}{2}s\frac{\bar{\omega}}{\bar{c}} & \frac{\bar{\omega}}{\bar{c}}(\nu-q_2)+e^2(\frac{\bar{\omega}^3}{\bar{c}^3}-\frac{1-\nu}{2}\frac{\bar{\omega}}{\bar{c}}s^2) \\ +\frac{1-\nu}{2}(1+e^2)s^2-\bar{\omega}^2 & & \\ \hline & \frac{\bar{\omega}^2}{\bar{c}^2}[q_1+\nu q_2+\frac{1-\nu}{2}(1+3e^2)] & -e^2(\frac{3-\nu}{2})s\frac{\bar{\omega}^2}{\bar{c}^2}-s(1+q_2) \\ & +s^2(1+q_2)-\bar{\omega}^2 & \\ \hline & & 1+e^2[(\frac{\bar{\omega}^2}{\bar{c}^2}+s^2)^2-2s^2+1] \\ & & +\frac{\bar{\omega}^2}{\bar{c}^2}(q_1+\nu q_2)+q_2 s^2 \\ & & -[1+\bar{\rho}\frac{a}{h}\frac{I_s(\xi)}{\xi I_s'(\xi)}]\bar{\omega}^2 \\ & & +[2\bar{\rho}\frac{a}{h}\frac{I_s(\xi)}{I_s'(\xi)}\bar{U}]\bar{\omega} \\ & & -[\bar{\rho}\frac{a}{h}\frac{I_s(\xi)}{I_s'(\xi)}\xi\bar{U}^2] \end{vmatrix} = 0. \tag{1.29}$$

SYMMETRIC

Results

We note that for the case $\overline{U} = 0.0$ equation (1.29) reduces to the frequency equation given in Reference 8 whereas the existence of a mean velocity introduces additional terms in the equilibrium equation for the radial direction. This frequency equation contains nine dimensionless parameters $q_1, q_2, \nu, s, h/a, \overline{\omega}, \overline{c}, \overline{\rho}$ and $\overline{U}$. Young's modulus E, the density of the vessel wall ρ_w, the radius of the middle surface a and the mean flow velocity U do not appear explicitly in the equation but enter as scale factors in the parameters $\overline{\omega}, \overline{c}$ and $\overline{U}$. With the aid of an IBM 7094 digital computer, the dimensionless wave speed $\overline{c}$ has been calculated as a function of the eight remaining dimensionless parameters. For each circumferential wave number s there exist three distinct types of waves each having a characteristic propagation velocity and wall displacement pattern. These waves shall be denoted as type I, II and III. At high frequencies type I waves are characterized by predominantly radial displacements of the vessel wall, type II by circumferential and type III by axial displacements. The influence of a mean blood flow on the dispersion and mode shapes of these waves is illustrated in Figures 1 through 10. In these graphs the dimensionless phase velocity $\overline{c}$ and the normalized displacement amplitudes $|u|, |v|, |w|$ are given as functions of dimensionless frequency $\overline{\omega}$ for $s = 0, 1, 2, 3$ and for zero transmural pressure and axial stretch ($q_1 = q_2 = 0.0$). The value of h/a (wall thickness to radius ratio) corresponds to that of a large artery.

The effects of transmural pressure, axial tethering and thickness to radius ratio as well as Poisson's ratio and the density ratio on the wave speed

have been discussed extensively by Anliker and Maxwell[8]. We will therefore direct our attention only to the influence of the mean flow velocity on the wave speeds.

It should be noted that since $\bar{c}$ and $\bar{U}$ are both normalized by the factor c_p, the relative effects of a mean flow on the phase velocity are the same for dimensional and dimensionless variables. We can attribute physical significance to the dimensionless mean flow velocity by considering values for the parameters E, ρ_w and ν usually ascribed to the circulatory system. A value of $\bar{U} = 0.1$, for example, corresponds to an actual mean flow velocity of about 115 cm/sec if $E = 10^6$ dynes/cm^2, $\rho_w = 1.0$ gm/cm^3 and $\nu = 0.5$.

Discussion of Type I Waves

The effects of a mean flow on the mode shapes and phase velocities of type I waves are shown in Figures 1 through 6. In general the speed of signals traveling in the direction of the flow increases with increasing flow velocity for all values of the circumferential wave number s, and the frequency dependence of the wave speed remains relatively unaffected. For axisymmetric disturbances (s = 0) Figure 1 shows that the wave speed in the presence of a mean flow is increased by an amount approximately equal to the velocity of the flow for small values of $\bar{\omega}$. This difference in signal speed progressively decreases with increasing frequency and is less than half the flow velocity for $\bar{\omega} > 1.0$. The corresponding changes in mode shape are given in Figure 2. Notice that for $\bar{\omega} < 1.0$ the relative amplitude of the radial displacement decreases with flow while the axial displacement shows an increase for a given frequency. The increase in wave speed and the decrease in radial displacement may be attributed to an apparent stiffening of the vessel

with respect to distension as a result of the increase in inertia or apparent mass of the fluid in the radial direction.

Considering waves with $s = 1$, the influence of a mean flow is most pronounced for values of $\bar{\omega}$ below 0.5. Although the absolute difference in wave speeds for $\bar{U} = 0.0$ and 0.1 is not as great as in the case $s = 0$, the relative difference is appreciable and for small values of $\bar{\omega}$ exceeds 100 percent. Figure 3 shows a definite change in the wall displacement amplitudes with mean flow at a given frequency. Note, however, that the displacement pattern for the different values of $\bar{U}$ is similar. As illustrated in Figure 4 the effect of $\bar{U}$ on dispersion is similar for type I waves with $s = 2$ and $s = 3$. For values of $\bar{\omega}$ near the cut-off frequency the influence of the mean flow is difficult to assess since the wave speed is inherently quite sensitive to small variations in $\bar{\omega}$ because of the singularity in the frequency equation. For frequencies slightly above cut-off and higher the wave speed is increased by an amount less than half the mean flow velocity for both $s = 2$ and $s = 3$. Similar behavior has also been noted for values of s greater than 3. Mode shapes corresponding to these waves are given in Figures 5 and 6. In both cases the addition of a mean flow causes significant changes in the mode shapes corresponding to a given frequency. The overall wall displacement pattern, however, is similar to that for $\bar{U} = 0.0$ and the mean flow tends only to shift the curves in the direction of increasing frequency.

Discussion of Type II and Type III Waves

Waves of type II and III do not exhibit any significant changes in phase velocity or mode shape in the presence of physiologically meaningful values of

mean flow velocity. As shown in Figures 7 and 8 the dimensionless phase velocity $\overline{c}$ for $s = 0, 1, 2, 3$ is the same within drawing accuracy for $\overline{U} = 0.0$, 0.05 and 0.1. Mode shapes are also unaffected by the mean flow as illustrated in Figures 9 and 10. For axisymmetric waves this behavior is expected since we have considered the blood to be inviscid and the vessel wall undergoes essentially only circumferential or axial displacements thereby preventing any strong coupling between the fluid and wall motions. When s is not zero, radial displacements of the vessel wall occur at all frequencies above cut-off. Their relative magnitudes, however, are consistently small, and compared to waves of type I, the corresponding pressure flucuations are minute. The flow parameter U enters the analysis only through equation (1.10) for the pressure perturbation $p_i - p_{io}$ which is initially quite small for type II and III waves and remains the same order of magnitude for all meaningful values of mean flow velocity. It may be expected, therefore, that the effect of a streaming flow in the vessel on the propagation of these waves is not significant.

Conclusions and Experimental Observations

It is possible to compare our results for the speeds of axisymmetric type I waves with those of Morgan and Ferrante[14] for both an inviscid and viscous fluid. In order to nondimensionalize the dispersion curves for the viscous case it was necessary to prescribe values for the blood viscosity as well as the radius of the vessel and the effective Young's modulus and density of the vessel wall. The viscosity of blood normally ranges from about 4 to 7 centipoise[1] depending on the hematocrit and temperature, and as a representative average we

have chosen a value of 5 centipoise. The radius of 8 mm corresponds to that of the larger vessels and the wall density is taken as 1 gm/cm^3. In view of the results of wave transmission studies in the aorta and vena cava of anesthetized dogs[11,13], we assume that the elastic modulus of the vessel is 10^6 dynes/cm^2. Figure 11 gives dispersion curves from the two analyses for $\bar{U} = 0.0$ and 0.1. In the absence of a mean flow the wave speeds determined from Reference 14 for the inviscid case are consistently higher than ours for $\bar{\omega}$ below about 0.7 while above this frequency just the opposite behavior is observed. The marked difference between the results can be attributed to the effects of bending rigidity of the vessel wall which are included in our theory and are of particular importance at all but the lowest frequencies. Note that for increasing frequency the wave speed calculated from the inviscid analysis of Reference 14 approaches zero and for sufficiently large values of $\bar{\omega}$ the velocity can even become negative. Similar behavior is observed for the case $\bar{U} = 0.1$ although the relative difference in speeds is not as great as for $\bar{U} = 0.0$. In a strict sense this comparison is not valid since the approximate solution presented by Morgan and Ferrante requires that the stream velocity be small compared to the Moens-Korteweg wave speed, i.e. $U^2 << \frac{Eh}{2\rho_f a}$ or $\bar{U} << \frac{h(1-\nu^2)}{2\bar{\rho}a}$. Our analysis did not impose this restriction on the mean flow and it can be seen that even for values of $\bar{\omega}$ as large as 0.3 there is no great difference between the results for an inviscid fluid.

For the case of small viscosity, the results of Morgan and Ferrante show that the wave speeds for the frequency range $0.0 < \bar{\omega} < 1.0$ are essentially

nondispersive irrespective of the mean flow velocity. Furthermore, the phase velocity of pressure waves is given to a good approximation by the sum of the wave speed for zero mean flow and the average stream velocity. The marked difference between our results and the viscous fluid analysis of Reference 14 may be due in part to the reasons cited previously for the inviscid case but perhaps more importantly to the fact that the radial inertia of the vessel wall was neglected by Morgan and Ferrante. Note, however, that for $0.0 < \bar{\omega} < 0.2$ which corresponds to an actual frequency range of 0.0 to about 50 Hz for the dimensioned parameters chosen above, the three analyses yield results which are the same within 10 to 12 percent.

The effect of a mean flow on the propagation velocity of waves in blood vessels is pronounced only for pressure or distension waves which we have denoted as type I. With only a single exception[12], experimental investigations of the wave transmission characteristics of blood vessels have dealt exclusively with the propagation of naturally occurring or artificially induced pressure waves (type I). Since the effect of a mean flow on phase velocity is theoretically only pronounced for this type of wave it is clear that an accurate interpretation of wave speed data requires information regarding the nature of the blood flow during the time the data were obtained.

While studying the transmission characteristics of large amplitude artificial pressure waves in the vena cava of anesthetized dogs, we found that the signal speeds varied with respiration and were generally greater at inspiration than during the resting phase of the respiratory cycle (see Chapter III). By

measuring simultaneously the total and static venous pressure and the speed of induced pressure pulses we concluded that the difference in wave speeds could be attributed to the increased flow velocity during inspiration. To assess more accurately the validity of this theoretical analysis, a systematic study of the relationship between wave transmission velocity and blood flow in the aorta of anesthetized dogs has been undertaken[11] and initial results indicate agreement with the predicted behavior.

II. THEORETICAL ANALYSIS OF THE EFFECTS OF ANISOTROPY ON THE PROPAGATION OF WAVES IN BLOOD VESSELS

Introduction

The walls of blood vessels are complex structures composed of layers of various biological substances including elastin, collagen and smooth muscle which have different elastic properties and which appear in varying proportions according to the nature of the vessel[7]. Estimates of the elastic moduli of these materials range from as little as 6×10^4 dynes/cm^2 for relaxed smooth muscle to about 10^8 dynes/cm^2 for collagen fibers[20-23].

Judging from histological features which indicate the structural inhomogeneity of blood vessels, their mechanical properties should not be expected to be uniform and isotropic. That is, the vessel may respond differently to stresses in the longitudinal and circumferential directions. Experimental evidence for this type of behavior has been presented by Bergel[20] who found the circumferential Young's modulus in an excised canine thoracic aorta to be about 1.5 times greater than the longitudinal modulus. Furthermore, McDonald[1] has expressed little doubt that arteries are anisotropic, with maximum stiffness in the circumferential direction. But he argues that strong axial tethering results in the vessel being relatively inextensible in that direction and therefore does not move longitudinally in the presence of a propagating pulse wave. According to McDonald this behavior then renders the vessel as functionally equivalent to an isotropic tube.

To determine the actual extent of anisotropy in a single blood vessel,

Anliker and Moritz[12] have been studying the transmission characteristics of type III waves in the carotid artery of anesthetized dogs. Their results provide some information regarding the magnitude of the various elastic constants as well as a firm basis for refining our mathematical description of wave propagation in blood vessels.

Basic Equations

Postulating the existence of anisotropy, a more general theoretical description of the mechanical behavior of blood vessels can be obtained by considering the vessel wall to be orthotropically elastic with different elastic properties in the longitudinal and circumferential directions. The two-dimensional analysis presented in Chapter I can be extended to include this type of behavior by simply introducing a modified form of the elastic laws in which stress and strain are still directly proportional but the proportionality constant is dependent upon the direction of the applied stress.

We denote the elastic moduli for the longitudinal and circumferential directions by E_x and E_β respectively, the shear modulus by G and the two Poisson's ratios by ν_x and ν_β where $\nu_x(\nu_\beta)$ is the ratio of contraction in the direction $\beta(x)$ to elongation in the direction $x(\beta)$. Hooke's law relating the stresses and strains then takes the form

$$\epsilon_x = \frac{\sigma_x}{E_x} - \frac{\nu_\beta \sigma_\beta}{E_\beta}$$

$$\epsilon_\beta = \frac{\sigma_\beta}{E_\beta} - \frac{\nu_x \sigma_x}{E_x} \qquad (2.1)$$

$$\gamma_{x\beta} = \frac{1}{G}\tau_{x\beta}$$

where the strains $\epsilon_x, \epsilon_\beta, \gamma_{x\beta}$ and the stresses $\sigma_x, \sigma_\beta, \tau_{x\beta}$ are defined as usual[19]. In general the Young's moduli and Poisson's ratios are mutually independent. However, when the system being analyzed is initially unstressed we can show by means of the Maxwell-Betti reciprocity theorem[24] that

$$\frac{E_\beta}{E_x} = \frac{\nu_\beta}{\nu_x}. \qquad (2.2)$$

The shear modulus G must also be retained as an independent parameter since the usual relation between E, ν and G for isotropic materials is a direct consequence of their isotropy. Hence, for this plane stress formulation the constitutive law for the material is specified by five elastic parameters. For convenience we introduce a dimensionless shear modulus $\tilde{g}$, the ratio of the two elastic moduli γ_1 and the ratio of the two Poisson's constants γ_2:

$$\tilde{g} = G\left(\frac{1 - \nu_x \nu_\beta}{E_x}\right)$$

$$\gamma_1 = \frac{E_\beta}{E_x}, \quad \gamma_2 = \frac{\nu_\beta}{\nu_x}. \qquad (2.3)$$

The dimensionless stress resultants in the axial and circumferential directions and the inertia quantities associated with the vessel wall and the fluid are modified for the orthotropic case and are distinguished from the parameters in Chapter I by "tildes":

$$\tilde{q}_1 = \frac{T_{10}(1 - \nu_x \nu_\beta)}{E_x h} \qquad \tilde{\mu}_w = \frac{1 - \nu_x \nu_\beta}{E_x h} a^2 \rho_w h$$

$$\tilde{q}_2 = \frac{a\Delta p(1 - \nu_x \nu_\beta)}{E_x h} \qquad \tilde{\mu}_f = \frac{1 - \nu_x \nu_\beta}{E_x h} a^2 m_f \tag{2.4}$$

With these changes the linearized equations of motion for a thin shell in terms of the displacement components u, v, w can be rederived for an orthotropic material[19] and become:

$$\begin{aligned}
&\tilde{L}_{11}(u) + \tilde{L}_{12}(v) + \tilde{L}_{13}(w) + (\tilde{q}_1 + \nu_x \tilde{q}_2)\frac{\partial^2 u}{\partial \alpha^2} \\
&\quad + \tilde{q}_2\left(\frac{\partial^2 u}{\partial \beta^2} - \frac{\partial w}{\partial \alpha}\right) - \tilde{\mu}_w \frac{\partial^2 u}{\partial t^2} = 0 \\
&\tilde{L}_{21}(u) + \tilde{L}_{22}(v) + \tilde{L}_{23}(w) + (\tilde{q}_1 + \nu_x \tilde{q}_2)\frac{\partial^2 v}{\partial \alpha^2} \\
&\quad + \tilde{q}_2\left(\frac{\partial^2 v}{\partial \beta^2} + \frac{\partial w}{\partial \beta}\right) - \tilde{\mu}_w \frac{\partial^2 v}{\partial t^2} = 0 \\
&\tilde{L}_{31}(u) + \tilde{L}_{32}(v) + \tilde{L}_{33}(w) - (\tilde{q}_1 + \nu_x \tilde{q}_2)\frac{\partial^2 w}{\partial \alpha^2} \\
&\quad - \tilde{q}_2\left(\frac{\partial u}{\partial \alpha} - \frac{\partial v}{\partial \beta} + \frac{\partial^2 w}{\partial \beta^2}\right) + (\tilde{\mu}_w + \tilde{\mu}_f)\frac{\partial^2 w}{\partial t^2} = 0.
\end{aligned} \tag{2.5}$$

The modified differential operators $\tilde{L}_{ij}$ are defined by:

$$\tilde{L}_{11} = \frac{\partial^2}{\partial\alpha^2} + \tilde{g}\frac{\partial^2}{\partial\beta^2}(1+e^2)$$

$$\tilde{L}_{22} = \gamma_1\frac{\partial^2}{\partial\beta^2} + \tilde{g}\frac{\partial^2}{\partial\alpha^2}(1+3e^2)$$

$$\tilde{L}_{33} = \gamma_1 + e^2\left(\frac{\partial^4}{\partial\alpha^4} + 2(\gamma_1\nu_x + 2\tilde{g})\frac{\partial^4}{\partial\alpha^2\partial\beta^2} + \gamma_1\frac{\partial^4}{\partial\beta^4} + 2\gamma_1\frac{\partial^2}{\partial\beta^2} + \gamma_1\right)$$

$$\tilde{L}_{12} = (\gamma_2\nu_x + \tilde{g})\frac{\partial^2}{\partial\alpha\partial\beta}$$

$$\tilde{L}_{13} = \gamma_2\nu_x\frac{\partial}{\partial\alpha} - e^2\left(\frac{\partial^3}{\partial\alpha^3} - \tilde{g}\frac{\partial^3}{\partial\alpha\partial\beta^2}\right) \qquad (2.6)$$

$$\tilde{L}_{21} = (\gamma_1\nu_x + \tilde{g})\frac{\partial^2}{\partial\alpha\partial\beta}$$

$$\tilde{L}_{23} = \tilde{L}_{32} = \gamma_1\frac{\partial}{\partial\beta} - e^2(\gamma_1\nu_x + 3\tilde{g})\frac{\partial^3}{\partial\alpha^2\partial\beta}$$

$$\tilde{L}_{31} = \gamma_1\nu_x\frac{\partial}{\partial\alpha} - e^2\left(\frac{\partial^3}{\partial\alpha^3} - \tilde{g}\frac{\partial^3}{\partial\alpha\partial\beta^2}\right).$$

The equation of continuity, the linearized Euler equation and the boundary condition developed in the previous section remain valid and therefore can be reudced to the same expressions for the velocity potential (Φ) and apparent mass of the fluid (m_f). We again assume solutions to equation (2.5) of the form

$$u = \tilde{A}_{sc} \exp[i \frac{\omega}{c}(x - ct) + is\beta]$$

$$v = \tilde{B}_{sc} \exp[i \frac{\omega}{c}(x - ct) + is\beta] \qquad (2.7)$$

$$w = \tilde{C}_{sc} \exp[i \frac{\omega}{c}(x - ct) + is\beta + i \frac{\pi}{2}]$$

and obtain a set of three linear homogeneous equations for the amplitude factors $\tilde{A}_{sc}$, $\tilde{B}_{sc}$ and $\tilde{C}_{sc}$ which leads to a frequency equation in the form of a vanishing determinant. We introduce the following dimensionless parameters:

$$C_p^{*2} = \frac{E_x}{\rho_w(1 - \nu_x \nu_\beta)} \qquad \tilde{C}^2 = \frac{C^2}{C_p^{*2}} \qquad \tilde{\omega}^2 = \frac{\omega^2 a^2}{C_p^{*2}}$$

$$\tilde{\rho} = \frac{\rho_f}{\rho_w}. \qquad (2.8)$$

Then the determinant takes the form:

$$
\begin{vmatrix}
\frac{\tilde{\omega}^2}{\tilde{c}^2}(1+\tilde{q}_1+\nu_x\tilde{q}_2)+\tilde{q}_2 s^2 & -\frac{\tilde{\omega}}{\tilde{c}}s(\gamma_2\nu_x+\tilde{g}) & \frac{\tilde{\omega}}{\tilde{c}}(\gamma_2\nu_x-\tilde{q}_2)+ \\
+\tilde{g}s^2(1+e^2)-\tilde{\omega}^2 & & +e^2\left(\frac{\tilde{\omega}^3}{\tilde{c}^3}-\frac{\tilde{\omega}}{\tilde{c}}s^2\tilde{g}\right) \\
\hline
-\frac{\tilde{\omega}}{\tilde{c}}s(\gamma_1\nu_x+\tilde{g}) & \frac{\tilde{\omega}^2}{\tilde{c}^2}(\tilde{q}_1+\nu_x\tilde{q}_2+\tilde{g}(1+3e^2)) & -e^2(\gamma_1\nu_x+3\tilde{g})\frac{\tilde{\omega}^2}{\tilde{c}^2}s \\
 & +s^2(\gamma_1+\tilde{q}_2)-\tilde{\omega}^2 & -s(\gamma_1+\tilde{q}_2) \\
\hline
\frac{\tilde{\omega}}{\tilde{c}}(\gamma_1\nu_x-\tilde{q}_2) & -e^2(\gamma_1\nu_x+3\tilde{g})\frac{\tilde{\omega}^2}{\tilde{c}^2}s & \gamma_1+e^2\left[\frac{\tilde{\omega}^4}{\tilde{c}^4}\right. \\
+e^2\left(\frac{\tilde{\omega}^3}{\tilde{c}^3}-\frac{\tilde{\omega}}{\tilde{c}}s^2\tilde{g}\right) & -s(\gamma_1+\tilde{q}_2) & +2\frac{\tilde{\omega}^2}{\tilde{c}^2}s^2(\gamma_1\nu_x+2\tilde{g}) \\
 & & \left.+\gamma_1 s^4-2\gamma_1 s^2+\gamma_1\right]+ \\
 & & \frac{\tilde{\omega}^2}{\tilde{c}^2}(\tilde{q}_1+\nu_x\tilde{q}_2)+\tilde{q}_2 s^2 \\
 & & -\left(1+\tilde{\rho}\frac{a}{h}\frac{I_s(\xi)}{\xi I_s'(\xi)}\right)\tilde{\omega}^2
\end{vmatrix} = 0. \qquad (2.9)
$$

Results

The frequency equation in the form of the determinant (2.9) for an orthotropic vessel contains eleven dimensionless parameters: $\tilde{q}_1, \tilde{q}_2, s, h/a, \tilde{\rho}, \tilde{\omega}, \tilde{c}, \nu_x$, γ_1, γ_2 and $\tilde{g}$. With the exception of the parameters $\nu_x, \gamma_1, \gamma_2$ and $\tilde{g}$ the above quantities are the same as those which appear in the analysis for an isotropic vessel with the only difference entering through the normalizing factor $E_x/(1 - \nu_x \nu_\beta)$. For the analysis in terms of nondimensional variables this normalization effectively reduces the number of explicit independent elastic constants from five to four. It must be remembered however, that any physical interpretation of the dimensionless results requires that we specify values for the original five elastic constants.

In order to arrive at physiologically meaningful conclusions we should restrict, to some degree, the range of acceptable values for these additional parameters. For example, by requiring the material of the vessel wall to be incompressible the Poisson's ratios must satisfy certain incompressibility relations which are obtained directly from Hooke's law. These equations show that ν_x and ν_β can lie between 0.0 and 1.0 and that the Poisson's ratios for the radial direction (although they do not appear explicitly in the equilibrium equations for the vessel) may not be neglected when considering incompressibility and must assume values compatible with those chosen for ν_x and ν_β. In this analysis we will assume that these restrictions regarding the contraction of the vessel wall through its thickness are fulfilled. From equation (2.3) we have $\nu_\beta = \gamma_2 \nu_x$ and it follows that both ν_x and $\gamma_2 \nu_x$ satisfy the condition

$$0.0 \leq \nu_x, \gamma_2 \nu_x \leq 1.0 \qquad (2.10)$$

For an isotropic vessel the dimensionless shear modulus $\tilde{g}$ is a function only of the Poisson's ratio and for an incompressible material (Poisson's ratio = 0.5) $\tilde{g} = 0.25$. Unfortunately, no experimental information is yet available on which to base assumptions regarding the value of the shear modulus of blood vessels. The Young's modulus ratio γ_1 may theoretically assume any positive value. However, experimental measurements indicate that the circumferential and axial elastic moduli of blood vessels are well within an order of magnitude of each other with E_β generally 2 to 3 times greater than E_x[20,25]. It seems appropriate therefore, to consider values of γ_1 within the range 0.0 to 5.0.

For this analysis the determinant no longer retains its symmetry since the parameter γ_2 appears in the equation for axial equilibrium while γ_1 appears in the circumferential and radial equations. In the limiting case of vanishingly small initial stresses the reciprocity relation $\gamma_1 = \gamma_2$ is applicable and the determinant becomes symmetric. In the orthotropic shell we again find three classes of propagating waves denoted as type I, II or III according to the previous convention.

For the limiting case of vanishing frequency we can directly obtain the approximate phase velocities of axisymmetric waves (s = 0). Taking $\tilde{\rho} \cong 1$ and $\tilde{q}_1, \tilde{q}_2$ and h/a small compared to 1, the phase velocity of pressure waves (type I) as $\tilde{\omega} \to 0$ is given by

$$\tilde{c}_I^2 = \frac{\gamma_1}{2\tilde{\rho}a/h} + \frac{(\gamma_1\nu_x - \tilde{q}_2)(\gamma_2\nu_x - \tilde{q}_2)}{\gamma_1 - 2\tilde{\rho}\frac{a}{h}(1 + \tilde{q}_1 + \nu_x\tilde{q}_2)} \tag{2.11}$$

Note that both terms are of the same order; namely O(h/a). When the initial stresses $(\tilde{q}_1, \tilde{q}_2)$ are taken as zero and $h/a << 1$ this reduces to

$$\tilde{c}_I^2 = \frac{\gamma_1}{2\tilde{\rho}a/h}(1 - \gamma_2\nu_x^2) \tag{2.12}$$

or

$$c_I^2 = \frac{E_\beta h}{2\rho_f a} \tag{2.13}$$

the Moens-Korteweg equation. Observe that of the five elastic parameters only the circumferential Young's modulus has an effect on the phase velocity in this limiting example. Axisymmetric type II waves are characterized by pure circumferential wall displacements and propagate with a velocity

$$\tilde{c}_{II}^2 = \tilde{q}_1 + \nu_x\tilde{q}_2 + \tilde{g}(1 + 3e^2) \tag{2.14}$$

at all frequencies. The strong influence of the shear modulus $\tilde{g}$ in determining the wave speed is particularly apparent when the initial stresses are small. In terms of dimensional variables (2.14) becomes

$$c_{II}^2 = \frac{T_{10}}{\rho_w h} + \frac{\nu_x a\,\Delta p}{\rho_w h} + \frac{G}{\rho_w}(1 + 3e^2) \tag{2.15}$$

which is independent of either the axial or circumferential Young's modulus. As $\tilde{\omega} \to 0$ the phase velocity of type III or axial waves approaches

$$\tilde{c}^2_{III} = 1 + \tilde{q}_1 + \nu_x \tilde{q}_2 - \frac{(\gamma_1 \nu_x - \tilde{q}_2)(\gamma_2 \nu_x - \tilde{q}_2)}{\gamma_1 - 2\tilde{\rho} a/h(1 + \tilde{q}_1 + \nu_x \tilde{q}_2)} \tag{2.16}$$

In contrast to equation (2.11) the fractional term appearing here is of higher order compared to $1 + \tilde{q}_1 + \nu_x \tilde{q}_2$ and therefore its role in determining the wave speed is necessarily small. When $\tilde{q}_1$ and $\tilde{q}_2 \to 0$ and $h/a \ll 1$ we obtain

$$c^2_{III} = \frac{E_x}{\rho_w (1 - \nu_x \nu_\beta)} \tag{2.17}$$

indicating the predominant influence of the axial modulus on the velocity of axial waves.

The extent to which orthotropy influences the wave transmission characteristics of the vessel can be determined from a parametric analysis of the frequency equation. The results presented here do not comprise a complete parametric study of the effects of anisotropy since our intentions have been only to obtain an initial indication of the role of anisotropy in determining the propagation velocities and mode shapes of various types of waves. Furthermore, it is hoped that the selected results may provide the information most useful to the experimentalist for determining the degree of anisotropy and its variations in blood vessels. More specifically, with only two exceptions, graphs illustrating the effects of anisotropy on the mode shapes are not included since the changes produced are relatively small and do not reflect any major deviations from the displacement patterns for isotropic vessels.

To facilitate comparison with other analyses, in particular Reference 8, but also References 26 and 27, we consider the vessel to be initially unstressed

which implies that $\gamma_1 = \gamma_2$. With this restriction we can eliminate the subscripts and denote the value of the parameter with γ.

Effect of the Ratio γ

Waves of Type I

The effect of the Young's modulus ratio γ on the dimensionless phase velocity of type I waves is illustrated in Figures 12 and 13 for $s = 0$ and $s = 2$. The values of ν_x and $\tilde{g}$ correspond to those of an isotropic incompressible vessel while the radius to wall thickness ratio a/h applies for the larger arteries and average size veins (Reference 7). As a consequence of the assumed incompressibility of the vessel wall and the fact that $\nu_x = 0.5$, the range of γ is restricted such that $0.0 \leq \gamma \leq 2.0$. From Figure 12 ($s = 0$) we see that for all frequencies the dimensionless phase velocity $\tilde{c}$ increases with increasing values of γ although the velocity is significantly affected by changes in γ only when $\tilde{\omega} < 0.5$. For $\tilde{\omega} > 0.5$ the influence of the Young's modulus ratio on the wave speed diminishes rapidly with increasing frequency as exemplified at $\tilde{\omega} = 1.0$ where a 400 percent increase in γ produces less than a 10 percent increase in $\tilde{c}$.

The corresponding effect on the dimensional phase velocity c is radically different and depends not only on the values chosen for the elastic moduli but, even more importantly, on the manner in which the two Young's moduli vary with γ. For example, if we assume that E_x is constant and equal to 10^6 dynes/cm^2 the phase velocity of type I waves corresponding to a frequency of $\tilde{\omega} = 1.0$ increases about 50 percent as γ is increased from 0.5 to 2.0. On the other hand, for $E_\beta = 10^6$ dynes/cm^2 and constant, the wave speed decreases about

30 percent for the same increase in γ at $\tilde{\omega} = 1.0$. As the frequency approaches zero the value of the phase velocity is approximated by equation (2.12) for dimensionless variables and by equation (2.13) for the dimensional case. Obviously, if E_β is constant, c will not vary with changes in γ at zero frequency even though a marked increase in $\tilde{c}$ is observed as γ increases from 0.5 to 2.0.

With the exception of the cut-off frequency which increases slightly with rising γ, the dispersion of type I waves with $s = 2$ is not appreciably changed by variations in γ as shown in Figure 13. Nonaxisymmetric waves with $s \geq 2$ exhibit similar behavior with respect to variations in γ. By considering smaller values of the Poisson's ratio ν_x we can explore the effect of larger values of γ on the wave speeds while still satisfying the condition of vessel incompressibility (equation 2.10). The graph in Figure 14 gives dispersion curves for $s = 0$ and for various γ between 1.0 and 5.0 with $\nu_x = 0.2$. In this instance a marked influence of the Young's modulus ratio on the nondimensional phase velocity extends throughout the frequency range 0.0 to 1.0 and relative increases in $\tilde{c}$ with γ are significantly greater than those for the example given in Figure 12. When $s = 2$ the larger values of γ again tend only to increase slightly the cut-off frequencies.

Waves of Type II

According to equations (2.14 and 2.15) the phase velocity of axisymmetric type II waves is independent of the Young's moduli for all frequencies and in the absence of initial stresses is governed entirely by the shear modulus and the

wall thickness to radius ratio. For $s = 2$ the ratio γ exhibits only a mild influence on the dispersion as indicated in Figure 15 which shows the effect to be limited to a range of frequencies near the cut-off value. The behavior for large values of γ is quite similar.

Waves of Type III

The transmission velocity of axial waves with $s = 0$ is also relatively insensitive to variations in γ as is evident from Figure 16. Inspection of equation (2.16) reveals that even at low frequencies the ratio γ is contained in a term which is of second order small for the parameter values considered. As shown in Figure 17, when $s = 2$ it is primarily the cut-off frequencies which change with γ and show a consistent increase as γ is varied between 0.5 and 2.0. Note the different scale used in this figure.

We recall that γ is defined in terms of either the Poisson's ratios as ν_β/ν_x or the Young's moduli as E_β/E_x. Since the parameter ν_β is only implicitly contained in the frequency equation through the ratio γ, the results of this section also reflect the effect of variations in ν_β on the dimensionless phase velocities for fixed values of ν_x.

Effect of the Poisson's Ratio

Unlike the other elastic parameters, ν_x appears in the frequency equation as a multiplier of one of the stress resultants in terms of the form $\nu_x \tilde{q}_2$. Hence the degree of initial prestress will have a definite influence on the extent to which ν_x affects the wave speeds in an orthotropic vessel. It is necessary therefore, to include in the analysis both the case for zero and nonzero

values of $\tilde{q}_2$ to approximately assess the importance of variations in the parameter ν_x.

Waves of Type I

Figure 18 illustrates the dispersion of axisymmetric type I waves in the absence of initial stresses for $\nu_x = 0.0, 0.4, 0.6$ and 0.8, while γ and $\tilde{g}$ have values corresponding to isotropy in the axial and circumferential directions. In addition it is understood that the elastic parameters for the radial direction, although they do not appear explicitly in the analysis, assume values compatible with the requirement of vessel incompressibility. At all frequencies we see that the dimensionless phase velocity decreases with rising values of ν_x. For $\tilde{\omega} < 0.4$ this decrease in $\tilde{c}$ is particularly pronounced, while in the region $\tilde{\omega} > 0.6$ the speed varies only slightly with changes in ν_x. The similarity between this figure and Figure 12, which depicts the effect of variations in γ on $\tilde{c}$, may be attributed to the fact that for $s = 0$ and $\tilde{q}_2 = 0.0$, ν_x enters the frequency equation only through the product $\gamma\nu_x$ and no distinction can be made between variations in γ with fixed ν_x and variations in ν_x with constant γ. For the case of nonvanishing $\tilde{q}_2$, variations in ν_x are manifested in an entirely different fashion as evidenced in Figure 19 where we have taken $\tilde{q}_2 = 0.4$. It should be emphasized that these dispersion curves, as well as others for which $\tilde{q}_2 \neq 0.0$, are approximate since the assumption that $\gamma_1 = \gamma_2 = \gamma$ is valid only when all initial stresses vanish. This illustration shows that the wave speed consistently <u>increases</u> with increasing ν_x and that the influence of ν_x is relatively minor at low frequencies ($\tilde{\omega} < 0.3$) but becomes increasingly pronounced for $\tilde{\omega} > 0.5$.

Interestingly, this behavior is completely opposite that observed for $\tilde{q}_2 = 0.0$ and it appears that any effect the terms $\gamma\nu_x$ might have on the wave speeds at low frequencies is negated by the quantity $\nu_x\tilde{q}_2$.

For all values of $\tilde{q}_2 > 0.0$ the dispersion pattern is similar to that in Figure 19 although the range of values assumed by $\tilde{c}$ for $0.0 < \nu_x < 0.8$ becomes greater as $\tilde{q}_2$ increases. Nonaxisymmetric waves with $s \geq 2$ are only affected by variations in the Poisson's ratio when $\tilde{q}_2 > 0.0$, i.e. in the presence of an initial transmural pressure. Figure 20 shows that for $s = 2$ the phase velocities undergo substantial increases as ν_x is raised although the dispersion remains essentially unchanged and the cut-off frequency is not shifted. Similar behavior is observed for $s > 2$ and to a lesser degree for smaller values of $\tilde{q}_2$.

To determine the corresponding effect of variations in ν_x on the actual phase velocities of these waves it is necessary to multiply $\tilde{c}$ by the normalization factor which, for constant E_x and $\gamma = 1.0$, is proportional to $(1 - \nu_x^2)^{-1/2}$.

Waves of Type II

Referring once again to equation (2.14) which is valid at all frequencies, we see that the phase velocity of axisymmetric torsion waves is independent of ν_x when the initial stress $\tilde{q}_2$ vanishes, whereas for $\tilde{q}_2 \neq 0.0$ the square of the wave speed is a linear function of the Poisson's ratio. This behavior is illustrated in Figure 21 where $\tilde{q}_2 = 0.4$ and γ and $\tilde{g}$ assume the values for isotropy in the axial and circumferential directions. Again, the Poisson's ratio for the radial direction must be of a value such that incompressibility of the vessel is assured. As we allow ν_x to vary from 0.0 to 0.8 the phase

velocity shows an overall increase of about 50 percent and the dispersion is unchanged.

For $s = 2$ and zero transmural pressure, the dispersion characteristics for vessels with different ν_x are given in Figure 22. The cut-off frequency as well as the velocity for large values of $\tilde{\omega}$ are unaffected by ν_x. A significant decrease in phase velocity with increasing values of Poisson's ratio is apparent for the frequency range $1.0 < \tilde{\omega} < 4.0$. Of particular interest is the double-valuedness of $\tilde{c}$ which is evident here in the dispersion curve for $\nu_x = 0.8$. Inspection of the corresponding mode shapes in Figure 23 indicates that these different velocities apply to two distinct waves propagating in the positive direction. Although these disturbances are of the same frequency, they each possess a characteristic displacement pattern and wave length in addition to their different phase velocities. Note that for the parameter values chosen here this behavior is possible only when $\nu_x \geq 0.6$. It may be stressed that the existence of two mode shapes at a single frequency is not in conflict with any physical or mathematical principles underlying this analysis (e.g. continuity, uniqueness) and both waves constitute equally admissible solutions to the frequency equation (2.9).

A somewhat different relationship between dispersion and Poisson's ratio occurs when $\tilde{q}_2 = 0.4$ as is evident from the graph in Figure 24. Here the phase velocity is again a single-valued function of $\tilde{\omega}$ and for frequencies less than about 3.0, $\tilde{c}$ decreases as ν_x is varied from 0.0 to 0.8. However, for $\tilde{\omega} > 3.2$ the phase velocity shows a consistent increase with ν_x. This interesting pattern has

been observed in the dispersion curves for various values of $\tilde{q}_2$ between 0.1 and 0.8 and for waves with $s > 2$.

Waves of Type III

The nondimensional phase velocity of type III axisymmetric waves is insensitive to variations in ν_x for zero transmural pressure ($\tilde{q}_2 = 0.0$) and only mildly affected when $\tilde{q}_2 \neq 0.0$. In either case the waves are nondispersive and for all $\tilde{q}_2 > 0.0$ their speeds increase with rising ν_x. For example, when $\tilde{q}_2 = 0.4$ and ν_x is varied from 0.0 to 0.8 the phase velocity increases only about 15 percent. Considering waves with $s = 2$, the influence of the Poisson's ratio is reflected in the dispersion curves similarly for all values of $\tilde{q}_2$. Figure 25 depicts the typical changes in wave speed brought about by variations in ν_x for type III waves with $s = 2$. Although the cut-off frequency remains unchanged the velocities show an increase with ν_x for all $\tilde{\omega}$.

Effect of $\tilde{g}$

For an orthotropic material the shear modulus is an independent parameter and is entirely unrelated to the other elastic constants. As mentioned previously, no information is available regarding the behavior of blood vessels when subjected to shear stresses and therefore, we can only make educated guesses as to the acceptable range of values for the dimensionless shear modulus $\tilde{g}$. Since $\tilde{g} = 0.25$ for an isotropic incompressible material and we assume the vessel is not strongly anisotropic, we shall consider, initially, values for $\tilde{g}$ between 0.2 and 1.0. The results are also indicative of the effect of variations in G on the true wave speed since the normalizing factor is independent of the shear

modulus.

Waves of Type I

Inspection of the determinant (equation 2.9) reveals that when $s = 0$ the shear modulus $\tilde{g}$ appears only in the solution which describes the transmission of type II waves. Hence,the velocities of symmetric type I and type III waves are unaffected by variations in $\tilde{g}$. Figure 26 indicates for $s = 2$ the relationship between $\tilde{c}$ and $\tilde{\omega}$ for various $\tilde{g}$ from 0.2 to 1.0. The dimensionless phase velocity shows an increase with increasing $\tilde{g}$ for all frequencies although these changes are most pronounced in the range $0.1 < \tilde{\omega} < 0.6$. In addition the cut-off frequency is independent of $\tilde{g}$.

Waves of Type II

For $s = 0$ this vibrational mode is one of pure shear and does not involve any axial or radial displacements of the vessel wall and we therefore expect the shear modulus to have an important effect on the wave speeds. This is indeed the case as shown in Figure 27 where a very strong dependence of the phase velocity on $\tilde{g}$ is evident. Notice that the speeds are considerably higher than in any of the preceding cases for waves of this type,and for nonvanishing $\tilde{q}_1$ or $\tilde{q}_2$ would increase even more according to equation (2.14).

Dispersion curves for nonaxisymmetric waves with $s = 2$ are shown in Figure 28. Notice that for $\tilde{g} \geq 0.4$ the phase velocity becomes double-valued over a certain range of frequencies and indicates that two different vibrational modes can occur at the same frequency. Cut-off frequencies still exist in the sense that there are frequencies below which disturbances of the type considered

cannot propagate; however they do not necessarily coincide with values of $\tilde{\omega}$ for which the phase velocity becomes infinite. When $\tilde{g} = 1.0$, for example, the minimum admissible solution to the frequency equation ($\tilde{\omega}$) is about 1.35 and the phase velocity ($\tilde{c}$) at this frequency is about 0.85.

For values of $\tilde{\omega}$ and $\tilde{g}$ where two different modes can exist, increases in the shear modulus cause the speeds of the slower waves to increase slightly while the fast waves exhibit a decrease in velocity. When $\tilde{c}$ is single-valued the wave speeds increase with rising $\tilde{g}$.

Since these dispersion curves represent a strong deviation from the case for the two dimensionally isotropic vessel, we present in Figure 29 the corresponding mode shapes for $\tilde{g} = 0.2, 0.6$ and 1.0. We notice immediately that a marked influence of $\tilde{g}$ on the wall displacements, particularly in the axial and circumferential directions, is apparent throughout the frequency range considered. At high frequencies ($\tilde{\omega} > 2.0$) the circumferential displacements $|v|$ become smaller with increasing values of the shear modulus while the axial displacements $|u|$ show a progressive increase. For $\tilde{g} = 1.0$ the mode shape at high frequency does not strictly conform to that of a type II wave since the circumferential component of the displacement is not dominant. In fact, for this case, the axial and circumferential displacements are equal and the radial component approaches zero.

Waves of Type III

As mentioned previously, axisymmetric type III waves are independent of $\tilde{g}$ since the axial displacements of the vessel wall do not induce any shear strains.

Figure 30 depicts results for $s = 2$ and we observe a progressive increase in phase velocity with rising $\tilde{g}$. Although it is not clearly evident from this graph, the cut-off frequency is unaffected by variations in $\tilde{g}$.

Discussion

The results of the preceding section are incomplete in so far as they include the effects of anisotropy on the dispersion of only a few of the infinitely many waves which can theoretically occur and be propagated. However, the types of waves which have been discussed, it is felt, represent those which can most readily be induced or observed in the living system (particularly $s = 0$) and thus lend themselves to experimental investigation. These findings indicate that the dimensionless phase velocities of nonaxisymmetric waves are in general not strongly influenced by variations in the elastic parameters except in the neighborhood of the cut-off frequencies where these waves display rather dramatic dispersive properties. Although experimental verification of these waves has thus far eluded investigators, the eventual study of waves with $s \geq 2$ will provide valuable information regarding the elastic and viscoelastic properties of blood vessels.

The effects of anisotropy and its variations appear to be most pronounced in the dispersion curves for axisymmetric waves. For pressure waves (type I), the Young's modulus ratio γ and the Poisson's ratio ν_x are equally important factors in determining wave speed, although the role of ν_x is dependent upon the value of the initial transmural pressure. Characteristics of type II waves, on the other hand, are independent of γ and, as expected, are influenced

primarily by the shear modulus $\tilde{g}$. For nonvanishing $\tilde{q}_2$ variations in the Poisson's ratio also produced changes in the wave speed. As plotted, the dispersion curves for axial waves (type III) reflect little change for variations in any of the three elastic parameters considered although we have shown (equation 2.17) that the phase velocity depends directly on the axial Young's modulus E_x. This apparent discrepancy is accounted for by the fact that we have normalized the velocity to $\tilde{c}$ with the reference velocity c_p^* which is also dependent upon E_x. This renders the dimensionless phase velocity $\tilde{c}$ independent of E_x and obscures the fact that the actual velocity c is directly proportional to $\sqrt{E_x}$ at all frequencies.

Recent papers by Mirsky[26] and Atabek[27] have investigated theoretically some aspects of wave transmission in orthotropic tubes filled with viscous fluid. Atabek considers as a model for the vessel a tethered initially stressed elastic membrane while Mirsky studies the effects of anisotropy in an unstressed thick walled shell with bending rigidity. In both cases, results are obtained only for small values of the parameter $\alpha = a\sqrt{\frac{\omega}{\nu}}$ which is essentially the square root of an unsteady Reynolds number, and the studies are limited to the propagation of axisymmetric type I and type III waves. Unfortunately we cannot compare our findings with those of Atabek or Mirsky since they do not discuss the transmission characteristics of these two waves in the inviscid limit, i.e. for $\alpha \to \infty$, and it is not possible to extrapolate their results for this contingency. Furthermore, questions may be raised regarding the significance of Atabek's results describing the propagation of axisymmetric pressure waves ($s = 0$, type I) as α approaches

zero since the wave speed also tends toward zero. This may be due to the fact that the linearized form of the Navier-Stokes equations do not accurately represent the flow for values of $\alpha < 2$.

Comparison with Experimental Results

Anliker and Moritz have undertaken an investigation of the transmission characteristics of artificially induced, axisymmetric type III waves in the carotid artery of anesthetized dogs[12]. Their initial results show that, depending on frequency, the speed of axial waves is about 2 to 4 times higher than that of pressure waves, and according to the approximate equations (2.13) and (2.17) these differences in wave speed indicate that the vessel is substantially stiffer in the circumferential than in the axial direction. The values of γ calculated from these data range from about 2 to 5 which is interpreted as being a strong indication of the anisotropic nature of the carotid artery. Data regarding the propagation of torsion waves are required before the shear modulus can be accurately determined.

III. THE TRANSMISSION CHARACTERISTICS OF LARGE AND SMALL PRESSURE WAVES IN THE ABDOMINAL VENA CAVA

Introduction

Extensive studies have been made on the mechanical behavior of larger arteries of various species, but little information is available regarding the dynamic elastic properties of veins even though their role in maintaining and controlling circulation is certainly no less important than that of arteries. This lack of knowledge may in part be attributed to the difficulties encountered in obtaining quantitative data on the distensibility of veins. These difficulties are primarily due to the inherently high flexibility of veins, their complex anatomy and the low transmural pressure that prevails in most parts of the venous system. Even small variations in the transmural pressure produced for example by respiration, changes in posture and muscular contraction may cause substantial changes in the geometry of the vessels, in their state of stress and in the elastic or viscoelastic properties of their walls, which all can strongly affect the distensibility of the vessels, Since these variations occur naturally and are not necessarily small, it must also be expected that veins exhibit a more complicated behavior than arteries.

It is well known that the mechanical behavior of individual blood vessels can be studied indirectly in terms of their wave transmission characteristics. This approach is particularly convenient since it does not require any trauma of the vessel wall and yields essentially local and instantaneous values for the changing elastic and viscoelastic parameters. Also, the availability of

ultrasound sensors has made it possible to adapt the wave transmission techniques validated in animal experiments to the noninvasive study of large arteries and veins in the extremities of man. This should facilitate extension of present knowledge of the behavior of individual superficial limb veins which has been obtained by measuring the pressure rises induced by the injection of known volumes of fluid into temporarily isolated segments of veins in situ [28]. However, before a meaningful quantitative interpretation of the wave transmission properties of these vessels is possible, we must establish a mathematical theory that predicts these properties with sufficient accuracy as functions of the geometric and physical features of the vessels.

Medical researchers have measured transmission properties of naturally occurring and artificially induced pressure waves in arteries as well as veins[1,29-35]. The data obtained in these studies and related work, however, do not lend themselves to an incisive assessment of the relevance and accuracy of the various mathematical models that have been postulated for the mechanical behavior of the blood vessels. In most cases the shapes of the pressure signals were too restricted or the amplitudes too large to allow for a broad evaluation of basic wave transmission properties such as dispersion and attenuation.

In view of the significance of certain nonlinear phenomena affecting the transmission of large amplitude pressure signals[11,31,36] we are presenting here our findings on the propagation of both large and small pressure waves in the abdominal vena cava of anesthetized dogs. As will be shown, the nonlinear behavior must be taken into account in the interpretation of much of the published

data and in the design of future experiments directed to the elucidation of the mechanisms mediating changes in the distensibility of blood vessels.

Experimental Methods

Waves in blood vessels can be characterized by either wall displacements, intraluminal pressure perturbations or flow fluctuations. Depending on the type and frequency of the waves considered we may find that only one or two of these variables are of sufficient magnitude to allow for accurate measurements. For example, distension waves are easily sensed in terms of their pressure or flow fluctuations, while for the detection of axial waves it is most convenient to minitor the corresponding axial wall displacements[12]. Obviously, the choice of variables to be measured depends not only on the nature of the waves but also on the sensitivity of available transducers and on whether the waves are to be recorded by an invasive or a noninvasive technique. Pressure or distension waves can be readily induced in arteries and are observable over distances that are relatively large compared to the vessel radii when the frequency is less than 100 Hz[11,12]. Guided by these facts we have generated artificial distension waves in the vena cava of anesthetized dogs.

The pressure perturbations in the vena cava were minitored by highly sensitive catheter-tip manometers utilizing Bytrex pressure cells Model HFD-5*. One of these transducers is shown in Figure 31. It has a diameter of 3 mm and a sensitivity of 80 to 100 μV/mm Hg with an excitation of 25 volts and therefore allows for a resolution of a fraction of one mm H_2O. The natural frequency of

*Schaevitz-Bytrex, Inc., 223 Crescent Street, Waltham, Mass. 02154

such pressure cells was found to be above 60 kHz in air and their response is linear within 1% from 0 to 300 mm Hg. The shielded leads and the venting tube are protected by a heat-shrinkable plastic tube forming a leak-proof flexible catheter. The pressure cell itself is gold plated to reduce the corrosive effects of body fluids. The signal from the solid state strain gauge bridge used in these transducers is amplified by Astrodata amplifiers Model 885** and recorded on a Honeywell Visicorder Model 1108 equipped with galvanometers whose frequency response is flat up to 3300 Hz.

By injecting into a blood vessel a given volume of blood or saline from a spring-loaded syringe one can produce a pressure pulse whose amplitude and shape depend on the volume and injection time as well as the distensibility of the vessel. In our experiments we induced such signals with the syringe shown in Figure 32. A volume of 0.5 or 1.0 cm^3 of blood or saline could be injected in 10 to 20 msec depending on the stiffness of the spring and the length and diameter of the cannula. The amplitudes of the resulting pressure signals were generally between 30 and 60 mm Hg for injections of 0.5 cm^3 and as much as 225 mm Hg for 1 cm^3.

Figure 33 shows representative tracings of pressure fluctuations in the carotid artery and the abdominal vena cava of an anesthetized dog during the transmission of a pressure pulse induced by the injection of 0.5 cm^3 of saline into a femoral vein. In this instance the arterial blood pressure (BP) was

**Astrodata, Inc., 240 E. Palais Road, Anaheim, Calif. 92805.

135/95 mm Hg while the unperturbed venous pressure (P_v) was 75 mm H_2O. The distance between the two catheter-tip manometers (Δx) was 5.0 cm and the radius to wall thickness ratio (a/h) for the vena cava was 47. The relative scales for the venous and arterial pressure tracings and time are indicated. Each of the two venous pressure curves has a different zero point since they were separated for illustration purposes.

The speed of the pressure pulse is usually defined by the transmission time Δt of a characteristic point of the wave front over a given distance Δx. As a characteristic point we have chosen here the intersection of the tangent in the inflection point of the wave front with a line approximating the unperturbed venous pressure. For this point Δt could be measured with a high degree of repeatability in contrast to other admissible choices for the characteristic point, which displayed a rather wide scatter in the measurement of the transmission times.

While spring-loaded syringes are convenient tools for inducing transient pressure waves, they do not allow for accurate control of the shape of the pulse. For example, slight changes in the orientation of the cannula at the point of injection can produce marked differences in the pulse shape. Moreover, in order to determine the wave velocity as a function of the frequency from such pulse waves it would be necessary to evaluate the Fourier spectra of the signal at different points along the vessel. These laborious Fourier transform computations can be avoided by generating a sinusoidal pressure signal. In some of our experiments this was done by the pump shown in Figure 34. The waves are

induced by a reciprocating piston connected to a 1/8 hp D. C. motor by means of a timing belt and scotch yoke to enforce pure sinusoidal motions of the piston. The stroke volume and frequency of the pump can be varied from 0 to 5.0 cm^3 and 0 to 40 Hz respectively. To eliminate high frequency pressure fluctuations due to inherent structural vibrations of the system, a damping device was installed between the cannula and pump cylinder. Damping is provided by an air cushion that is separated from the fluid by a rubber membrane and whose pressure can be varied to optimize the damping characteristics. Since no check valve is used the net flow of the pump is zero.

The pump was connected to the vena cava by a flexible plastic cannula that was inserted through a femoral vein. Typical tracings of sinusoidal pressure waves induced by the pump are shown in Figure 35. As illustrated in this figure, the speed of the signals over a known distance Δx was evaluated from the transmission time Δt of the points of intersection of the tangents to the sine wave at two successive inflection points.

With the pump used it was not possible to induce sine waves of small amplitudes over a frequency range wide enough for an extensive study of dispersion. Also, the inertia of the pump and of the fluid contained in it was sufficiently large to cause some distortions of the sine waves during the starting phase of the pump at essentially all frequencies between 4 and 40 Hz. By inserting an electrically driven piston (Figure 36) directly into a femoral vein and positioning it near the bifurcation, sine waves could be generated with frequencies between 15 and 100 Hz. The piston consists of a lightweight aluminum rod that is attached to the core of a solenoid and is protected by a

brass cylinder which also prevents any direct contact of the moving rod with the vessel wall. The piston diameter is 5.5 mm and its maximum travel is about 6.5 mm for frequencies between 20 and 100 Hz. The sinusoidal displacements of the piston are induced by means of an electronic oscillator and a high fidelity amplifier.

At high frequencies one can avoid noticeable reflection interference even when the amplitudes of the waves are not necessarily very small[11] and when no dissipative mechanisms are present. This is accomplished by generating finite trains of sine waves with the aid of a tone burst generator. For sufficiently short trains the waves can be recorded before the reflections arrive at the sites of the transducers. Tracings of representative pressure signals of this type are given in Figure 37.

The attenuation of these signals was determined by comparing the peak-to-peak amplitudes of corresponding waves at the two pressure recording sites. The amplitude is defined as shown and denoted by A_o at the proximal transducer and by A at the distal transducer.

For mildly dispersive media, i.e. those in which the phase velocity does not vary by more than a few percent whenever the frequency is changed by 10%, the speed of a finite train of sine waves can be interpreted as a good approximation of the phase velocity corresponding to the frequency of the sine waves. This is evident from the Fourier spectra of finite trains of sine waves shown in Figure 38. The uppermost pair of graphs illustrates a train of 2 1/2 sine waves of circular frequency ω_o (left) and the corresponding Fourier transform $F(\omega)$ (right). The

pairs of graphs in the center and at the bottom correspond respectively to trains of 4 1/2 and 8 1/2 sine waves of the same circular frequency ω_o. In each case the Fourier transform $F(\omega)$ has a distinct maximum at ω_o. With increasing length of the train, $F(\omega)$ peaks more sharply at $\omega = \omega_o$, and $F(\omega_o)$ dominates the spectrum in increasing proportion. In the limiting case of an infinitely long train $F(\omega_o)$ would be infinite at $\omega = \omega_o$ and zero everywhere else. The progressive dominance of $F(\omega_o)$ with increasing length of the sine wave train implies that in a mildly dispersive medium such signals should have a speed of propagation which is a close approximation to the phase velocity corresponding to ω_o. Most importantly, the dispersion of the vessel can be determined without having to perform extensive Fourier transform computations. Likewise, the attenuation characteristics of the vena cava can be obtained directly by measuring the amplitude ratio A/A_o for wave trains of various frequencies.

Experimental Procedure

The animals used in the experiments were mongrel male dogs of uncertain age and weighed between 15 and 40 kg. They were anesthetized intravenously with 30 mg/kg sodium pentobarbital (Nembutal). The dogs were kept in supine position throughout the experiment. As an indicator of the general physiologic state of the animals their arterial blood pressure was continuously recorded from a Statham manometer P23Dd connected to a cannula which was inserted into the left carotid artery or a femoral artery. In addition, their respiration was usually monitored by a mercury-filled silastic tube stretched across the chest. The variations in gauge resistance with breathing were recorded to allow for the

study of the effects of respiration on the wave transmission characteristics of the abdominal vena cava. Besides this, the venous pressure at the bifurcation was continuously measured with a Statham P23BB transducer and a saline manometer with the cannula inserted through a femoral vein. The outputs from the Statham gauges were amplified with Honeywell Accudata Amplifiers Model M-104 and recorded on the Visicorder.

The general experimental arrangement is schematically illustrated in Figure 39. To detect small pressure fluctuations two Bytrex catheter-tip manometers were inserted into the right external jugular vein and positioned in the abdominal vena cava with the aid of an X-ray fluoroscope. The catheter-tip manometers, the Statham gauges, amplifiers and recording equipment were calibrated as a system for each experiment. Depending on recording speed and amplitude of the signals we could evaluate Δt with an error of 0.3 to 1.0 milliseconds.

When the artificial pressure or distension waves were generated by the spring-loaded syringe or by the sinusoidal pump, the cannula from either device was inserted through a femoral vein and placed near the bifurcation. When the electrically driven vibrator was used, the brass sleeve which encloses the piston and has an outside diameter of 6.2 mm was disconnected from the vibrator, filled with heparnized saline and inserted through a femoral vein into the common iliac. The vibrator piston was then guided into the brass sleeve. This procedure was adopted to overcome the difficulties in manipulating the vibrator, which weighs 10 kg, and to facilitate the positioning of the relatively large brass

cylinder.

The distance between the tip of the cannula or the tip of the vibrating piston and the nearest catheter-tip manometer was usually 3 to 7 cm, while the distance separating the two manometers ranged in general from 2 to 7 cm. These distances were determined radiographically with an accuracy of .1 cm by using an image intensifier and a radio-opaque grid with a mesh size of 1 cm and taking into account the effects of parallax.

Theoretically the wave transmission properties of arteries and veins can be affected by changes in the transmural pressure and in the geometry of the vessels[8,9,37]. For accurate estimates of the elastic properties of blood vessels from their wave propagation characteristics it is therefore desirable to know the geometry of the vessel and the prevailing transmural pressure. To determine the dispersion and attenuation of waves in the abdominal vena cava in the presence of a well-defined transmural pressure, the abdomen of the dog was opened by a midline incision from the lower end of the sternum to the pubis and the vena cava was exposed to atmospheric pressure by displacing the viscera. This surgical process also enabled us to observe the vena cava during the experiment and to measure with calipers its external diameter and wall thickness. Variations in the level of the transmural pressure were achieved with the aid of a tilt-table or by occluding the vena cava above the hepatic branches with a balloon catheter.

Results

Waves Generated by Spring-Loaded Syringe

To assess the feasibility of utilizing wave transmission phenomena in large veins for the purpose of determining their mechanical properties under various conditions we induced relatively large pressure pulses in the vena cava of 20 anesthetized dogs with the spring-loaded syringe shown in Figure 32. The speed of the pressure signals normally ranged from 300 to 700 cm/sec and was found to depend strongly on the amplitude, the instantaneous transmural pressure and the general physiologic state of the animals. The amplitude itself depended on the volume of saline injected, the injection time, the orientation of the syringe cannula, the venous pressure and, of course, the local distensibility of the vessel. A typical example of the variation of the pulse speed with amplitude is illustrated in Figure 40 which shows that the signal induced by injecting 0.5 cm^3 saline has an amplitude of 60 mm Hg and travels at a velocity of 500 cm/sec while the signal produced by 1 cm^3 saline has an amplitude of 225 mm Hg and a speed of 774 cm/sec.

The marked increase in wave speed with signal amplitude indicates that the vena cava exhibits nonlinear behavior with respect to large pressure signals. As a rule, pressure signals travel at a greater speed when they are superimposed on a higher transmural pressure and this behavior has been consistently observed in experiments in which the venous pressure was increased by as much as 200 mm H_2O by tilting the animal. Because of the apparent strong dependence of the wave transmission characteristics on transmural pressure in the vena cava, a detailed study of the relationship between these two quantities was conducted.

These experiments and their results are described in Chapter IV.

By varying the location of the transducers we observed that the amplitude generally decreased with increasing distance from the cannula except in the neighborhood of the renal branches. The speed also varies as indicated in Figure 41 which depicts typical tracings of pressure waves induced by the spring-loaded syringe and recorded at four different relative locations (I-IV). In each case the maximum amplitude of the pulse at the proximal transducer is about the same while, as expected, the amplitude at the distal site progressively decreases with distance traveled as a result of dissipative mechanisms. Differences in the wave speed v indicate variations in the distensibility of the vena cava which are attributed either to geometrical changes or to variations in the elastic properties of the vessel wall caused, for example, by branch structure. Variations in the wave shape at the proximal transducer may be due to slight alterations in the orientation of the cannula at the point of injection. Near the renal branches we also noted changes in the wave shape which are presumably due to reflections.

In the presence of a mean flow the velocity of pulse waves propagating in the direction of the flow is predicted to be approximately equal to the wave speed at zero mean flow plus the average stream velocity,[14] which generally is expected to be rather small in the vena cava compared with the propagation velocity of pressure pulses[18,29]. We observed that the speeds of pressure signals generated during inspiration were consistently greater than those induced during expiration or at the resting phase of the respiratory cycle. In

some cases the difference exceeded 200 cm/sec as indicated in Table I. By measuring continuously the total and static (end and lateral) venous pressure we found that the blood flow velocity increased during inspiration by approximately the difference in the pulse wave speeds. Since we are primarily interested in studying the mechanical properties of the vena cava in terms of its wave transmission characteristics at known or negligible blood flow rates we have avoided these respiration-induced flow effects on the wave speed by consistently selecting data obtained during the resting phase of the respiratory cycle.

Significant increases in wave speed were also produced by vagal stimulation, fibrillation of the heart and by injection into the vena cava of massive or lethal doses of various drugs such as epinephrine, nembutal, KCl, NaCl, $MgCl_2$, $CaCl_2$ and KCN. In some cases the speed increased by more than 400%. These findings are currently under detailed investigation, with particular emphasis on venous motor control mechanisms including the effects of changes in venous pressure.

With a reduction in the injection volume it is possible to generate sufficiently small pressure pulses by the spring-loaded syringe to minimize the observed nonlinear behavior with amplitude. But to obtain the dispersion and attenuation we would still have to determine the Fourier spectra of the signals.

Waves Generated by Pump

Initial results on the dispersive nature of the vena cava were obtained by measuring the speeds of pressure signals of the form of long trains of sine waves induced by a pump. The frequency and amplitude of the sine waves were

systematically varied. For peak-to-peak amplitudes less than 3 mm Hg no evidence of reflection interference could be observed between the bifurcation and the renal branches. This was concluded from the fact that the signals retained their sinusoidal character during propagation independent of frequency. In the exposed vena cava the speeds of such sine waves with frequencies between 4 and 40 Hz ranged from about 60 to 400 cm/sec depending on pressure and the general physiological state of the animals. Representative dispersion curves are illustrated in Figure 42. In each case shown the speed varied by no more than $\pm$ 15% with frequency, which confirms that the exposed vena cava is not strongly dispersive. Each data point represents an average of 9 to 12 speed measurements in a series of wave trains induced during the resting phase of the respiratory cycle. The peak-to-peak amplitude of the waves at the proximal transducer was 2 to 4 mm Hg.

For sinusoidal wave trains of sufficiently small amplitude the velocity was not dependent on the selection of the characteristic point and could be determined with greater certainty than in the case of single pressure pulses such as those generated by the spring-loaded syringe. Also, the signals clearly retained their sinusoidal form during propagation and no "forerunners"[38] were observed. These facts lend further support to the conclusion that the vena cava is not strongly dispersive and that effects of reflections are not noticeable. Consequently, when the amplitude of a sinusoidal pressure wave induced by the pump is small, the speed of such a signal can be interpreted as the phase velocity corresponding to the frequency of the sine waves.

An example of the manner in which the wave shape can be affected by the amplitude is shown in Figure 43. The four pairs of tracings illustrated represent the pressure fluctuations induced by the pump for different stroke volumes at two fixed stations in the abdominal vena cava. The distance between the transducers was 4.0 cm and the frequency was 7.5 Hz. As the stroke volume of the pump is successively increased the peak-to-peak amplitude at the proximal site rises in this case from 3.5 to 9.8 mm Hg and the pressure waves become increasingly non-sinusoidal. One can readily discern a relative steepening of the wave front with respect to the phase of diminishing pressure as the amplitude of the wave increases.

This amplitude phenomenon may be attributed to a pressure dependence of the wave speed. Whenever the speed increases markedly with pressure the peaks of the sinusoidal pressure waves travel faster than the valleys. This is further illustrated in Figure 44 in which the velocities of the peaks and valleys of near sinusoidal waves produced by the pump are given as a function of signal amplitude. For peak-to-peak amplitudes larger than about 5 mm Hg the speed of the wave peaks is noticeably greater than that of the valleys and the difference increases progressively with amplitude. Each data point corresponds to 9 to 12 measurements of the transmission time.

The vessel apparently behaves in a nonlinear fashion with respect to large pressure pulses which precludes the possibility of performing a harmonic analysis of such signals for the purpose of determining dispersion and attenuation.

The extent to which reflections can alter the apparent wave speed of an

induced pressure signal is illustrated in Figure 45 which shows five pairs of recordings that were obtained from identical transducer locations. Two possible manifestations of reflections can be discerned from the tracings. At 6.8 Hz the first peak and valley appear to arrive at the distal transducer site with a definite time lag. However, the second peak seems to reach both transducers simultaneously. As the frequency is increased the relationship between the wave patterns beyond the first peak changes dramatically. For example, the second peak completely disappears at the proximal transducer for 9.7 Hz.

Waves Generated by Vibrating Piston

By generating finite trains of sine waves with the aid of the electrically driven piston it was possible to obtain extensive dispersion and attenuation data for waves in the exposed vena cava. Representative tracings of trains of different frequencies generated in this manner are shown in Figure 46. Each of the tracings has a different zero point since they were separated for illustration purposes. Note that the signals are attenuated during propagation but retain their sinusoidal character for all frequencies.

Typical dispersion curves are given in Figures 47 and 48 for small pressure waves generated during the resting phase of the respiratory cycle. The amplitude of the signals was less than 20 mm H_2O and each data point represents an average of 9 to 12 speed measurements from recordings taken over a period of less than 5 seconds.

The speed of the induced sine waves ranged from 100 to 400 cm/sec for these experiments and exhibited only mild dispersion which was usually more

pronounced for frequencies below 50 Hz. For frequencies between 20 and 100 Hz the wave speed generally increased with increasing frequency. The significant differences in speed from animal to animal observed in our experiments may be attributed to differences in vessel geometry and to the physiological state of the animals which includes such factors as transmural pressure, depth of anesthesia and surgical trauma. An additional cause for these variations may be the location of the transducers relative to the bifurcation or renal branches. Figure 49 illustrates the dependence of wave speed and dispersion on transducer location in the vena cava of a single animal. In this experiment the distance between transducers was constant while their position relative to the bifurcation was systematically changed. Of particular interest are the marked variations in wave speed and dispersion with distance from the bifurcation. This behavior was investigated in 3 dogs and appears to be the result of significant variations in the local wave transmission characteristics of the vessel.

Most of the pressure waves generated with the vibrating piston had peak-to-peak amplitudes less than 20 mm H_2O and there was no significant or systematic variation in the speed of different wave peaks or valleys within the same wave train. It appears that for distension waves with amplitudes less than 20 mm H_2O and frequencies between 20 and 100 Hz the wave speed is independent of amplitude. For such small waves the vena cava behaves essentially in a linear fashion. For frequencies above 100 Hz the stoke of the vibrating piston used was too small to generate sufficiently strong pressure waves in the vena cava to allow for accurate measurements while below 20 Hz

the shape of the signals deviated too much from that of true sine waves.

Data regarding the attenuation characteristics of the vena cava with respect to sinusoidal pressure waves were obtained by comparing again the peak-to-peak pressures for various frequencies at the two transducer sites. Attenuation curves corresponding to the dispersion data given in Figures 47 and 48 are illustrated in Figures 50 and 51. As in the case of the thoracic aorta[11] the amplitude ratio A/A_o for pressure waves in the vena cava with frequencies between 20 and 100 Hz decays exponentially with distance traveled. Also, high frequency waves are dissipated much more rapidly over a given distance than low frequency waves. Knowing the wave speed and frequency we can plot A/A_o as a function of the distance traveled in wavelengths and we find again that the amplitude ratio decays in the same exponential fashion for all frequencies:

$$A/A_o = e^{-k\frac{\Delta x}{\lambda}} \qquad (3.1)$$

where k is the attenuation coefficient or logarithmic decrement. Data from 6 experiments indicate that k may vary from about 1 to 2.5 for the vena cava as compared with a range from 0.7 to 1.0 for the aorta.

Discussion and Conclusions

The propagation of large amplitude pressure waves induced by the spring-loaded syringe or by the pump appears to be affected by reflection interference and pronounced nonlinear phenomena. For waves with amplitudes exceeding a few mm Hg the speed increases markedly with signal amplitude and the wave front steepens during propagation. We also find an increase of the signal speed

by raising the level of the unperturbed transmural pressure. Therefore the observed amplitude dependence of the speed and the steepening of the wave front can be interpreted as nonlinear phenomena attributable to the fact that the wave speed increases with pressure. Accordingly the steepening of the wave front may correspond to the early phases of the formation of a shock wave. This implies that a sufficiently strong pressure pulse may generate a shock wave in the vena cava which would manifest itself in the form of a sharp and audible sound. Clinical evidence supporting the possibility of the actual development of shock waves is established by the occurrence of the venous pistol shot[39].

The wave transmission data obtained with signals induced by the spring-loaded syringe yielded valuable information regarding the gross behavior of the vena cava including the effects of pressure, respiration, various drugs, vagal stimulation and ventricular fibrillation. But these data did not allow for the actual determination of the dispersion and attenuation of pressure waves becuase of the strong nonlinearities that were observed.

With the vibrating piston we could induce only pressure waves of small amplitude. The maximum volumetric displacement of the piston was about 200 mm^3 for frequencies below 70 Hz and decreased rapidly with increasing frequency above 80 Hz. For displacements of about 150 mm^3 the peak-to-peak pressure amplitudes were generally of the order of 20 mm H_2O at normal transmural pressure levels and at a distance of 4 cm from the piston. The frequencies and shape of the waves generated in this fashion could be controlled with a high degree of accuracy and repeatability. Only distension waves were

observed; no attempts were made to record axial or torsion waves. Non-axisymmetric waves[8,9] if present did not exhibit sufficiently strong pressure fluctuations at the transducer sites to be recognizable. This was verified by placing the two transducers at various points of the same cross section (by twisting the catheter leads) and comparing the corresponding pressure variations. The fact that both transducers recorded the same signal with zero phase shift independent of transducer position suggests that the pressure waves were axisymmetric.

From our experimental results it follows that the abdominal vena cava of anesthetized dogs does not exhibit much dispersion of distension waves with frequencies between 20 and 100 Hz. Although the dispersion may be considered as mild, it appears to vary markedly with location as indicated in Figure 49. The absence of strong dispersion of small axisymmetric distension waves is clearly in agreement with theoretical predictions[8,10]. However, the observed changes in the dispersive nature with location have not been anticipated. This may be due to the fact that the local variations in geometry and in the elastic and viscoelastic properties of the vessel wall and the surroundings are usually disregarded in theoretical analyses. It should be noted that when the wave speeds are measured over longer distances (Figure 48) the fluctuations in <u>local</u> dispersion characteristics may no longer be evident since the speed of the pressure waves between any two points of the vessel is an average measure of the mechanical properties.

As in the aorta[11] small pressure waves in the vena cava appear to decay

exponentially with distance traveled in wavelengths independent of frequency. This dissipation of signal energy may be attributed primarily to viscoelastic damping in the vessel wall since theoretical considerations[10] indicate that the effects of blood viscosity are insignificant for the range of frequencies and type of waves investigated. Furthermore, radiation of energy into the surrounding medium cannot be a major contributing factor since the vessel was exposed during the experiments.

Differences in attenuation are also observed in various segments of the vena cava of each animal studied, but this aspect has not yet been systematically investigated. Before any definitive statement can be made regarding the accuracy of a mathematical model postulating the relationship between the dispersion, attenuation and mechanical properties of the vessel, we need additional information on the wave transmission characteristics of the vena cava. For example, the dispersion and attenuation of axial and torsion waves would allow for the evaluation of the degree of anisotropy in the elastic and viscoelastic behavior of the vessel wall.

Although the wave velocity itself can serve as a measure of the distensibility of a blood vessel, it is commonly used to estimate the effective Young's modulus of the vessel wall from the Moens-Korteweg equation:

$$c^2 = \frac{Eh}{2\rho_f a} \tag{3.2}$$

where c is the signal velocity, ρ_f the density of the blood, h/a the thickness-to-radius ratio and E the effective Young's modulus. Recent theoretical

studies[10,27,40] indicate that the Moens-Korteweg equation constitutes a meaningful approximation for the speed of low frequency pressure waves for parameter values associated with large veins such as the vena cava. Applying this formula we have computed the effective Young's modulus of the exposed abdominal vena cava from data obtained with the vibrating piston. For transmural pressures between 75 and 100 mm H_2O, signal frequencies from 20 to 100 Hz and $\frac{a}{h}$ values between 30 and 45, the effective Young's modulus ranges from about 5×10^5 to 5×10^6 dynes/cm^2. These values for E_{eff} for the vena cava wall are of the same order as those found for the aorta[8]. The distensibility of the veins however is much higher because of their large values for the radius to wall thickness ratio.

An even greater range of values for the elastic modulus would be obtained from the speeds of large pressure waves induced by the spring-loaded syringe or the pump. However, the actual significance of these data is questionable in the light of the observed nonlinear behavior and apparent reflection phenomena. In fact, even the effective Young's modulus derived from the speed of small amplitude pressure waves is relevant only when referred to the conditions under which the wave speeds were measured, which includes the respiratory phase and the transmural pressure. The relatively large variations in the effective Young's modulus from animal to animal at comparable transmural pressures is probably due to differences in the physiologic state of the animals.

IV. THE EFFECT OF VARIATIONS IN TRANSMURAL PRESSURE ON THE TRANSMISSION CHARACTERISTICS OF PRESSURE WAVES IN THE ABDOMINAL VENA CAVA

Introduction

Initial results of experiments in which the venous pressure was artifically varied indicated that the wave transmission characteristics of the vena cava were strongly affected by changes in transmural pressure. In addition, increases in wave speed produced, for example, by vagal stimulation or the injection of various drugs into the circulatory system could possibly be in part the result of a change in transmural pressure induced by the stimuli. Even under normal conditions, relatively large fluctuations in the hydrostatic pressure in veins caused by postural variations can have serious effects on the cardiovascular system as evidenced by the fainting of patients who are suddenly brought to an upright position after an extended period of bed rest.

Because of the important role of arterial and venous blood pressure in maintaining proper circulation, it is of particular interest to elucidate some of the aspects of vascular motor control and to determine the extent to which active and passive compensatory responses are invoked by changes in transmural pressure. As a single step toward this goal and in conjunction with our venous wave transmission studies we have investigated the effects of variations in transmural pressure on the propagation of waves in the vena cava.

Experimental Methods

Various techniques were used to change the venous pressure in order to determine its effect on the wave transmission characteristics of the vena cava.

Initially, it was felt that the infusion of a small amount of blood or normal saline from an elevated reservoir into a femoral vein would produce a substantial pressure increase in the vena cava. A few attempts with this procedure, however, revealed that the circulatory system was able to accommodate a moderate infusion of fluid over a period of minutes and exhibit only a slight rise in venous pressure. By progressively increasing the diameter of the infusion cannula and the height of the reservoir above the femoral vein the venous pressure could be raised 300 to 400 mm H_2O in less than three minutes by infusing 2 liters of fluid. With the exception of venous pressure, the physiological and chemical changes caused by the massive addition of fluid to the circulatory system could not be assessed and thereby rendered this technique of little practical use for our purposes.

With the aid of a tilt table we were able to change the hydrostatic pressure in the vena cava rapidly and repeatedly thus eliminating two of the major drawbacks associated with infusion. The table has a tilt capability of from -15^{o} to $+90^{o}$ with respect to the horizontal, and for the average anesthetized dog we could vary the transmural pressure at the venous bifurcation from about 0 to 300 or 400 mm H_2O in less than 10 seconds. The supine dog was restrained on the table with a harness which supported him at the axillae. To prevent the pressure transducers from accidentally moving relative to one another in the vena cava during the tilt maneuver, their catheters were tied together and the two manometers were inserted as a single unit. Again, however, we were faced with the problem of determining the extent to which additional physiological changes

induced by tilting affect the wave transmission characteristics. For example, corresponding variations in the hydrostatic pressure in vessels other than the vena cava and their influence on the baroreceptors can be expected to alter the cardiac rate and output as well as the peripheral resistance and blood pressure.

The method for varying venous pressure which eventually proved to be the most satisfactory for our purposes was occlusion of the vena cava. The pressure was increased by occluding the vessel below the heart with a balloon catheter inserted through the right external jugular vein and positioned in the inferior vena cava between the heart and the hepatic branches. By inflating the balloon for a period of usually less than 15 seconds the venous pressure would rise from its normal value of 50 to 100 mm H_2O to as much as 200 or 300 mm H_2O. As evidenced from the relatively stable heart rate and blood pressure during short periods of caval occlusion this technique appeared to involve a minimum of interference with normal cardiovascular functions. Furthermore, it was possible to occlude the vessel repeatedly without observing any deleterious effects on the animal as manifested in the control (or pre-occlusion) values of arterial and venous pressures and the heart and respiration rates.

Results

Tilt

More than 15 experiments were conducted in which a tilt table was used to vary the venous pressure. The artificial pressure waves were induced with either the spring-loaded syringe or pump and could not be considered small

since the signal amplitude usually exceeded several mm Hg. In general we found that pressure signals travel at a greater speed when superimposed on a higher transmural pressure. Figure 52 shows a typical example of the effects of tilting on the arterial and venous pressures and the speed of large pressure pulses in the abdominal vena cava. Arterial pressure was measured in the carotid artery and venous pressure in the abdominal vena cava at the bifurcation. Pressure signals were produced by the injection of 0.5 cm^3 of warm saline into a femoral vein. Tilting the animal immediately produced an elevation in the venous pressure and a substantial increase in the speed of large amplitude pressure signals. While the animal was kept at 60^o tilt for a period of 8 minutes the mean arterial pressure and the pulse pressure continuously decreased while the wave speed and venous pressure exhibited no major changes. Data obtained 4 minutes after returning the animal to its original position do not deviate substantially from the pre-tilt values. In addition we found that the amplitude of the pressure waves increased markedly as the transmural pressure was raised. However, because of the length of time required to adjust the stroke or injection volume of the wave generator, it was not practical to maintain control over the amplitude of the induced signals. In some cases during extended periods of tilt at a constant angle a gradual decrease in wave speed was observed even though the transmural pressure remained constant. Figure 53 provides an illustration of this behavior for the time period 18 to 35 minutes in which the wave speed decreases about 25 percent. In this example, the waves were generated by the pump and the peak-to-peak amplitudes varied

from about 2 mm Hg at 0^{o} tilt to about 10 mm Hg at 60^{o} tilt. This figure also illustrates the typical effect on the wave speed of one form of cardiac failure which was induced by prolonged tilting and manifested by an absence of arterial pulse pressure. Observe the dramatic increases in signal velocity immediately upon death followed by a gradual decrease to approximately the pre-death value over a period of about eight minutes. Of particular interest is the fact that no significant variations in venous pressure are associated with these changes in wave speed.

On some occasions, increases in transmural pressure above a certain value would cause the wave speed to decrease as depicted graphically in Figure 54. Here we have plotted as a function of tilt angle the systolic and diastolic arterial pressures, transmural venous pressure, heart rate and wave speed. Each point represents an average of 5 to 10 measurements and the dog was held at each position for 6 to 10 minutes and then raised to the next higher angle. As the animal is tilted from -15^{o} to 40^{o} the transmural pressure and wave speed both increase as expected while the arterial pressures drop slightly. When the tilt angle is increased to 60^{o} and 80^{o}, increases in transmural pressure are accompanied by marked decreases in wave speed and arterial pressures, which may serve as an indication of some form of cardiovascular collapse.

Occlusion

Occlusion experiments provided extensive data regarding the relationship between venous pressure and the transmission characteristics of small amplitude sine waves of various frequencies. The vibrating piston was used to generate

the signals and their amplitudes were controlled such that they never exceeded 2 mm Hg peak-to-peak for all values of transmural pressure. Typically, the phase velocity increased with increasing transmural pressure and a linear relationship between these two quantities was apparent for the range of frequencies and pressures considered. Results of a representative occlusion experiment are depicted in the graph in Figure 55 where we have plotted wave speed as a function of venous pressure for signals with a frequency of 35 Hz. In this example the speed increased from about 240 to 400 cm/sec as the pressure was raised from 60 to 155 mm H_2O. Assuming a linear dependence of the wave speed on transmural pressure, the slope of this curve based on the method of least squares is 1.6 cm/sec/mm H_2O. Figure 56 illustrates similar results for signals with frequencies of 30, 40 and 50 Hz. Although the complete data were collected over a period of about 8 minutes, the data corresponding to a single frequency were obtained in less than 20 seconds during a single occlusion of the vena cava. A linear regression line was calculated for the combined data and was found to have a slope of 2.1 cm/sec/mm H_2O. Further results of these pressure studies are summarized in Table II. Notice that the linear regression coefficients calculated from the data ranged from about 1.5 to 2.5 cm/sec/mm H_2O for all cases.

Discussion

The results of our experiments consistently show that variations in venous pressure strongly affect the tranmission characteristics of large and small pressure waves in the vena cava. The usual marked increase in the speed and

amplitude of induced waves with rising transmural pressure appears to be the result of substantial changes in the elastic and viscoelastic properties of the vessel wall. This behavior may also be interpreted as a decrease in the distensibility of the vessel which is defined mathematically by dV/dp, the ratio of the volume increment dV associated with the pressure perturbation dp. In light of the previously discussed nonlinear behavior of the vena cava with respect to the propagation of large amplitude pressure waves, the results of the tilt table experiments serve only as gross indicators of the effect of pressure on wave velocity since the amplitude of the signals was allowed to vary with transmural pressure. We were able to establish, however, that the artifically induced changes in distensibility depend to a great degree upon the severity and duration of the applied stimulus and, most importantly, appear to be mediated in part by some —— as yet unknown —— active mechanism. This active ability of the vessel to change its stiffness with changes in transmural pressure apparently can be expended and lead to some form of cardiovascular failure as illustrated in Figures 53 and 54. Additional support for this hypothesis was provided from experiments in which a dog was repeatedly tilted to 60^{o}, held in that position for about 30 seconds and then returned to the horizontal. A constantly decreasing tolerance to this type of stress was evident from the progressive decrease in wave speed at 60^{o} as well as at the horizontal position during successive cycles. To gain a better understanding of this phenomenon, the effects of humoral and neural stimuli on the wave transmission characteristics of the abdominal vena cava are currently being investigated.

When the venous pressure was increased by occluding the vessel, data for a single study could be collected in a period of a few seconds and before any compensatory response of the circulatory system, if present, was reflected in the arterial pressure and heart rate. In addition the amplitude of the waves was kept sufficiently small at all values of transmural pressure so that nonlinear effects were not noticeable. It should be noted that the observed increase in wave speed with pressure, normally about 2 cm/sec/mm H_2O, does not agree with the theoretical analysis of Anliker and Maxwell[8] which predicts increases of no more than a few percent of those we have obtained experimentally. This discrepancy can be explained in terms of marked changes in the effective Young's modulus of the vessel wall which are not accounted for in the theory.

The distensibility of a blood vessel is defined by its geometry as well as by the mechanical properties of its wall. Any evaluation of distensibility from the wave transmission characteristics of the vessel therefore requires that we determine all changes in vessel diameter associated with variations in wave speed. Attempts were made in our experiments to measure continuously the diameter of the vena cava as a function of transmural venous pressure. In one approach we monitored the electrical resistance of a mercury filled silastic tube which encircled the vena cava and could stretch and contract with the circumference of the vessel. We found however, that the force required to increase the length of the gauge was generally greater than that needed to constrict this highly distensible vessel. In other experiments we used a catheter-tip device developed by H. Pieper[41,42] for measuring the internal diameter of

blood vessels and the heart. The transducer consists of a linear differential transformer contained in a tube of small diameter. Attached to the tube are three hinged braces or feet which are spring-loaded and expand within a vessel until they touch the wall. The braces are linked to a ferromagnetic sleeve which slides along the tube as the braces open and close and causes a change in the output of the differential transformer. We found however, that the vessel tended to distort into a triangular shaped cross section due to the expansion of the braces, and efforts to eliminate this difficulty by using weaker springs resulted in the desired decrease in vessel distortion, but also in an inability of the transducer to accurately track all but the quasistatic motions of the vessel wall. In addition, the vena cava was subjected to varying degrees of contact with the Pieper gauge and this stimulus could be expected to alter in some way the wave transmission characteristics of the vessel.

Visually we were able to observe a definite increase in the vessel diameter with increasing venous pressure. This change in diameter was measured with calipers but never exceeded more than about 10 percent even when the transmural pressure was increased by four of five times its normal value.

Without additional information regarding the nature and function of active control mechanisms in the circulatory system, in particular their time constants, it is not possible to attribute the observed changes in wave speed directly to variations only in transmural pressure. It is clear from these results that the role of transmural pressure in determining the transmission characteristics of a blood vessel over both long and short periods of time must be considered in a

proper interpretation of wave propagation data.

The wave transmission approach presented here will be useful in the continued study of the distensibility of parts of the vascular capacitance system and its regulation. The suggested use of transcutaneous ultrasound sensors should prove valuable in the determination of the relative significance of different components of the reservoir system and in the evaluation of the range of variation in the distensibility of blood vessels in different individuals under normal and pathologic conditions as well as in states of stress.

REFERENCES

1. McDonald, D. A., Blood Flow in Arteries, Edward Arnold Ltd., London, 1960.

2. Fung, Y. C., Biomechanics, its Scope, History and Some Problems of Continuum Mechanics in Physiology, Journal of Applied Fluid Mechanics Reviews, 21:1-20, 1968.

3. Rudinger, G., Review of Current Mathematical Methods in the Analysis of Blood Flow, in Biomedical Fluid Mechanics Symposium, ASME, New York, 1966.

4. Skalak, R., Wave Propagation in Blood Flow, in Biomechanics, ASME, New York, 1966.

5. McDonald, D. A., Hemodynamics, in Annual Review of Physiology, 30:525-556, 1968.

6. Attinger, E. O., Pulsatile Blood Flow, New York, 1964.

7. Burton, A. C., Physiology and Biophysics of the Circulation, Year Book Medical Publishers, Chicago, 1965.

8. Anliker, M., Maxwell, J. A., The Dispersion of Waves in Blood Vessels, in Biomechanics Symposium, ASME, New York, 1966.

9. Maxwell, J. A., Anliker, M., The Dissipation and Dispersion of Small Waves in Arteries and Veins with Viscoelastic Properties, Biophysical Journal, 8:920-950, 1968.

10. Jones, E., Chang, I-Dee, Anliker, M., Effects of Viscosity and External Constraints on Wave Transmission in Blood Vessels, SUDAAR Report No. 344, Department of Aeronautics and Astronautics, Stanford University, Stanford, California, 1968.

11. Anliker, M., Histand, M. B., Ogden, E., Dispersion and Attenuation of Small Artificial Pressure Waves in the Aorta, Circulation Research, 23:539-551, 1968.

12. Anliker, M., Moritz, W., Ogden E., Transmission Characteristics of Axial Waves in Blood Vessels, Journal of Biomechanics, 1(4):235-246, 1968.

13. Anliker, M., Wells, M. K., Ogden, E., The Transmission Characteristics of Large and Small Pressure Waves in the Abdominal Vena Cava, SUDAAR Report No. 362, Department of Aeronautics and Astronautics, Stanford University, Stanford, California, 1968. Accepted for publication in IEEE Transactions on Bio-Medical Engineering.

14. Morgan, G. W., Ferrante, W. R., Wave Propagation in Elastic Tubes Filled with Streaming Liquid, Journal of the Acoustical Society of America, 27:715-725, 1955.

15. Klip, W., Velocity and Damping of the Pulse Wave, The Hague, Martenus Nijhoff, 1962.

16. Womersley, J. R., Elastic Tube Theory of Pulse Transmission and Oscillatory Flow in Mammalian Arteries, WADC Tech. Rept. TR 56-614, Defense Documentation Center, 1957.

17. Atabek, H. B., Lew, H. S., Wave Propagation Through a Viscous Incompressible Fluid Contained in an Initially Stressed Elastic Tube, Biophysical Journal, 6:481-503, 1966.

18. Brecher, G. A., Venous Return, Grune and Stratton, New York, 1956.

19. Flügge, W., Stresses in Shells, Springer-Verlag, Berlin, 1962.

20. Bergel, D. H., The Static Elastic Properties of the Arterial Wall, Journal of Physiology, 156:445-457, 1961.

21. Bergel, D. H., The Dynamic Elastic Properties of the Arterial Wall, Journal of Physiology, 156:458-469, 1961.

22. Burton, A. C., Relation of Structure to Function of the Tissues of the Wall of Blood Vessels, Physiological Reviews, 34:619-642, 1954.

23. Peterson, L. H., Jensen, R. E., Parnell, J., Mechanical Properties of Arteries In Vivo, Circulation Research, 8:622-639, 1960.

24. Biot, M. A., Mechanics of Incremental Deformations, John Wiley and Sons, New York, 1965.

25. Patel, D. J., Greenfield, J. C., Fry, D. L., in Pulsatile Blood Flow, New York, 1964.

26. Mirsky, I., Wave Propagation in a Viscous Fluid Contained in an Orthotropic Elastic Tube, Biophysical Journal, 7:165-186, 1967.

27. Atabek, H. B., Wave Propagation Through a Viscous Fluid Contained in a Tethered, Initially Stressed, Orthotropic Elastic Tube, Biophysical Journal, 8:626-649, 1968.

28. Burch, G. E., Murtadha, M., A Study of the Venomotor Tone in a Short Intact Venous Segment of the Forearm of Man, American Heart Journal, 51:807-828, 1956.

29. Caeiro, A., Velocidad de Propagacion de las Distintas Ondas del Pulso Venoso, Revista Argentina de Cardiologia, 8:329-339, 1941-42.

30. Peterson, L. H., Participation of the Veins in Active Regulation of Circulation, Federation Proceedings, 10:104, 1951.

31. Peterson, L. H., The Dynamics of Pulsatile Blood Flow, Circulation Research, 2:127-139, 1954.

32. Landowne, M., Wave Propagation in Intact Human Arteries, Federation Proceedings, 13:83, 1954.

33. Landowne, M., A Method Using Induced Waves to Study Pressure Propagation in Human Arteries, Circulation Research, 5:594-601, 1957.

34. Landowne, M., Characteristics of Impact and Pulse Wave Propagation in Brachial and Radial Arteries, Journal of Applied Physiology, 12(1):91-97, 1958.

35. MacKay, I. F. S., Van Loon, P., Campos, J. T., de Jesus, N., A Technique for the Indirect Measurement of the Velocity of Induced Venous Pulsations, American Heart Journal, 73:17-23, 1967.

36. Gow, B. S., Taylor, M. G., Measurement of Viscoelastic Properties of Arteries in the Living Dog, Circulation Research, 23:111-122, 1968.

37. Kresch, E. N., Design of a Nonlinear Electrical Model for Veins, Ph. D. Dissertation in Biomedical Engineering, University of Pennsylvania, 1968.

38. Brillouin, L., Wave Propagation and Group Velocity, Academic Press, New York, 1960.

39. Hultgren, H. N., Venous Pistol Shot Sounds, American Journal of Cardiology, 10:667-672, 1962.

40. Klip, W., Van Loon, P., Klip, D., Formulas for Phase Velocity and Damping of Longitudinal Waves in Thick-Walled Viscoelastic Tubes, Journal of Applied Physics, 38:3745-3755, 1967.

41. Pieper, H., Catheter-tip Instrument for Measuring Left Ventricular Diameter in Closed-chest Dogs, Journal of Applied Physiology, 21(4):1412-1416, 1966.

42. Pieper, H., Paul, L. T., Catheter-tip Gauge for Measuring Blood Flow Velocity and Vessel Diameter in Dogs, Journal of Applied Physiology, 24(2):259-261, 1968.

TABLE I

EFFECT OF RESPIRATION ON THE SPEED OF PRESSURE PULSES IN THE ABDOMINAL VENA CAVA INDUCED BY THE INJECTION OF 0.5 CM^3 SALINE WITH A SPRING-LOADED SYRINGE

Experiment	P_v mmH_2O	Δx cm	n	Velocity, cm/sec Inhale	Resting	$V_{in} - V_r$ cm/sec
36	150	4.4	6	593	490	103
37	75	9.4	4	582	459	123
47	120	5.8	6	591	383	208
63	140	3.6	7	626	547	79
67	90	4.9	10	437	385	52
68	90	4.5	13	495	349	146
73	60	4.4	4	776	739	37
93	50	5.1	3	637	564	73
123	-	6.0	5	575	480	95
132	120	6.0	2	533	425	108

P_v transmural pressure

Δx distance between transducers

n number of wave speed measurements during inhalation and corresponding resting phase

V_{in} wave speed at inhalation

V_r wave speed during resting phase

TABLE II

EFFECTS OF TRANSMURAL PRESSURE* ON THE SPEED OF SMALL AMPLITUDE SINE WAVES IN THE ABDOMINAL VENA CAVA

Experiment	Δx cm	Freq. Hz	P_v*, mmH_2O Initial	P_v*, mmH_2O Max.	Velocity, cm/sec Initial	Velocity, cm/sec Max.	$\frac{\Delta V}{\Delta P_v}$ $\frac{cm/sec}{mmH_2O}$
294	4.0	30	60	200	230	500	1.59
	4.0	30	60	235	213	597	1.75
	4.0	50	65	235	265	635	2.13
	4.0	40	60	235	234	615	1.85
	3.0	50	70	240	256	612	1.97
	3.0	50	60	210	236	638	2.34
298	4.0	35	60	155	239	406	1.62
319	3.0	40	45	195	200	643	2.43
	3.0	55	97	215	273	486	1.69

* The transmural pressure was increased by occluding the vena cava for 15 to 30 seconds with a balloon catheter positioned near the diaphragm.

ΔP_v change in transmural pressure

ΔV change in wave speed associated with pressure variation ΔP_v

$\frac{\Delta V}{\Delta P_v}$ linear regression coefficient

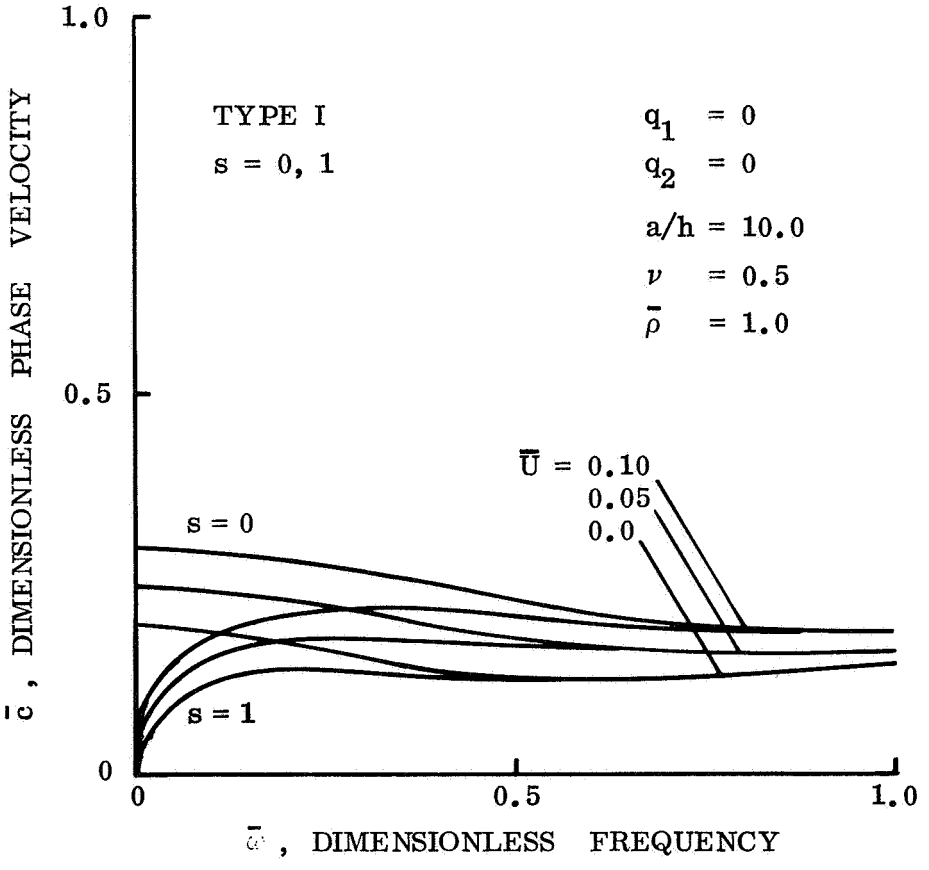

Figure 1. Dispersion curves for type I waves with s = 0 and 1 for different values of mean flow velocity.

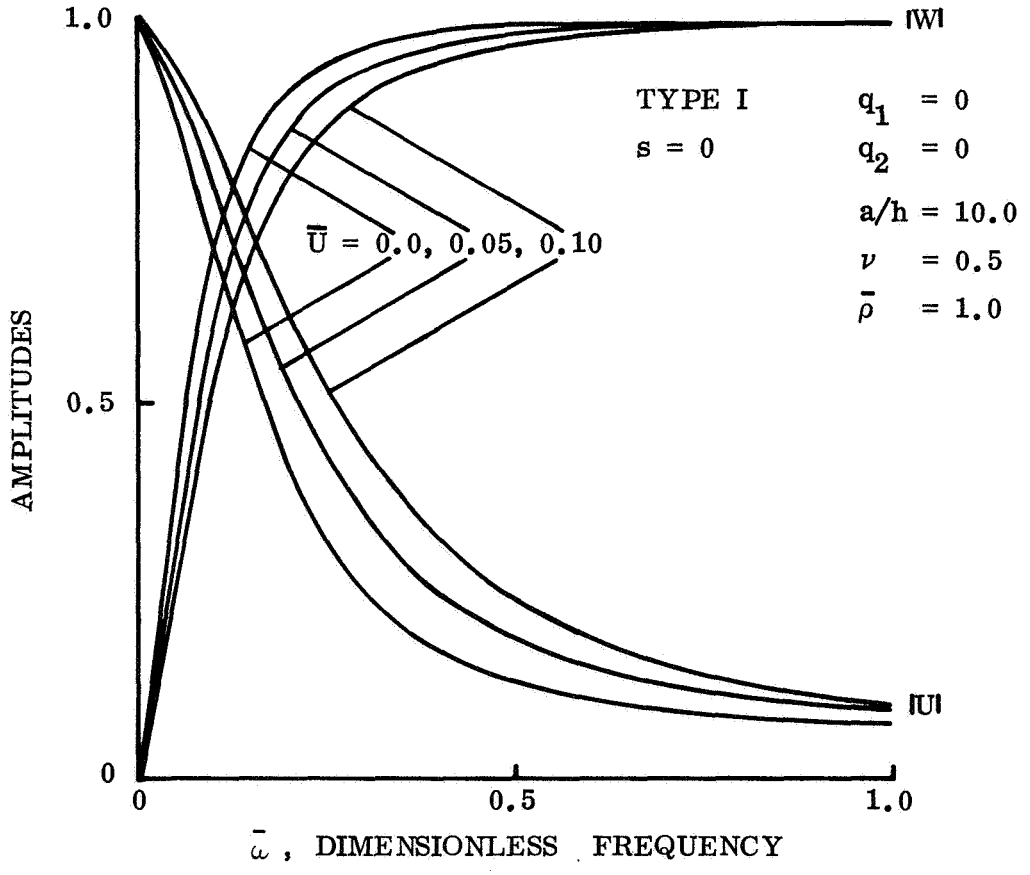

Figure 2. Mode shapes of type I waves with s = 0 for different values of mean flow velocity.

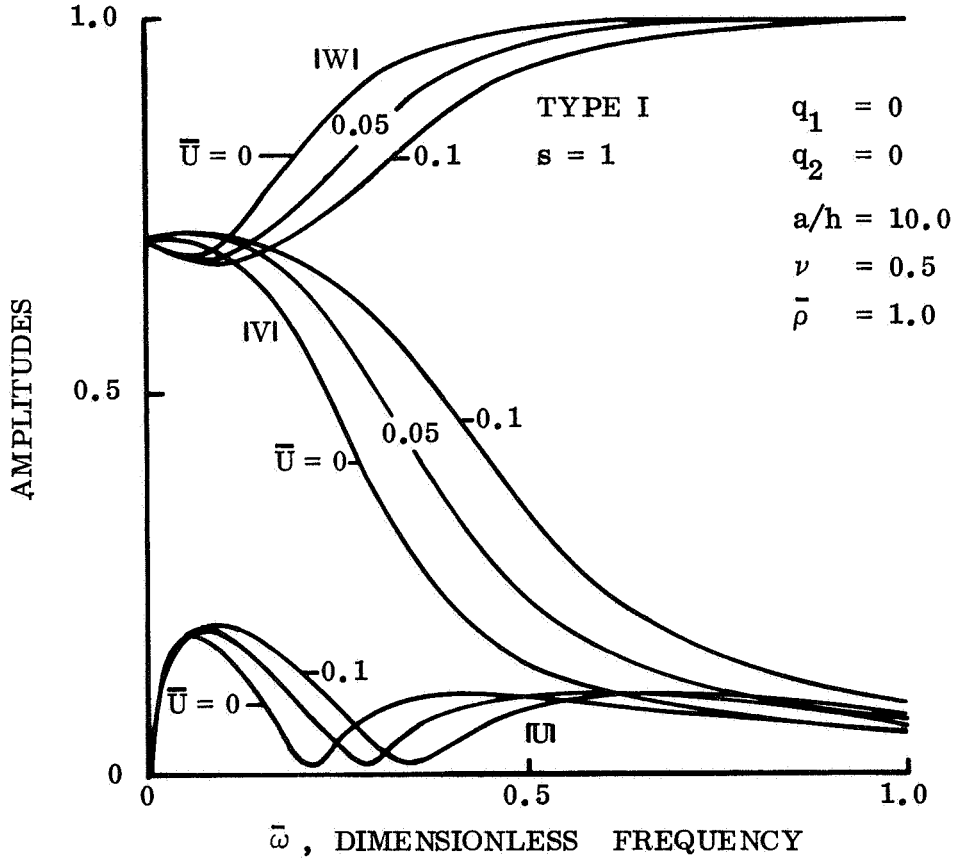

Figure 3. Mode shapes of type I waves with s = 1 for different values of mean flow velocity.

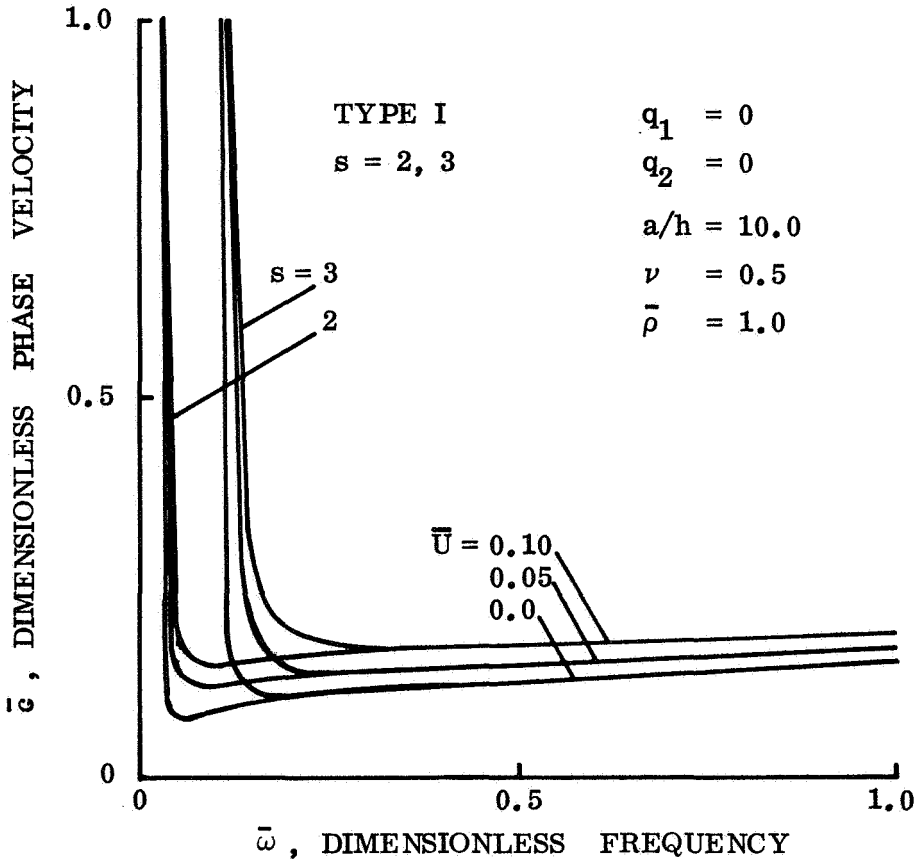

Figure 4. Effect of mean flow on the dispersion of type I waves with s = 2 and 3.

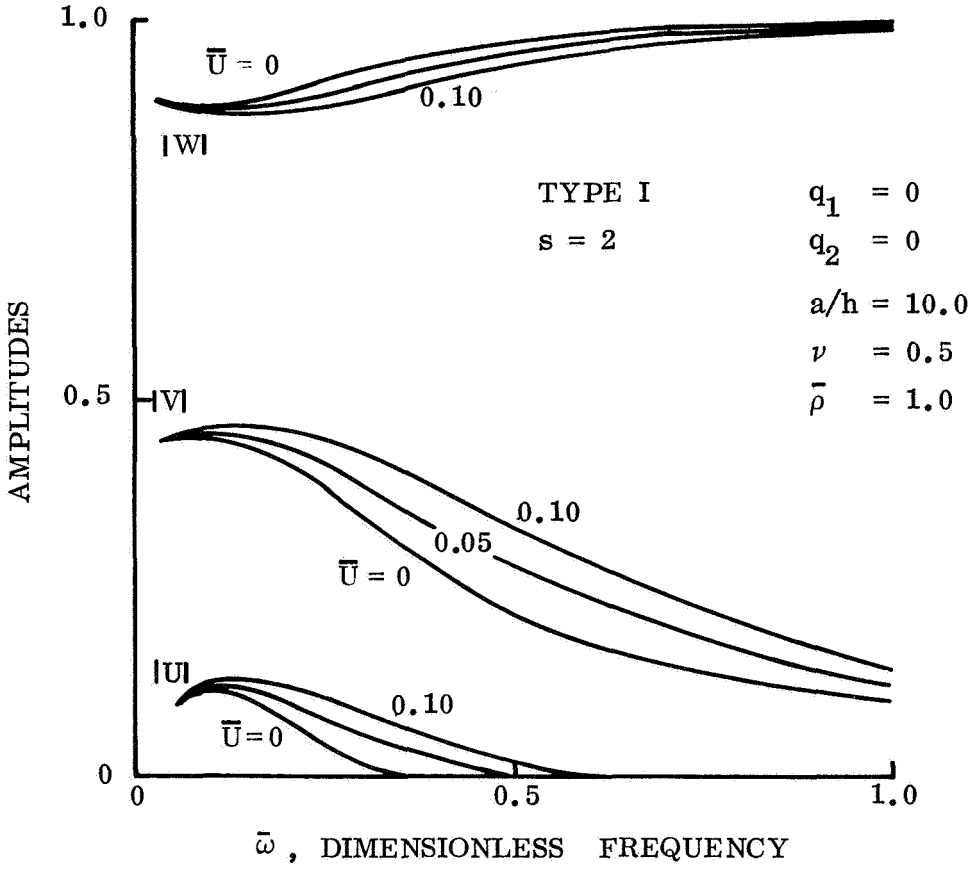

Figure 5. Effect of mean flow on the mode shapes of type I waves with s = 2.

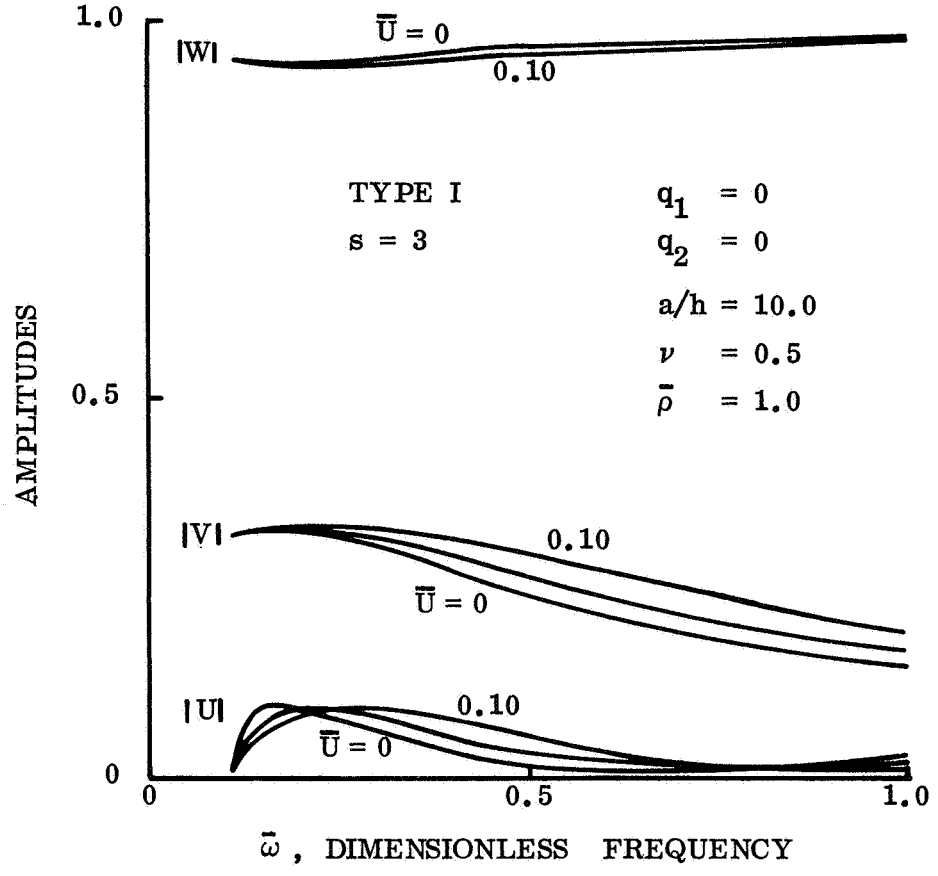

Figure 6. Effect of mean flow on the mode shapes of type I waves with s = 3.

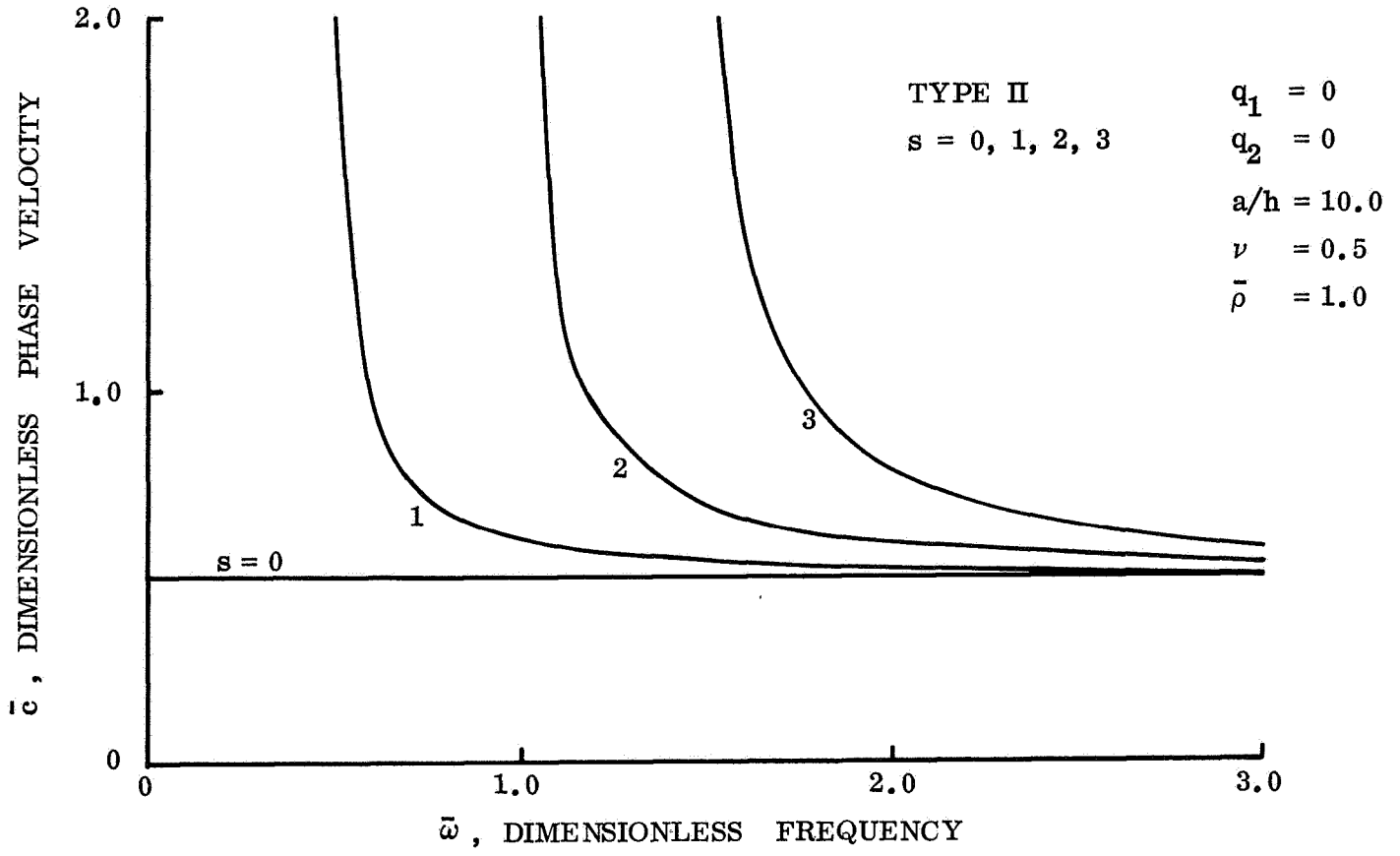

Figure 7. Changes in dispersion of type II waves due to mean flow velocities of $\bar{U} = 0.05$ and 0.10 within drawing accuracy.

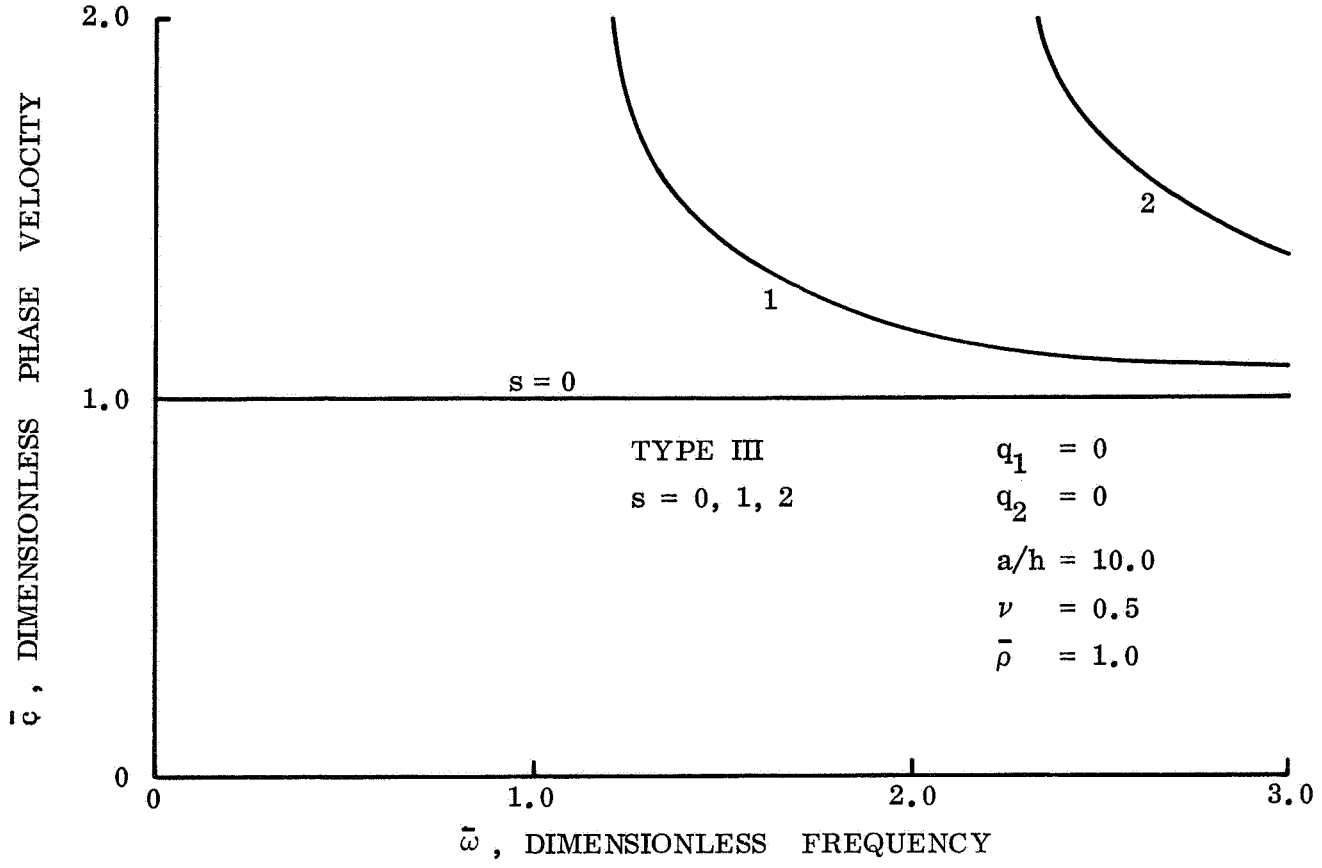

Figure 8. Changes in dispersion of type III waves due to mean flow velocities of $\bar{U} = 0.05$ and 0.10 within drawing accuracy.

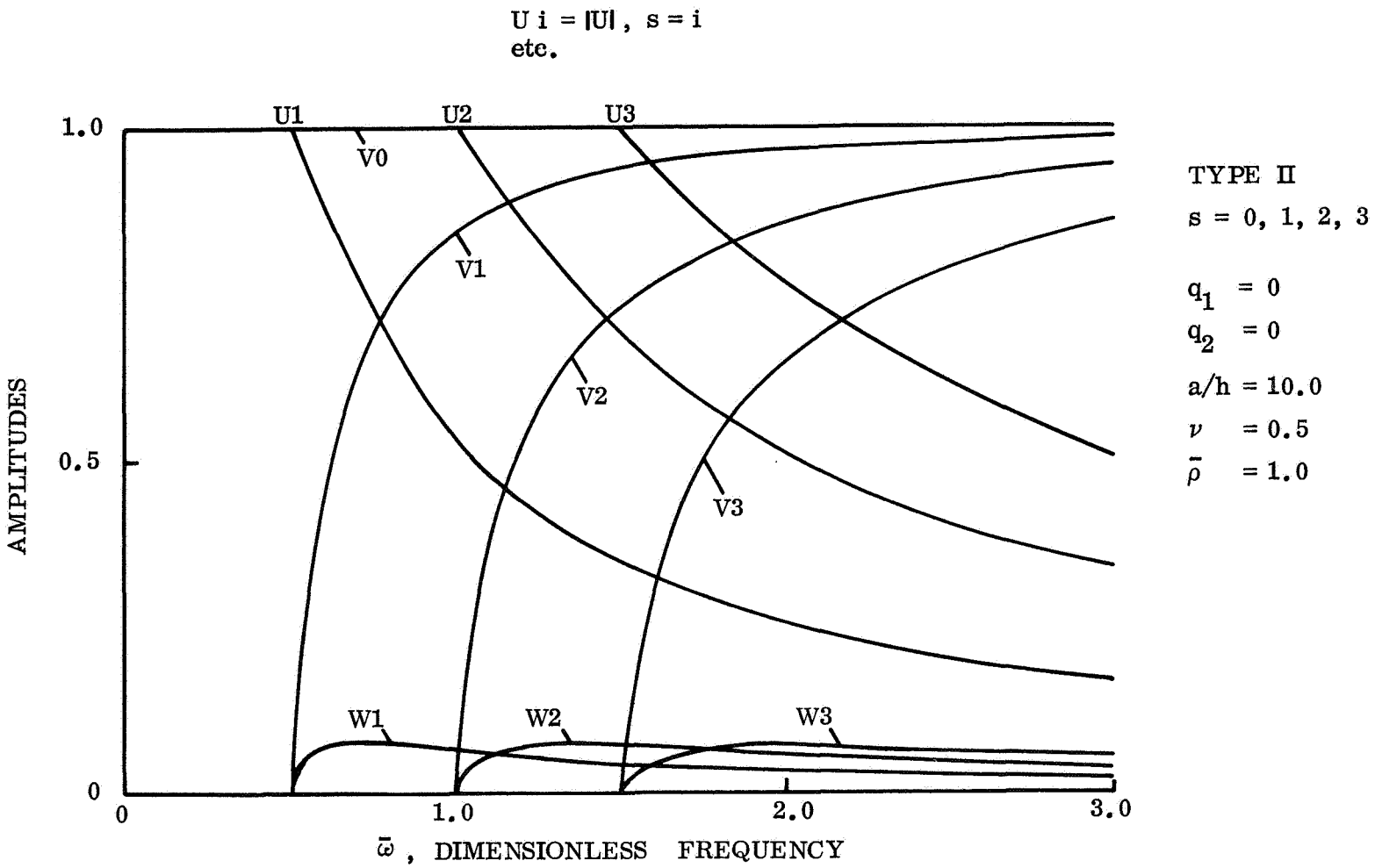

Figure 9. Mode shapes of type II waves for $\bar{U} = 0.0,\ 0.05$ and 0.10.

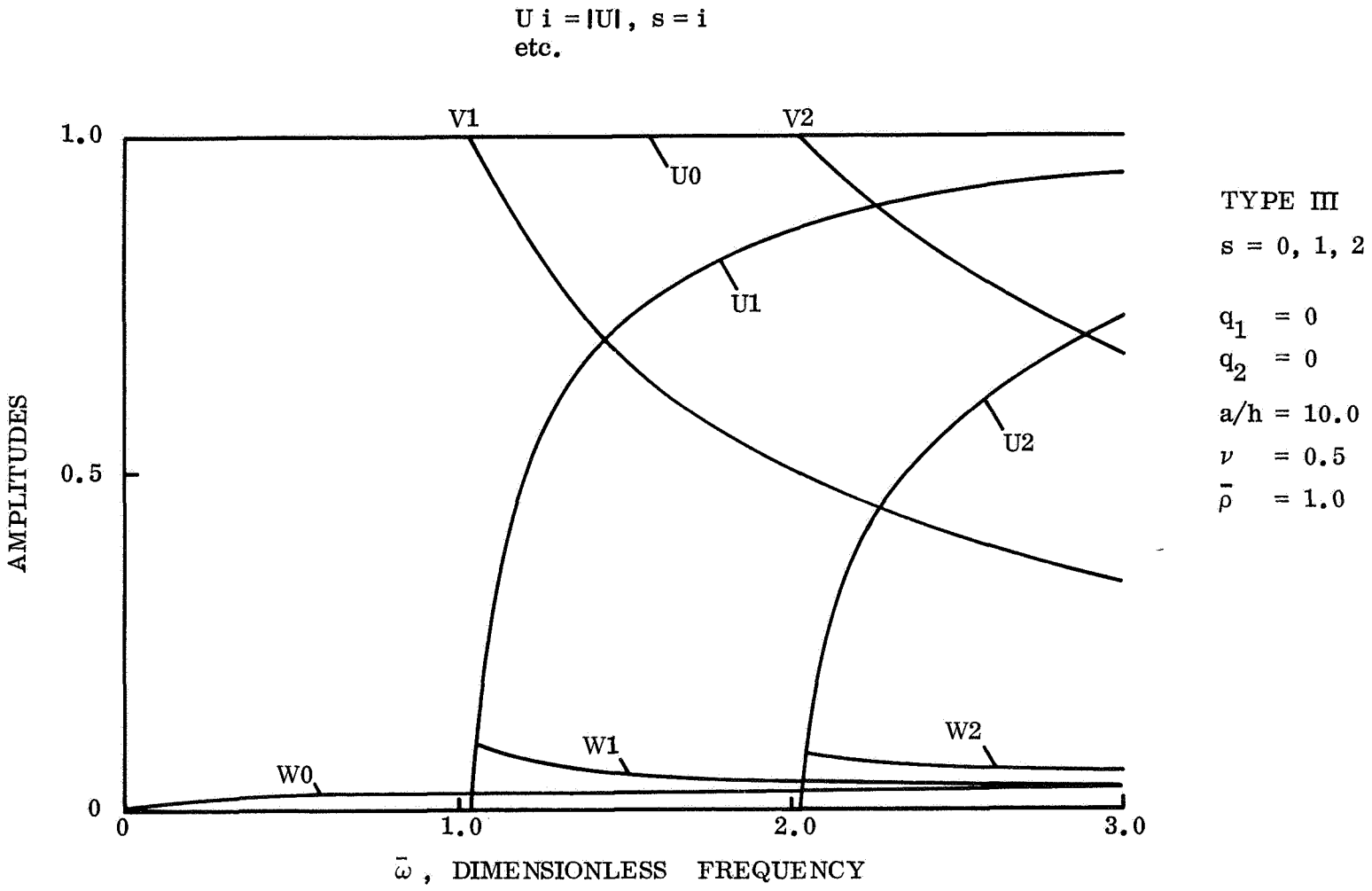

Figure 10. Mode shapes of type III waves for $\bar{U} = 0.0,\ 0.05$ and 0.10.

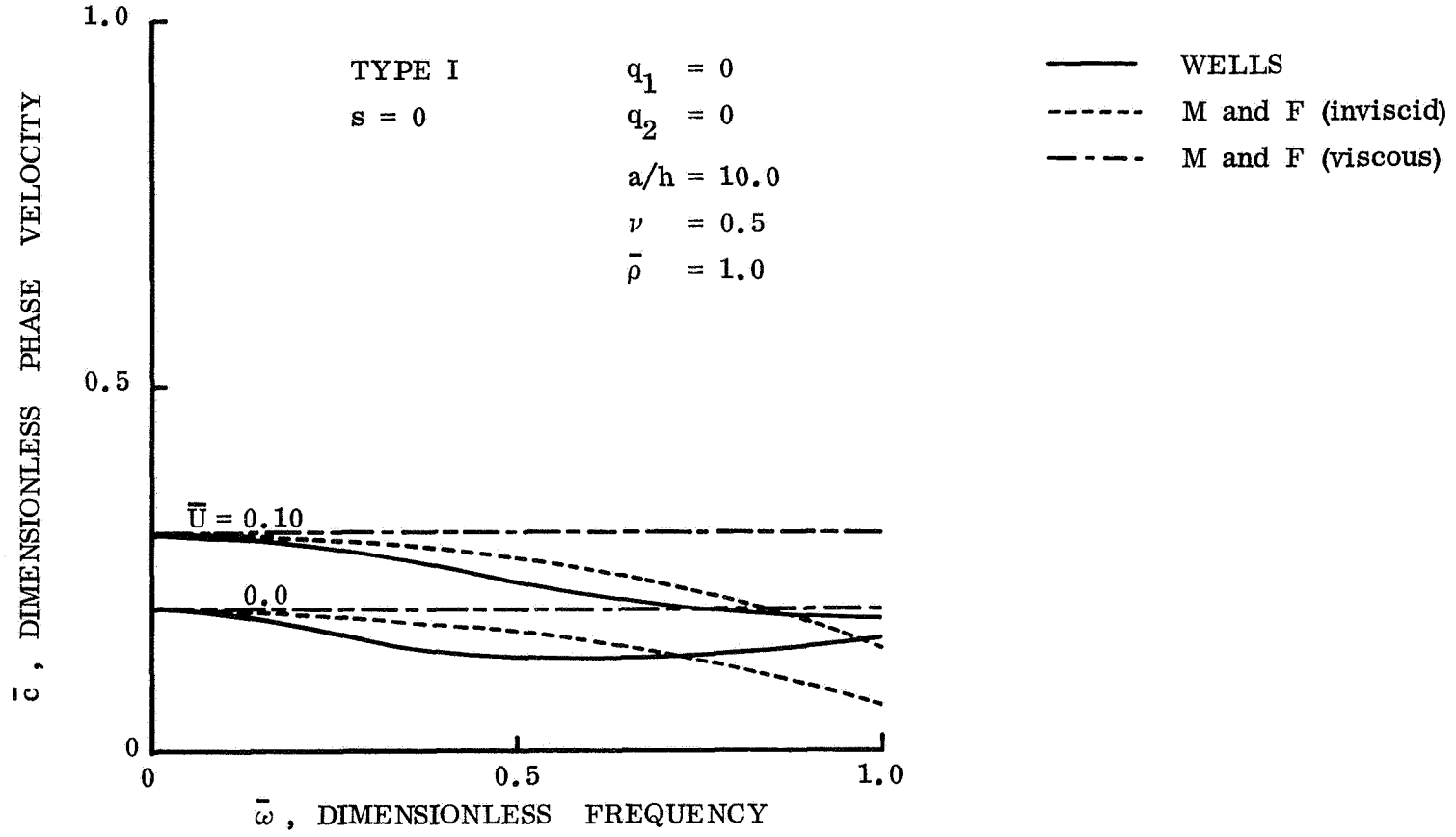

Figure 11. Comparison of theoretical results with those of Morgan and Ferrante.

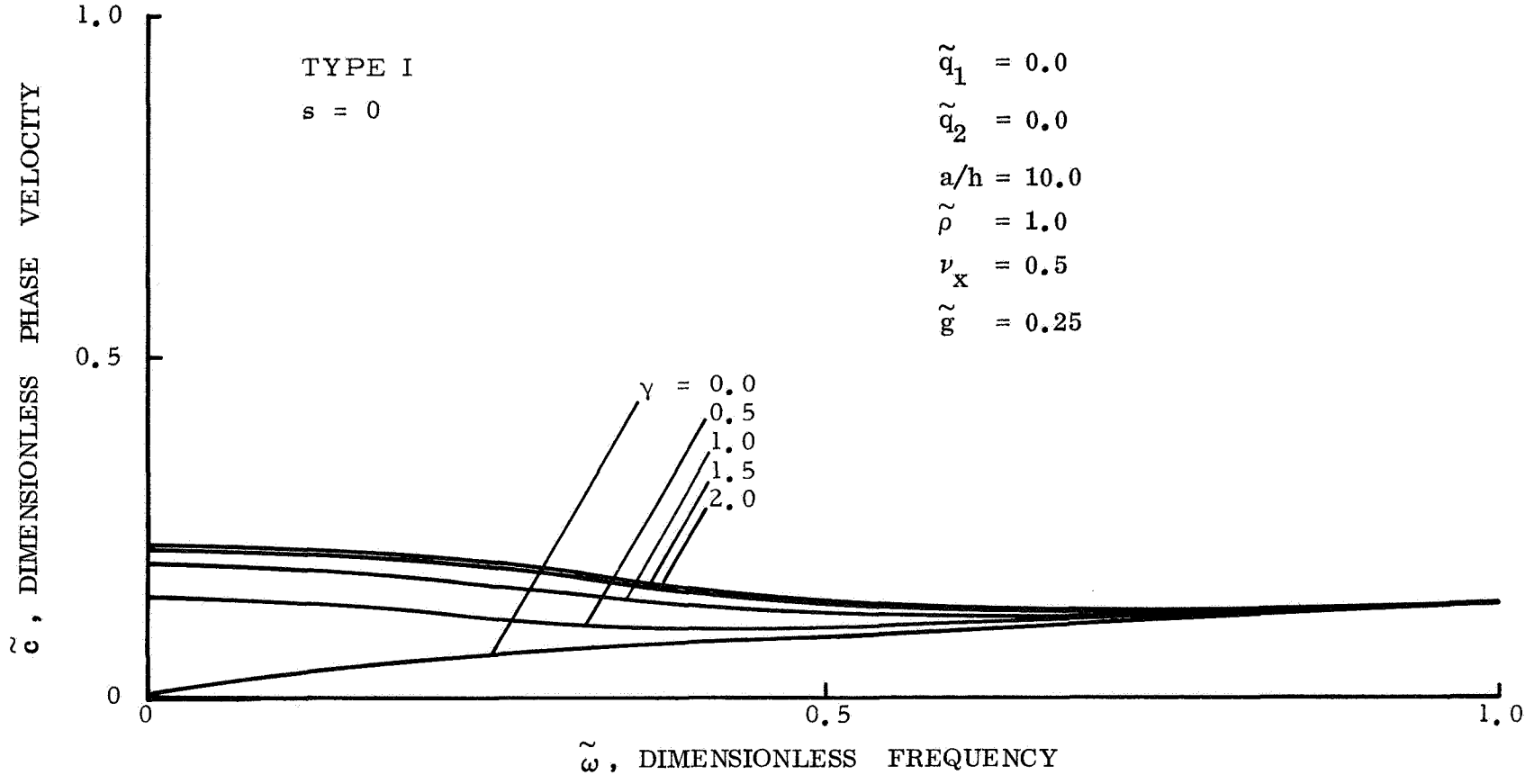

Figure 12. Effect of γ on dispersion of type I waves with s = 0 and $\nu_x = 0.5$.

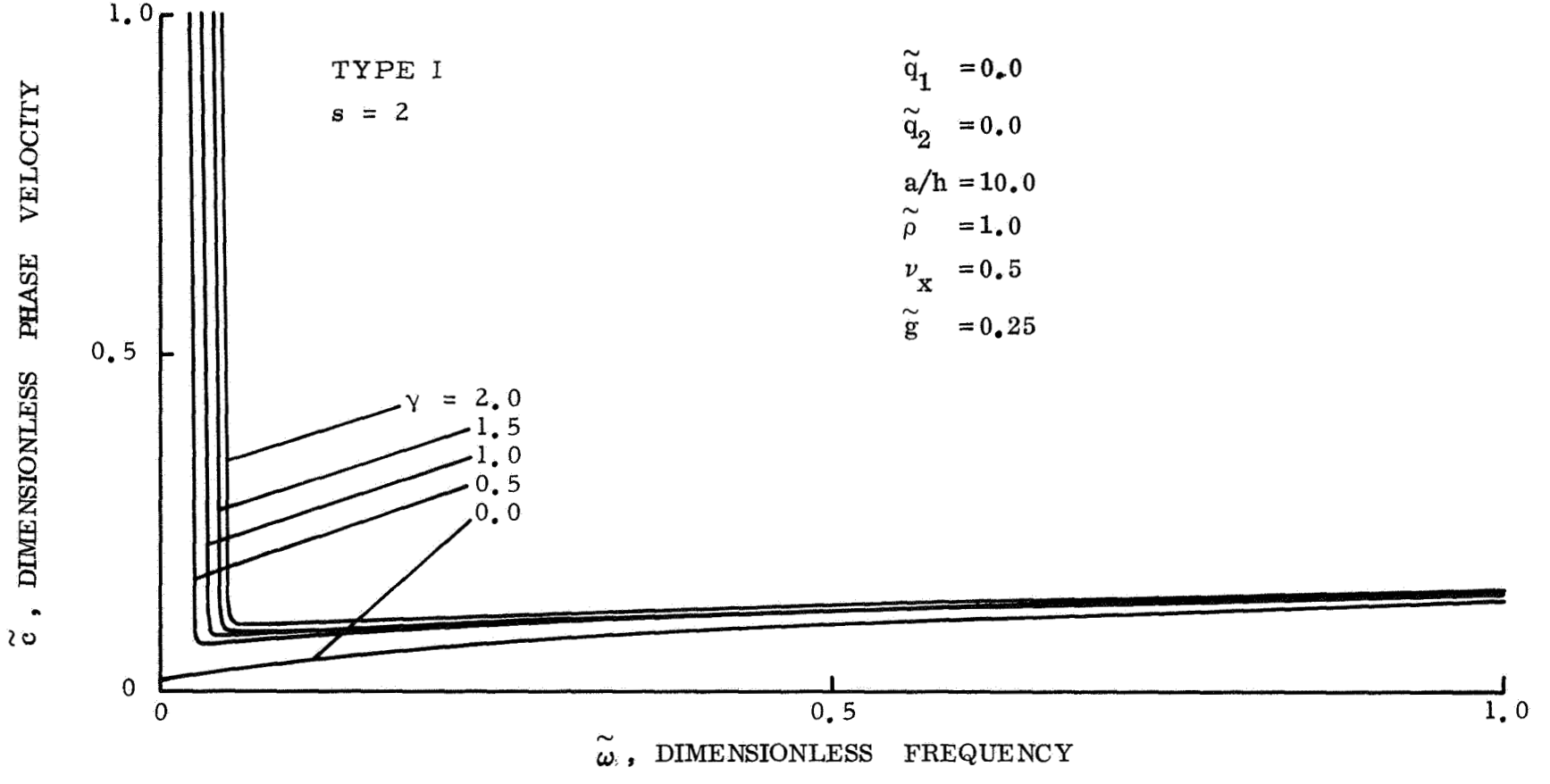

Figure 13. Effect of γ on dispersion of type I waves with s = 2.

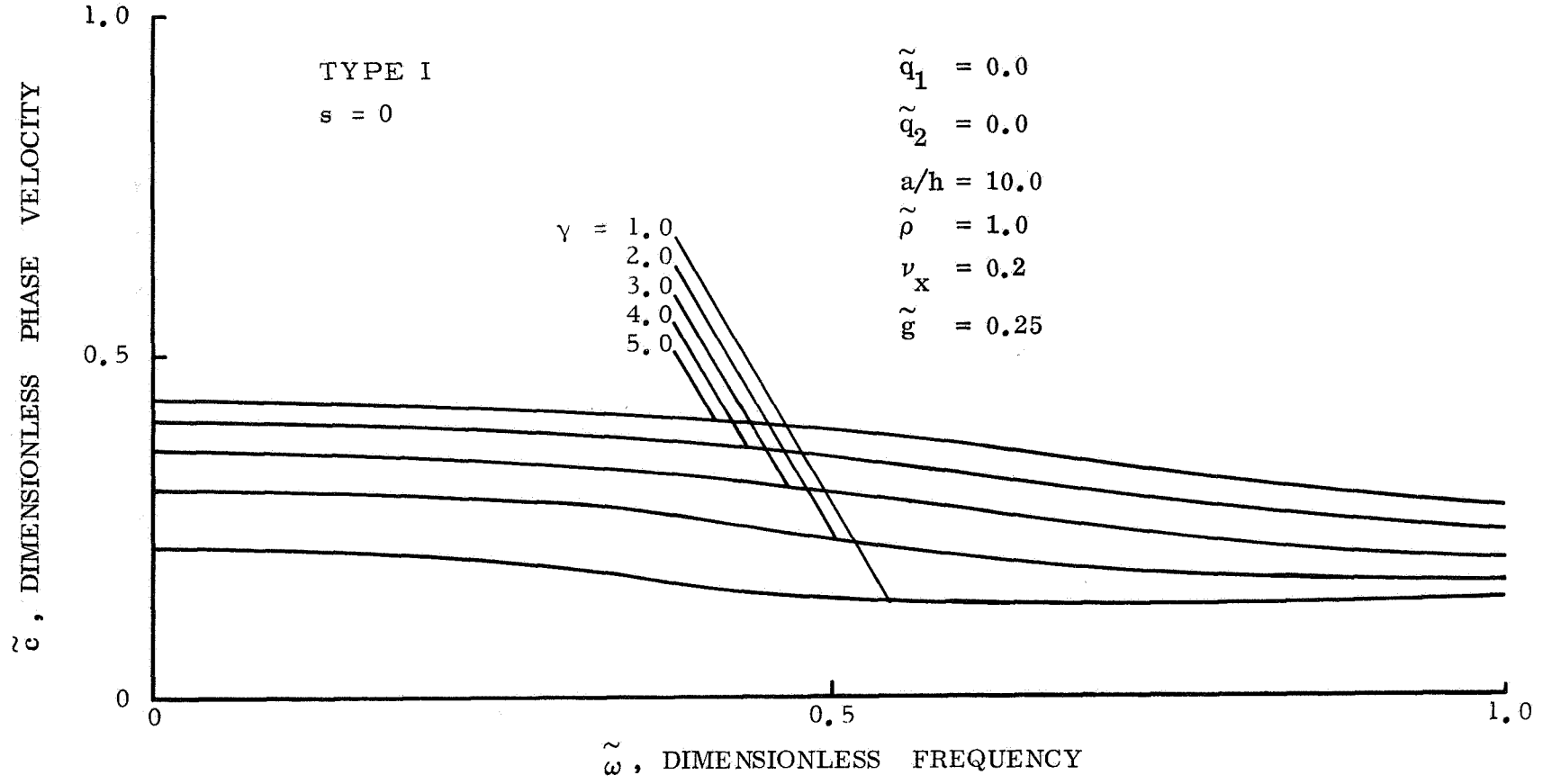

Figure 14. Effect of γ on dispersion of type I waves with $s = 0$ and $\nu_x = 0.2$.

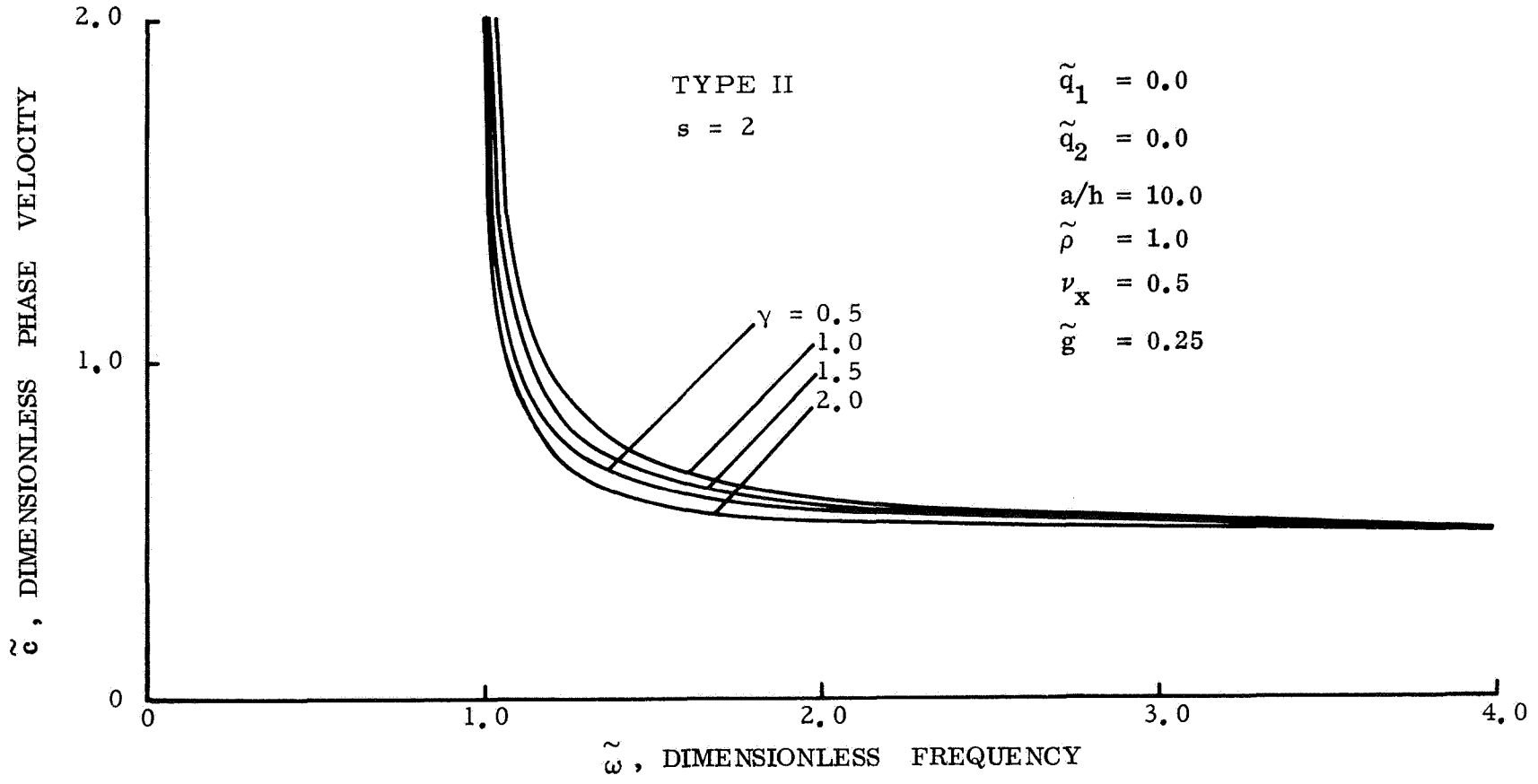

Figure 15. Effect of γ on dispersion of type II waves with s = 2.

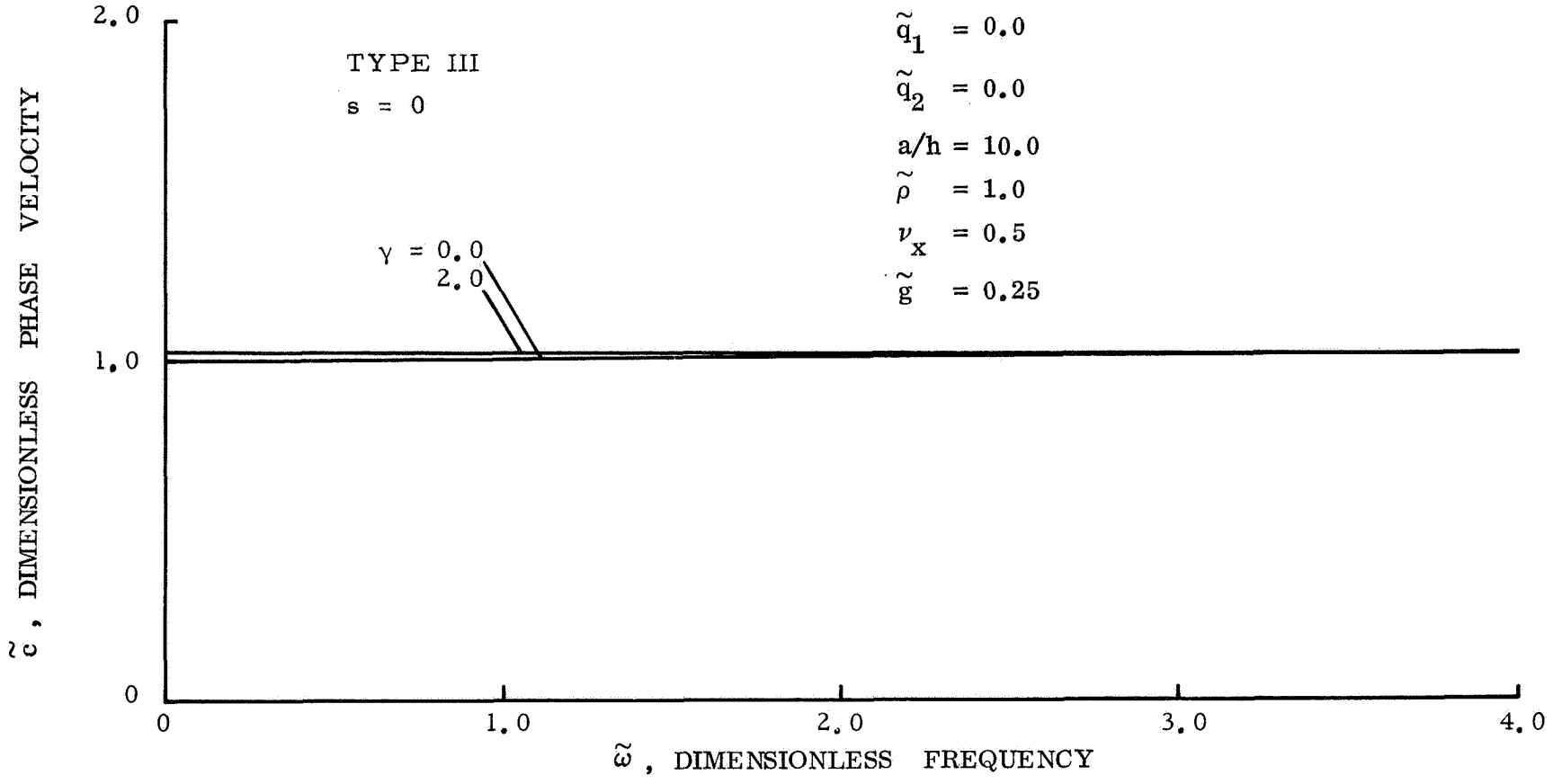

Figure 16. Effect of γ on dispersion of type III waves with s = 0.

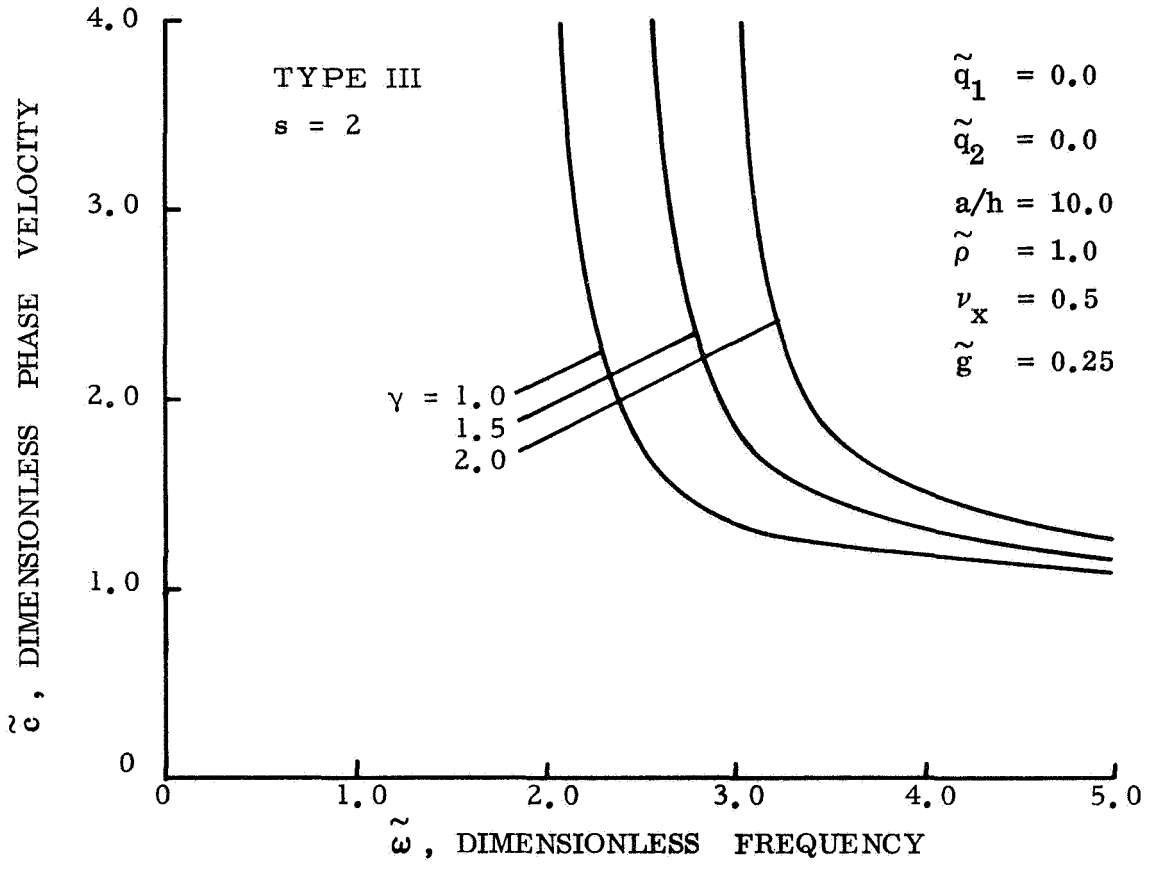

Figure 17. Effect of γ on dispersion of type III waves with s = 2.

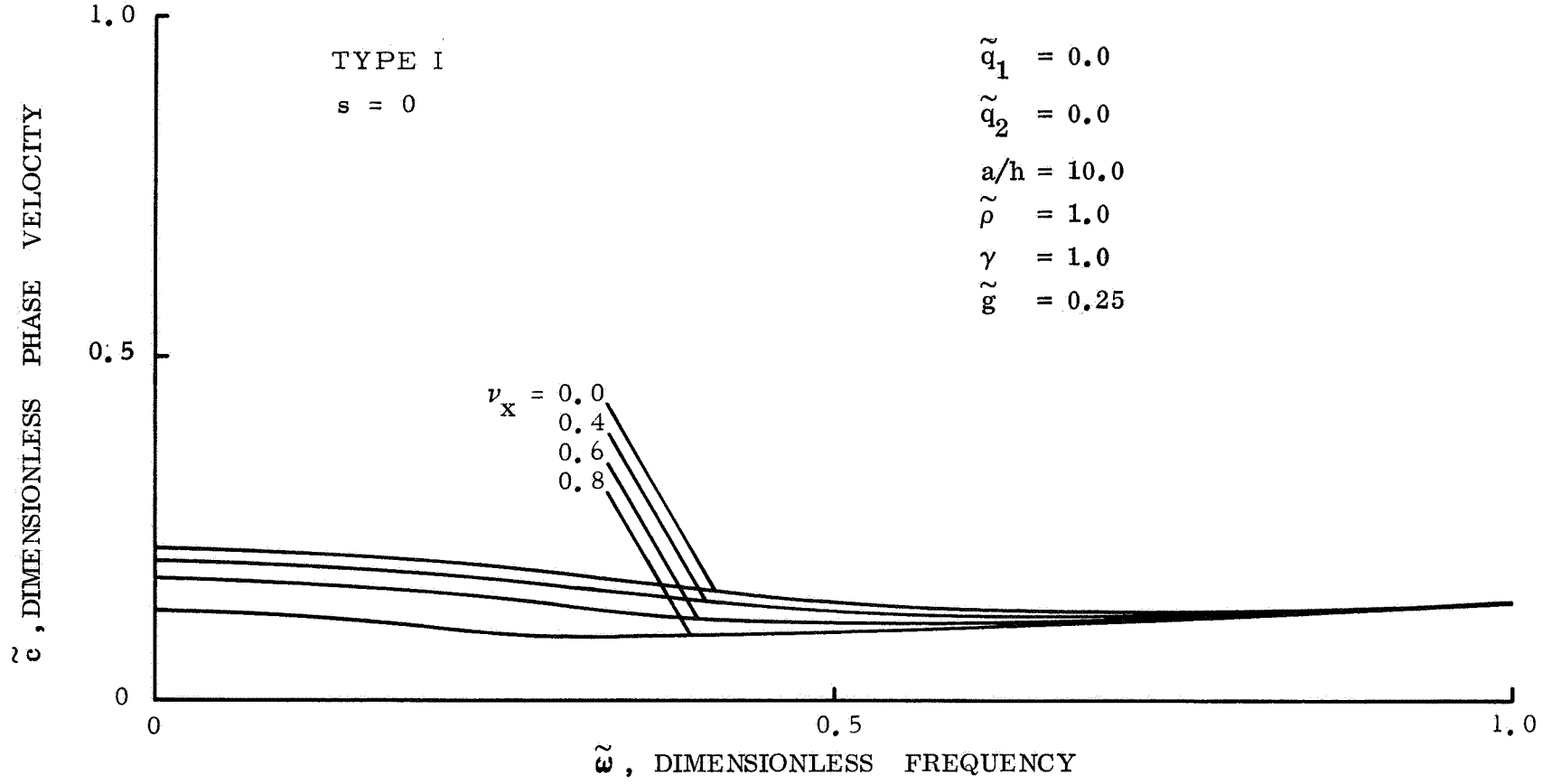

Figure 18. Dispersion of type I, s = 0 waves for $\tilde{q}_2 = 0.0$ and various ν_x.

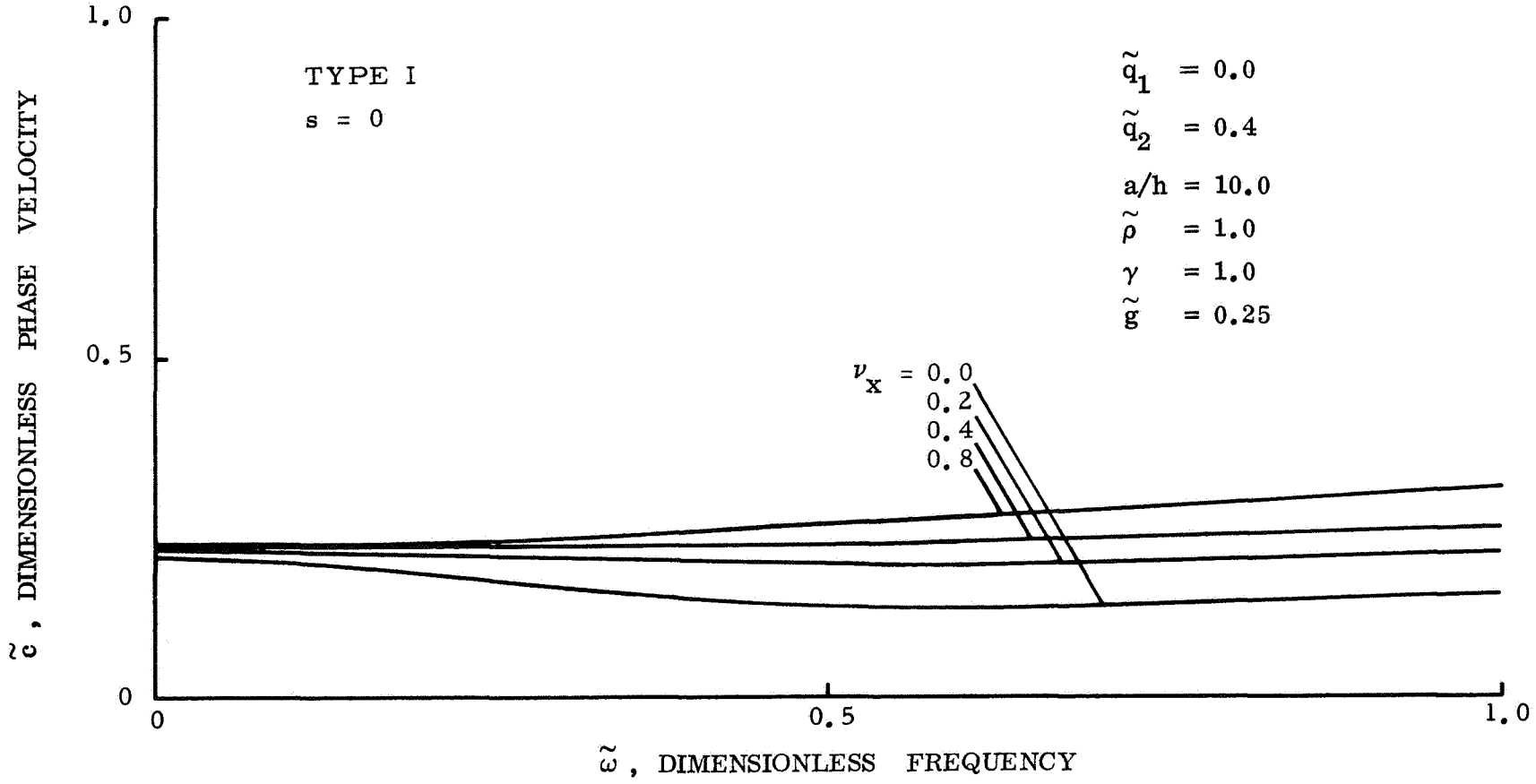

Figure 19. Dispersion of type I, s = 0 waves for $\tilde{q}_2 = 0.4$ and various ν_x.

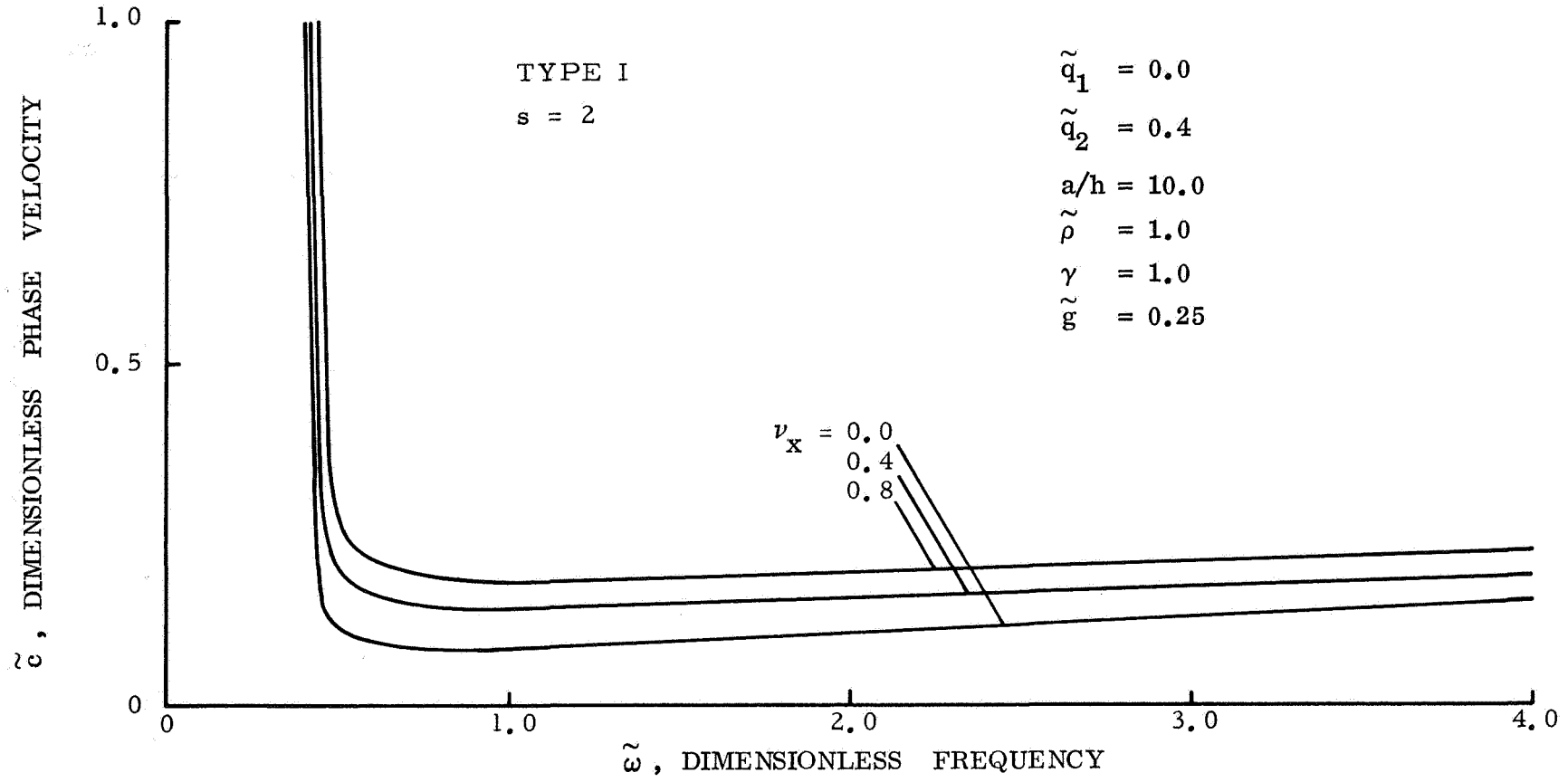

Figure 20. Dispersion of type I, s = 2 waves for $\tilde{q}_2 = 0.4$ and various ν_x.

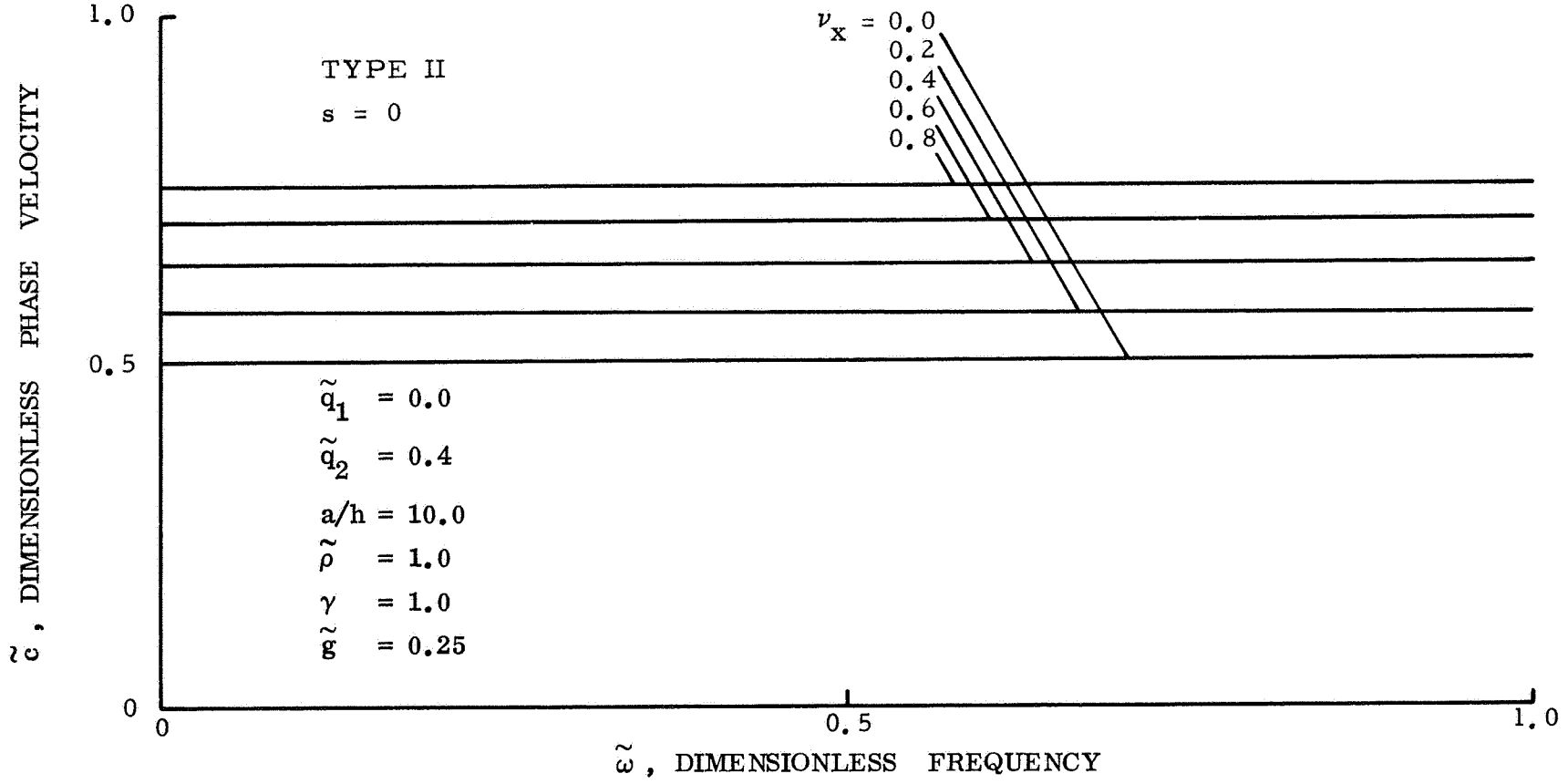

Figure 21. Dispersion of type II, s = 0 waves for $\tilde{q}_2 = 0.4$ and various ν_x.

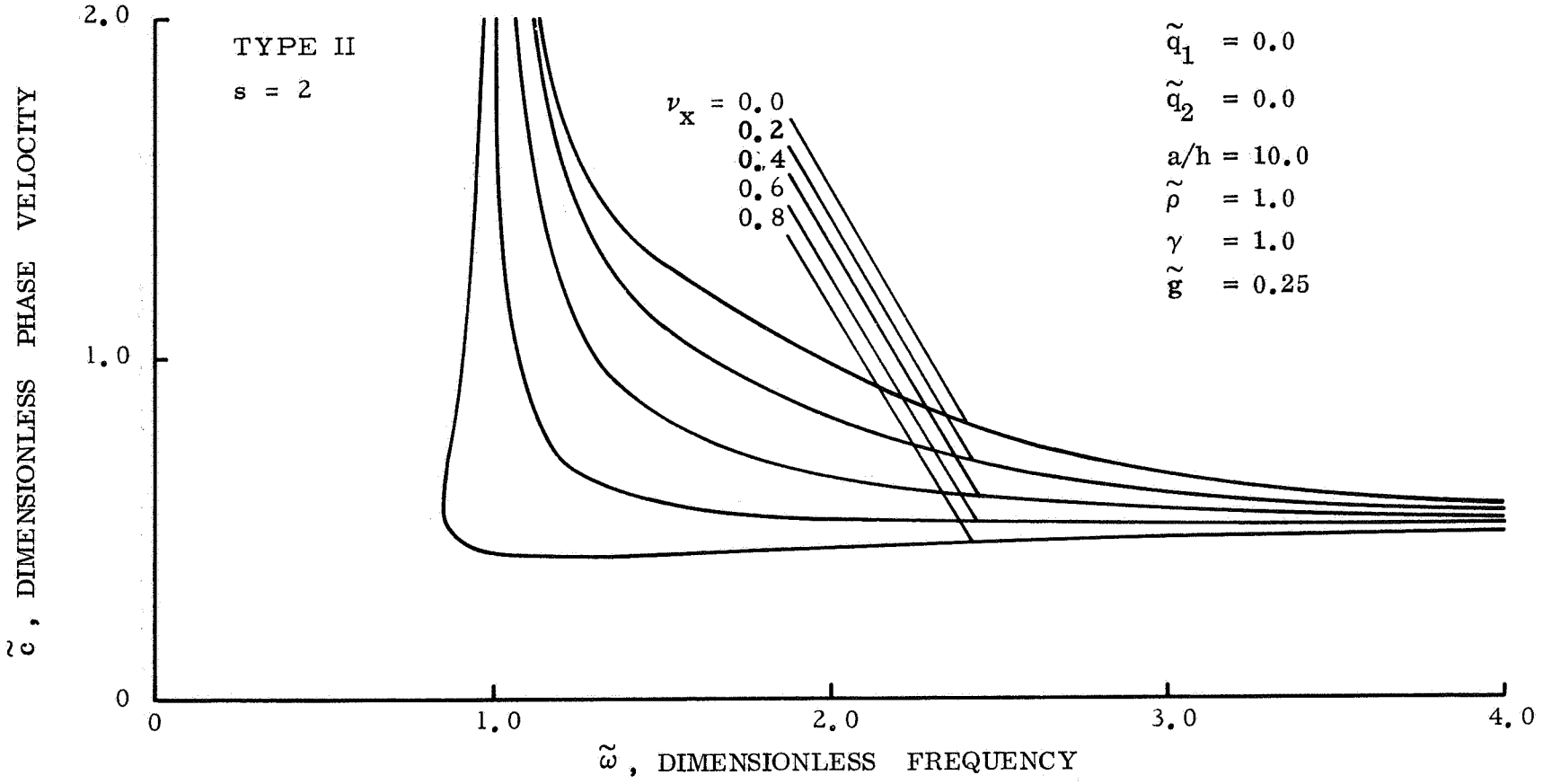

Figure 22. Dispersion of type II, s = 2 waves for $\tilde{q}_2 = 0.0$ and various ν_x.

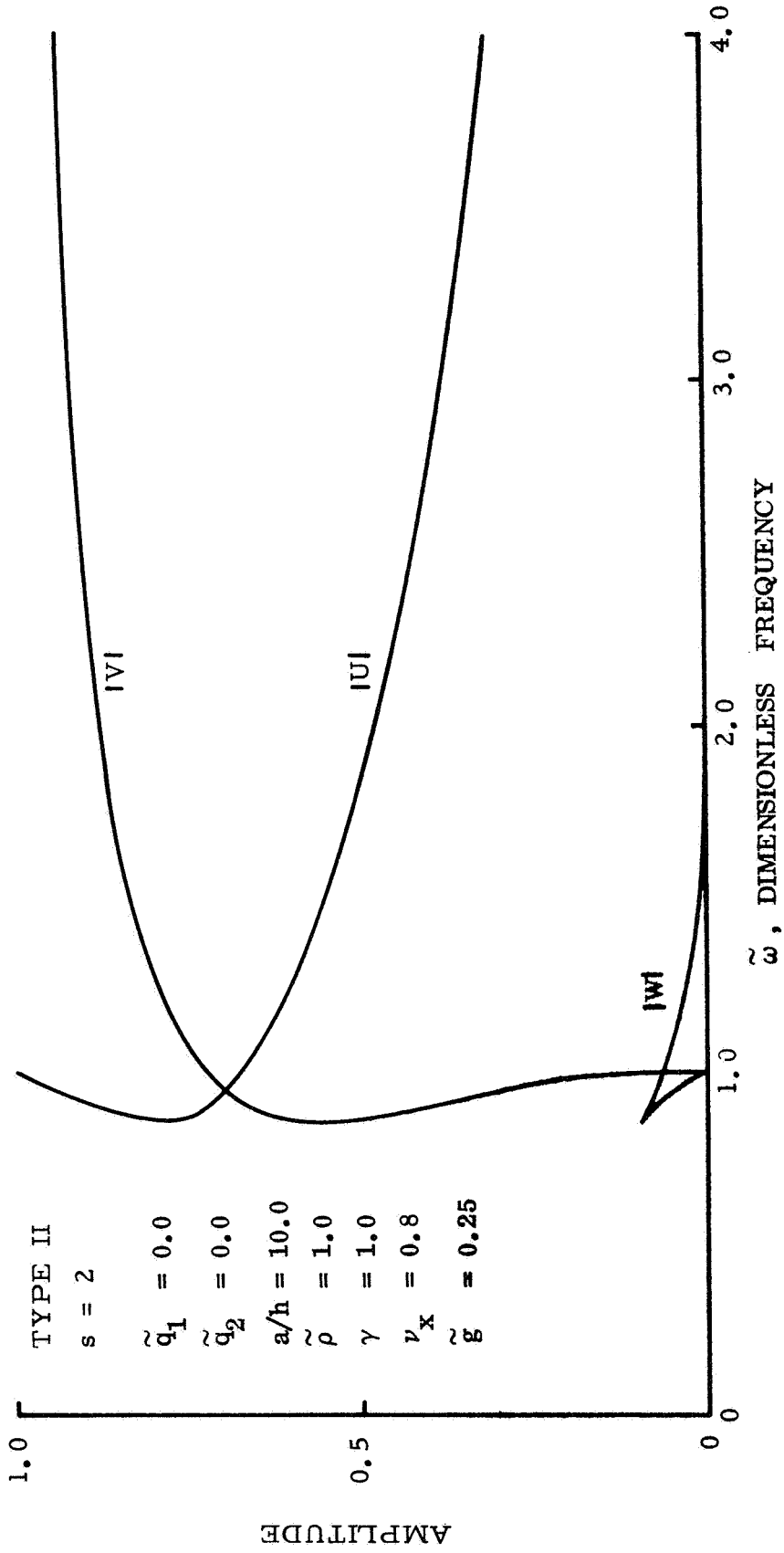

Figure 23. Mode shapes of type II, s = 2 waves for $\tilde{q}_2 = 0.0$ and $\nu_x = 0.8$.

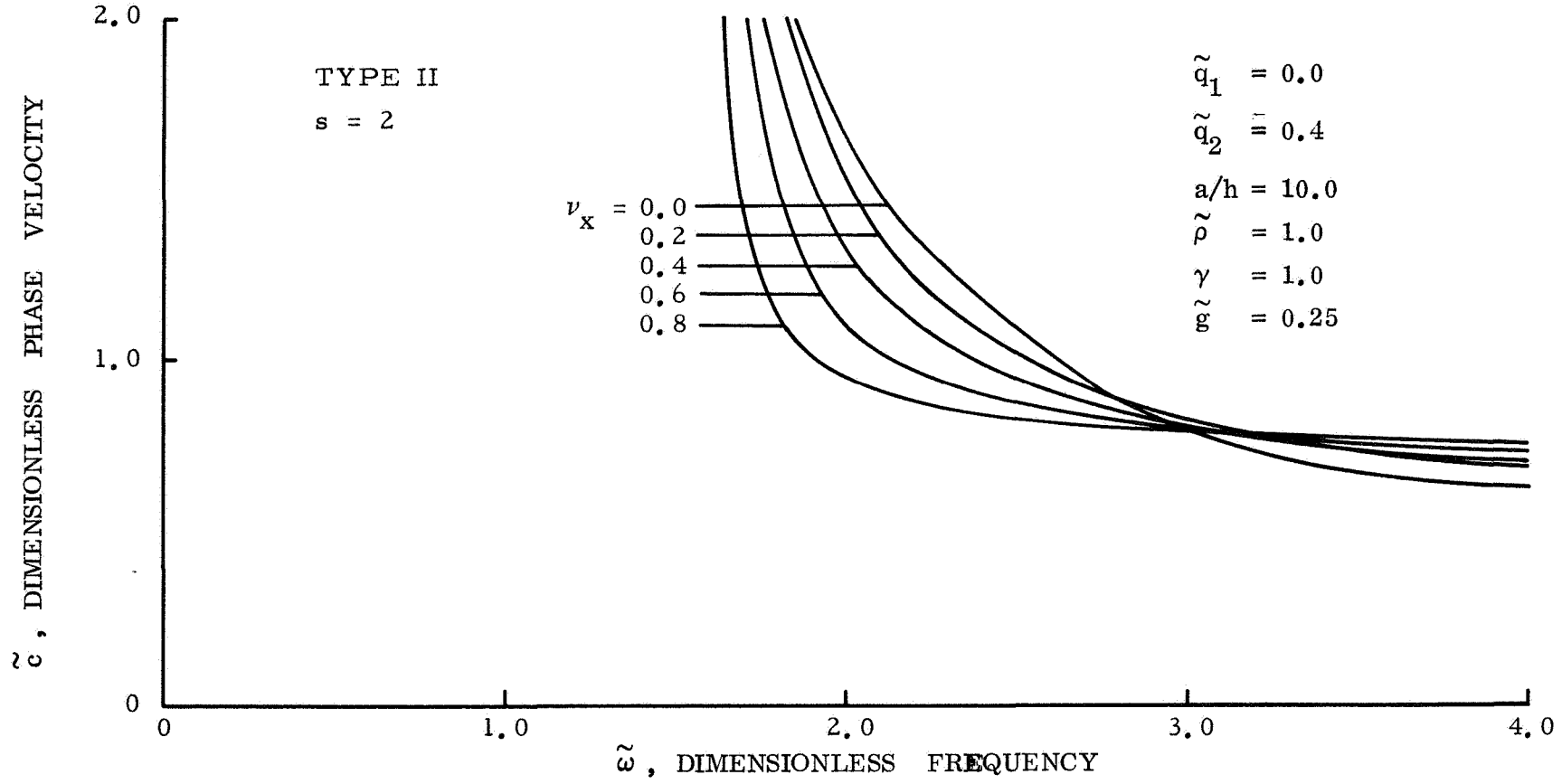

Figure 24. Dispersion of type II, s = 2 waves for $\tilde{q}_2 = 0.4$ and various ν_x.

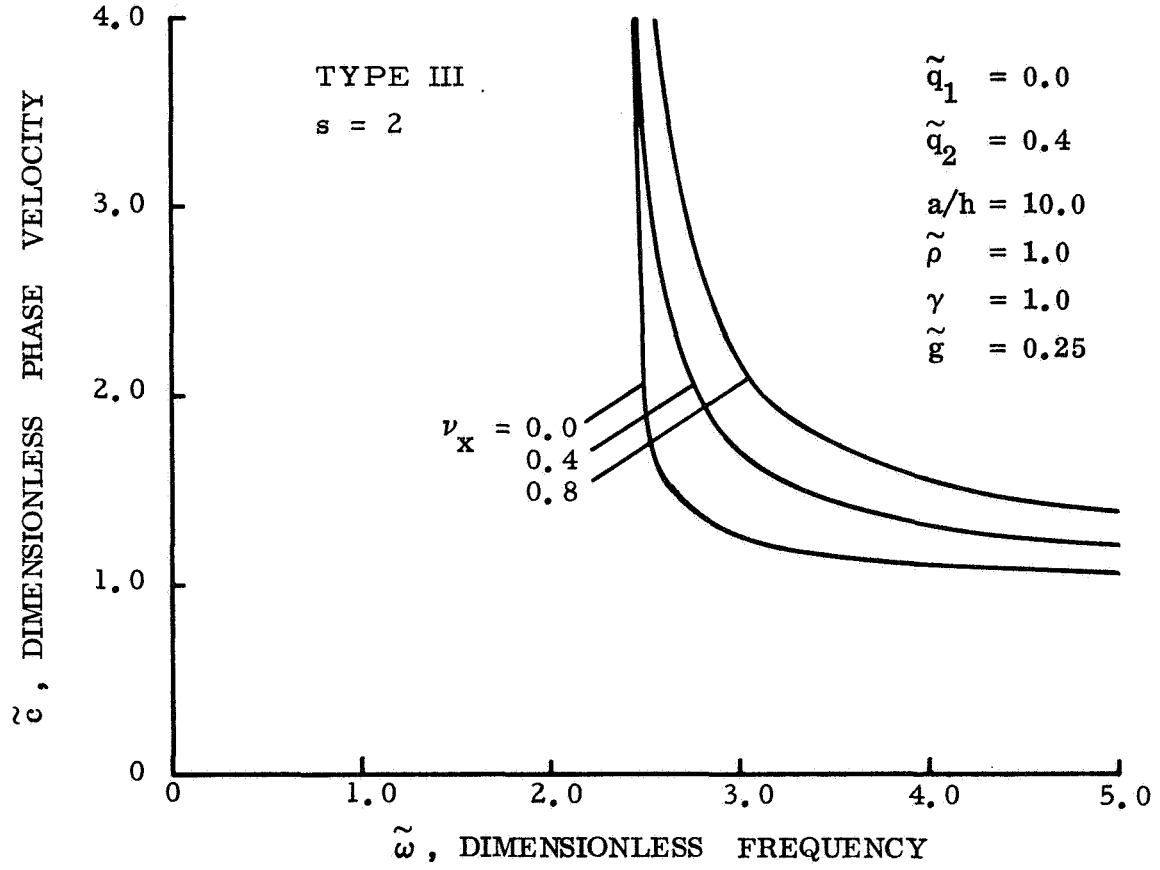

Figure 25. Dispersion of type III, s = 2 waves for $\tilde{q}_2 = 0.4$ and various ν_x.

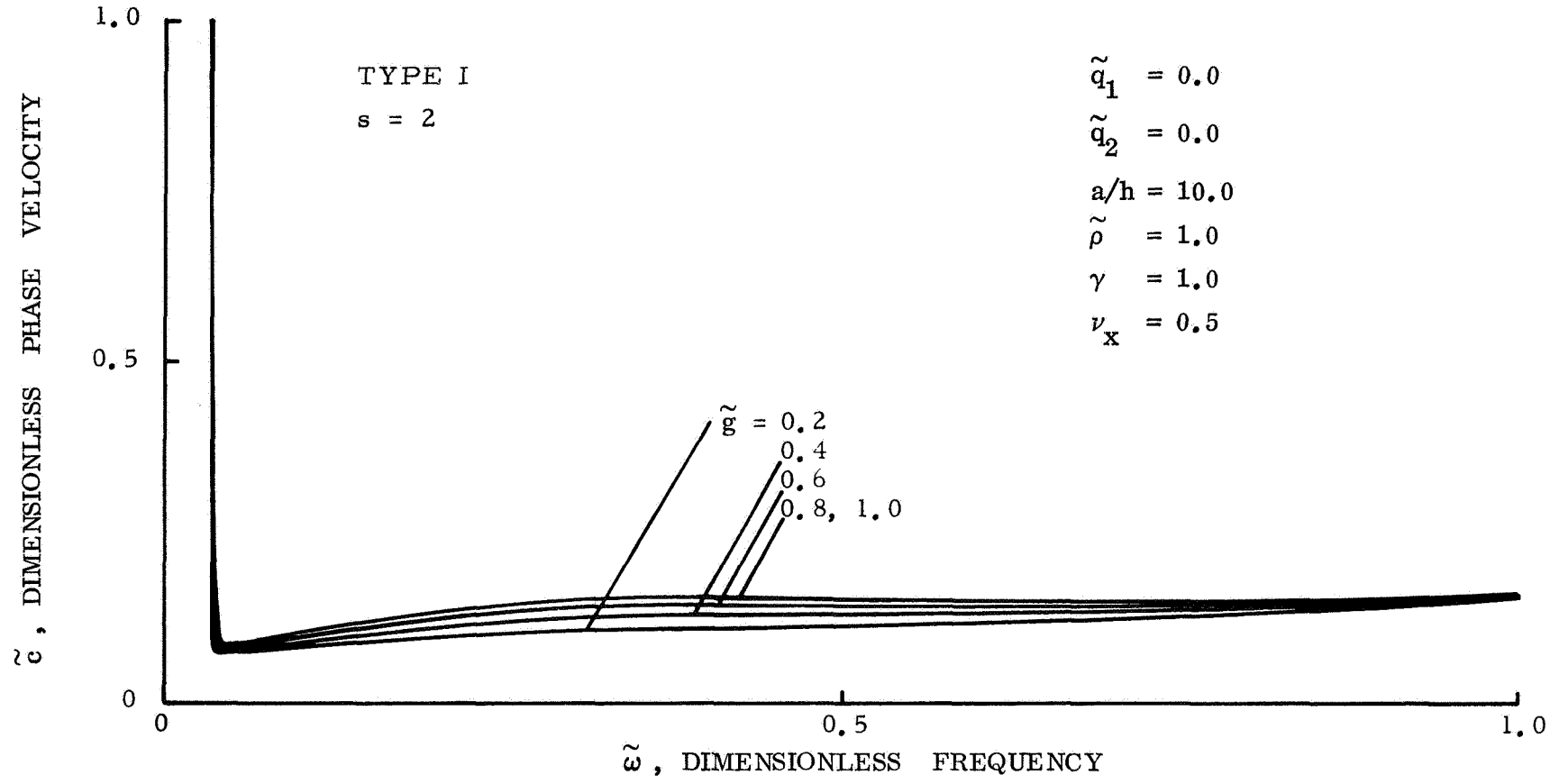

Figure 26. Effect of $\tilde{g}$ on the dispersion of type I waves with s = 2.

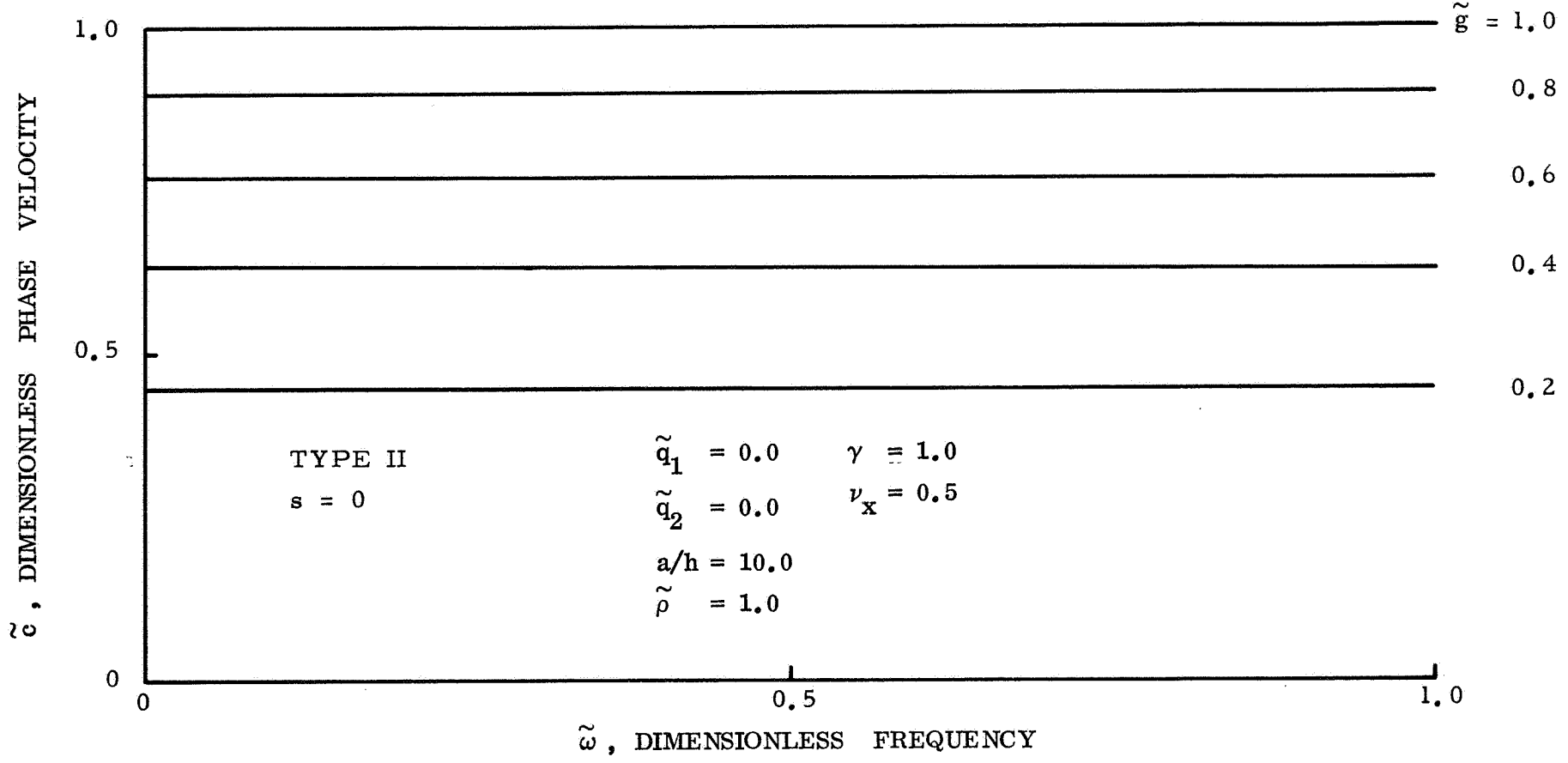

Figure 27. Effect of $\tilde{g}$ on dispersion of type II waves with s = 0.

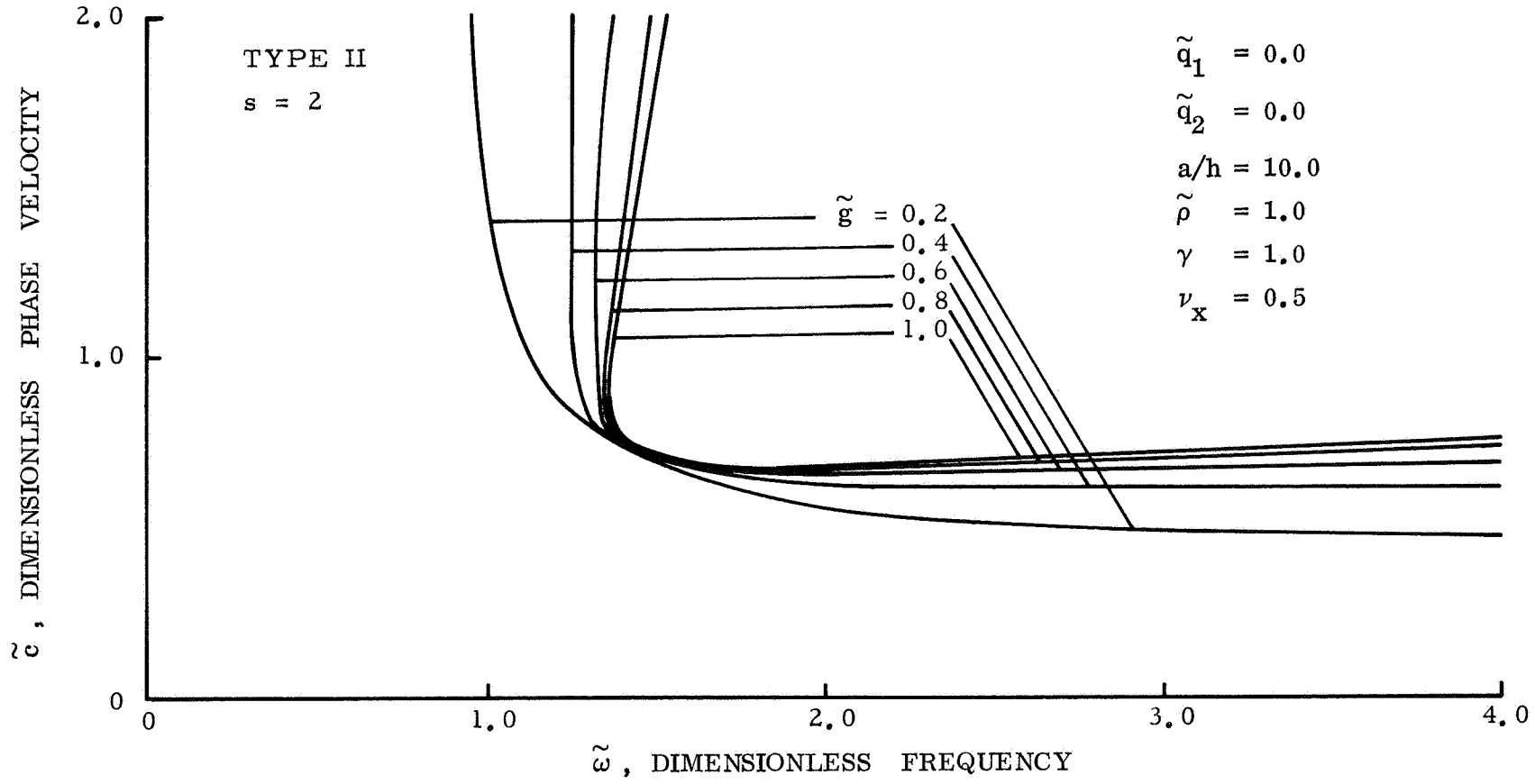

Figure 28. Effect of $\tilde{g}$ on dispersion of type II waves with s = 2.

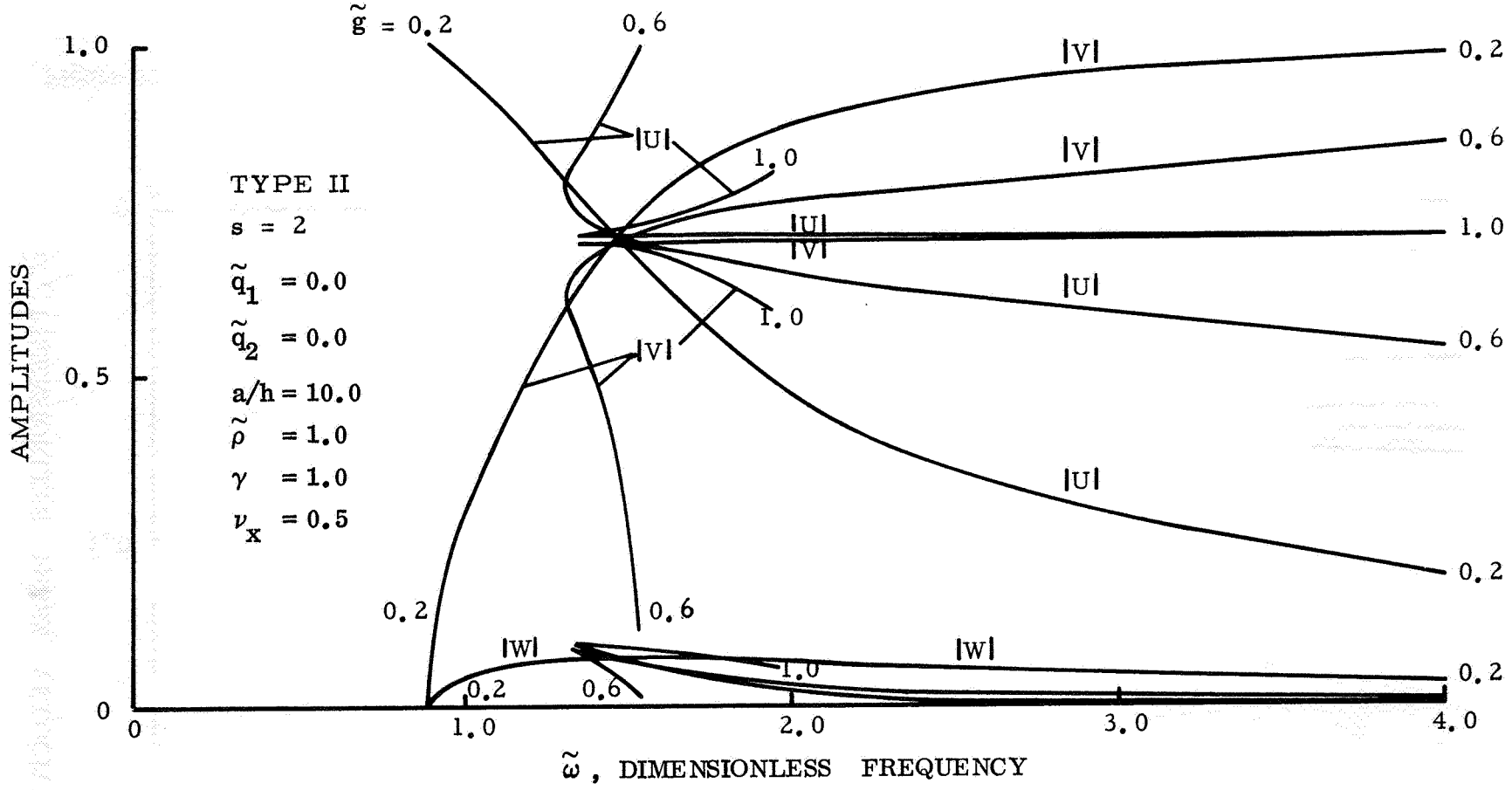

Figure 29. Mode shapes of type II, s = 2 waves for various $\tilde{g}$.

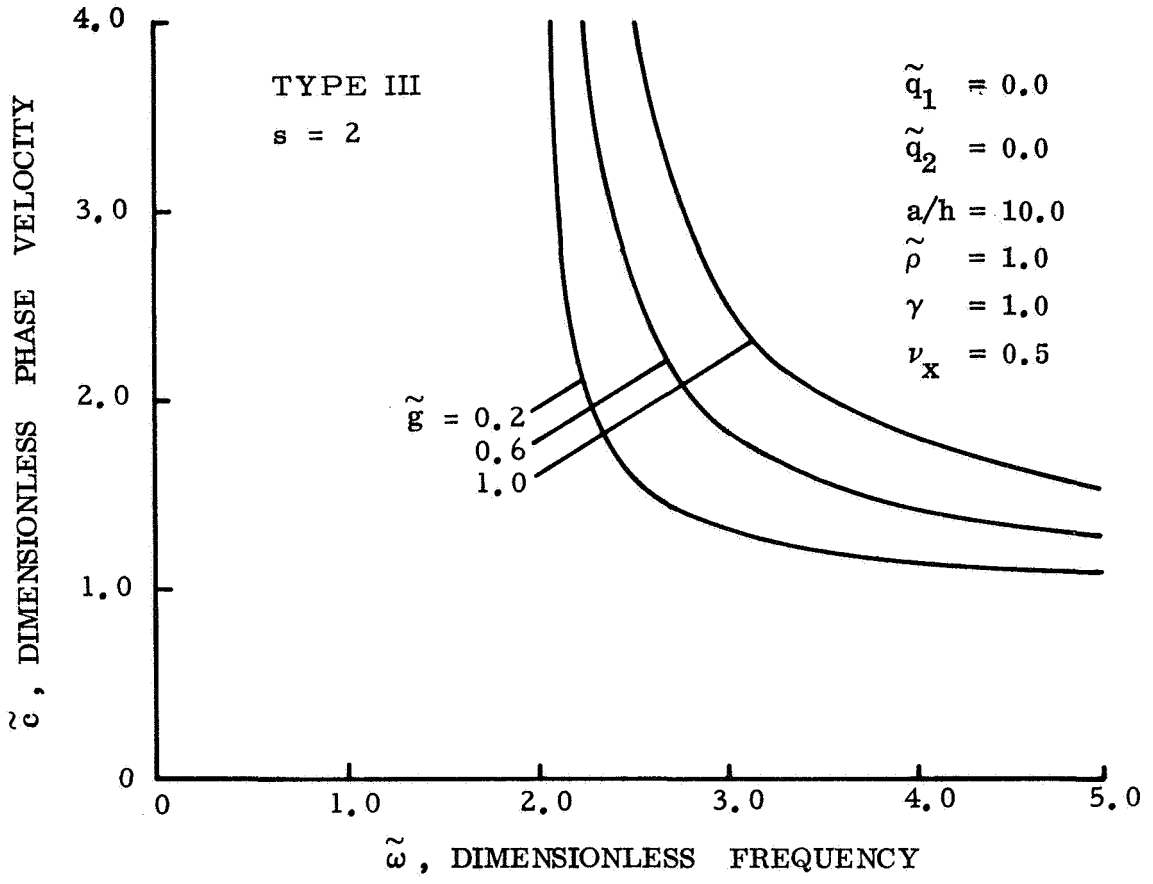

Figure 30. Effect of $\tilde{g}$ on dispersion of type III waves with s = 2.

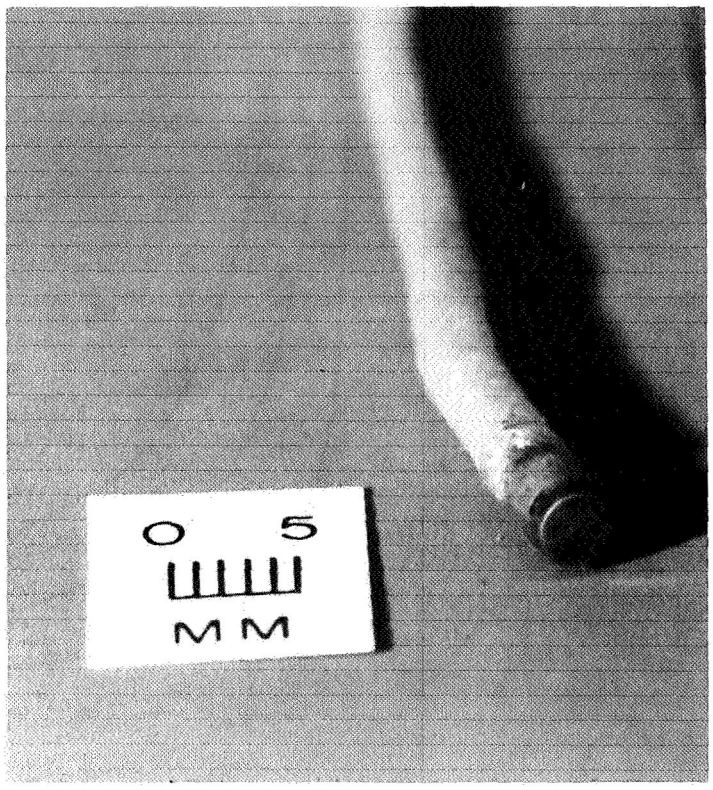

Figure 31. Schaevitz-Bytrex pressure transducer model HFD-5.

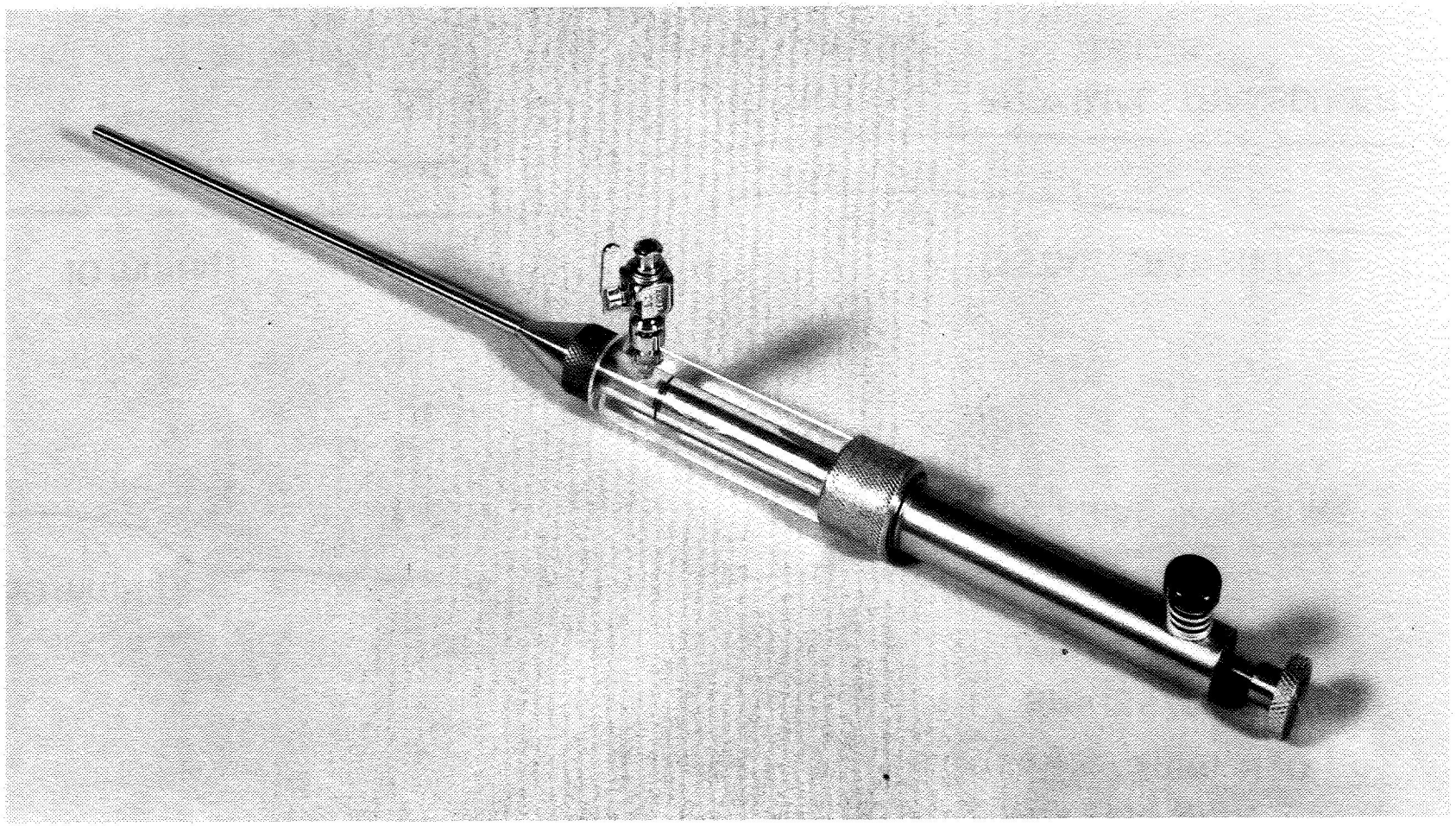

Figure 32. Spring-loaded syringe used to generate large amplitude pressure waves in blood vessels.

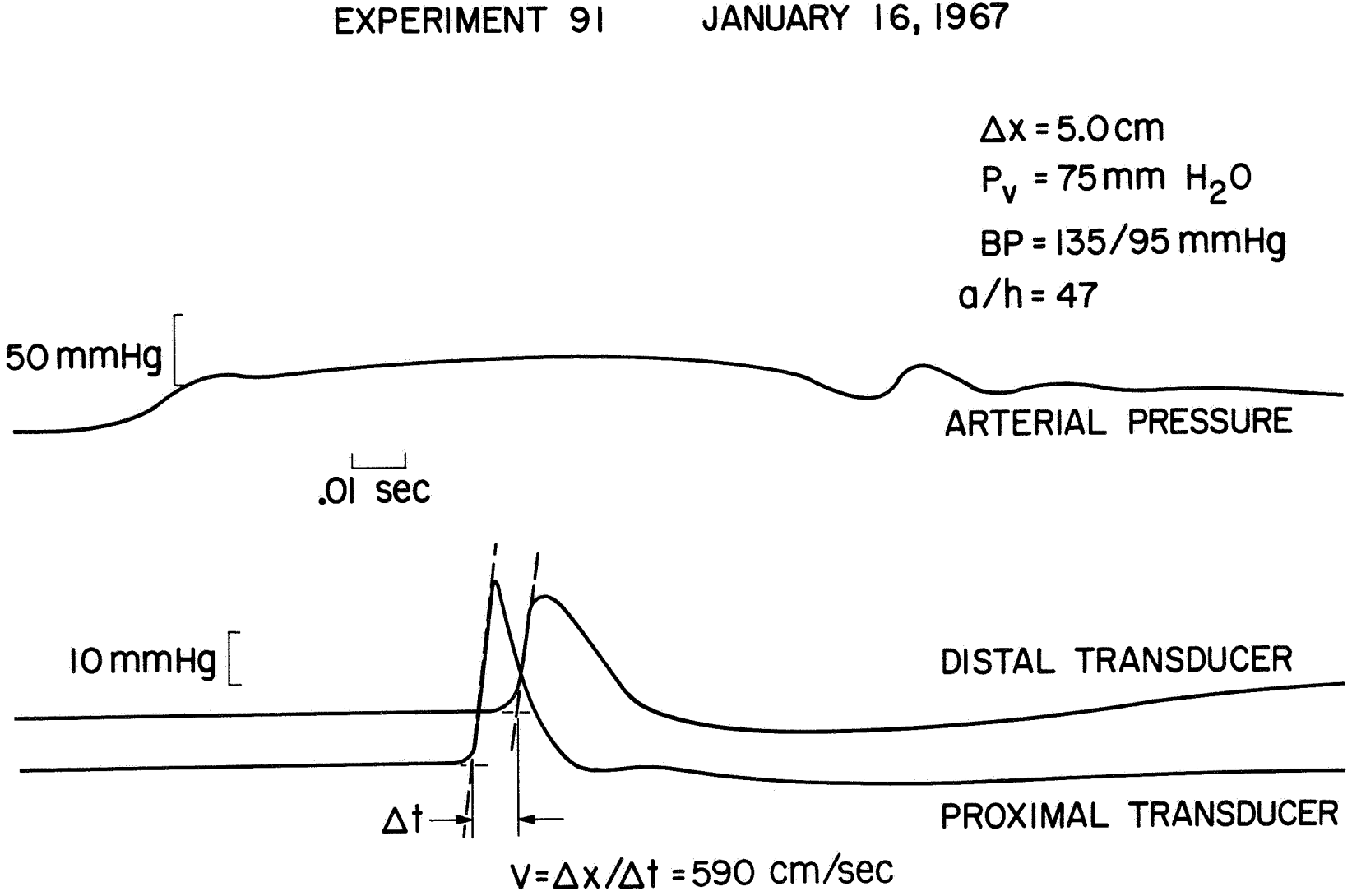

Figure 33. Representative tracings of pressure fluctuations in the carotid artery and in the abdominal vena cava of an anesthetized dog during the transmission of a pressure pulse induced by the injection of 0.5 cm^3 of saline into a femoral vein.

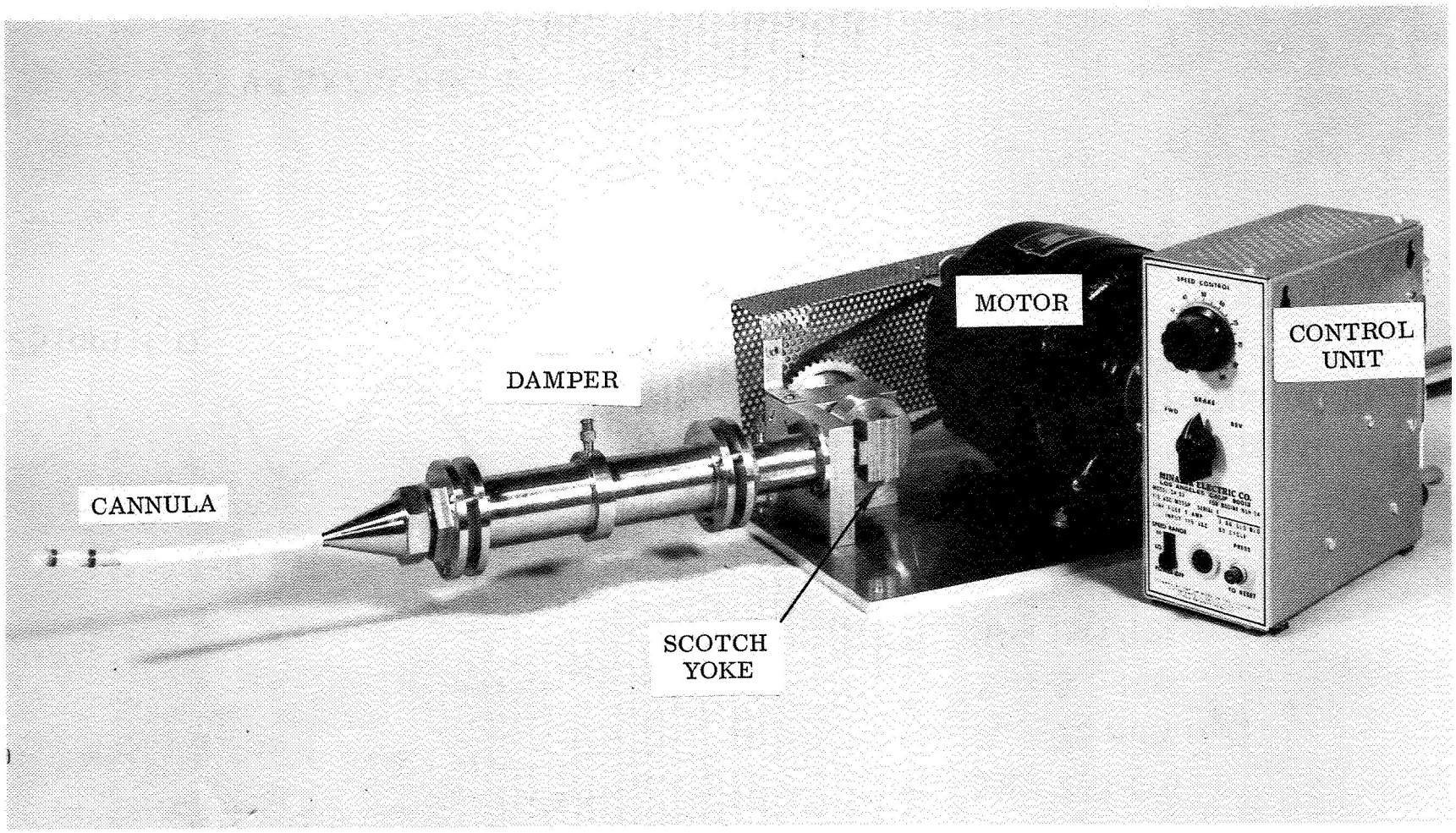

Figure 34. Pump with frequency control unit used to generate sinusoidal pressure waves in blood vessels.

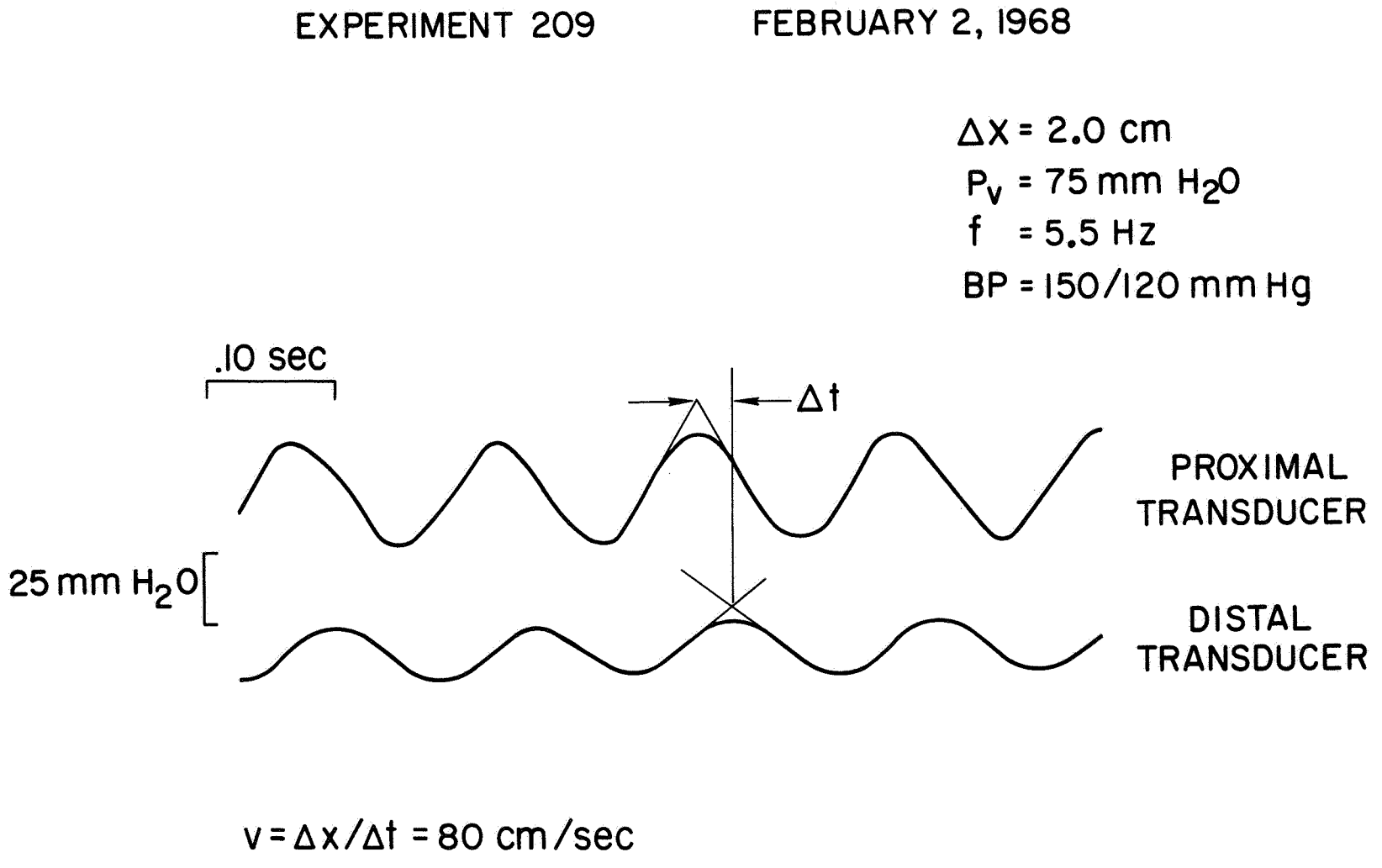

Figure 35. Trains of sinusoidal pressure waves in the abdominal vena cava produced by the pump.

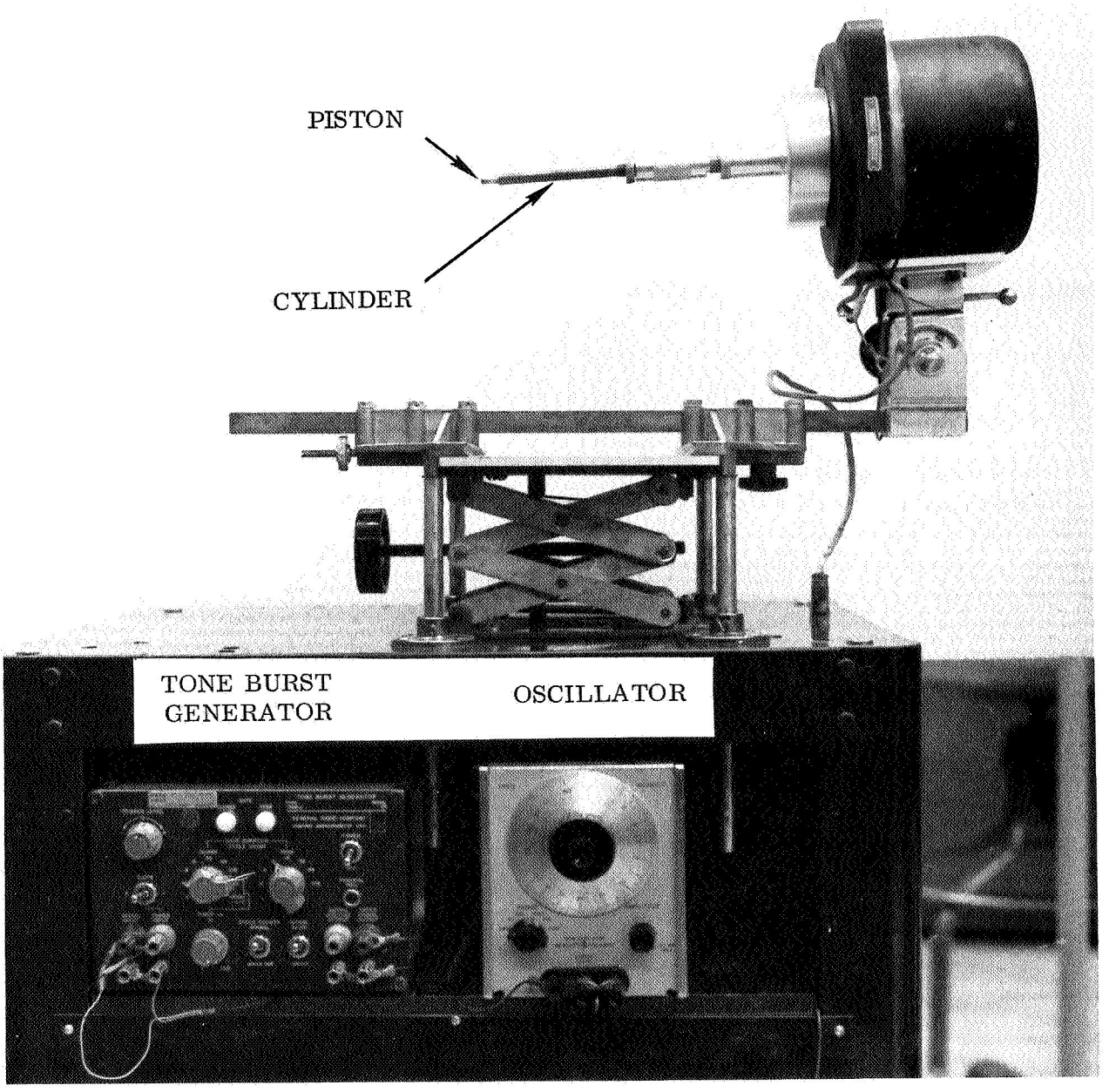

Figure 36. Electrically driven piston with tone burst generator and oscillator.

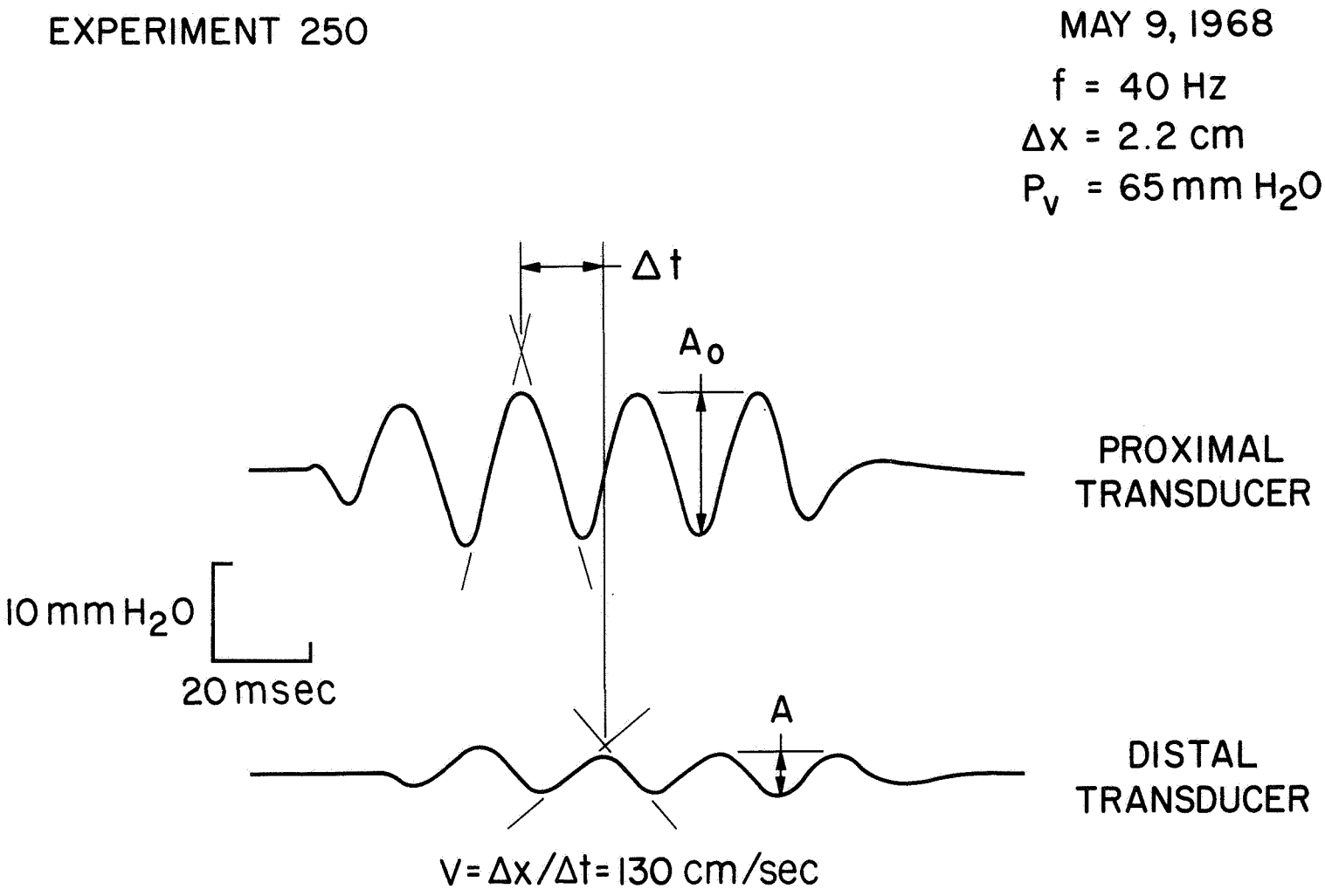

Figure 37. Recording of a finite train of sine waves produced by the vibrating piston.

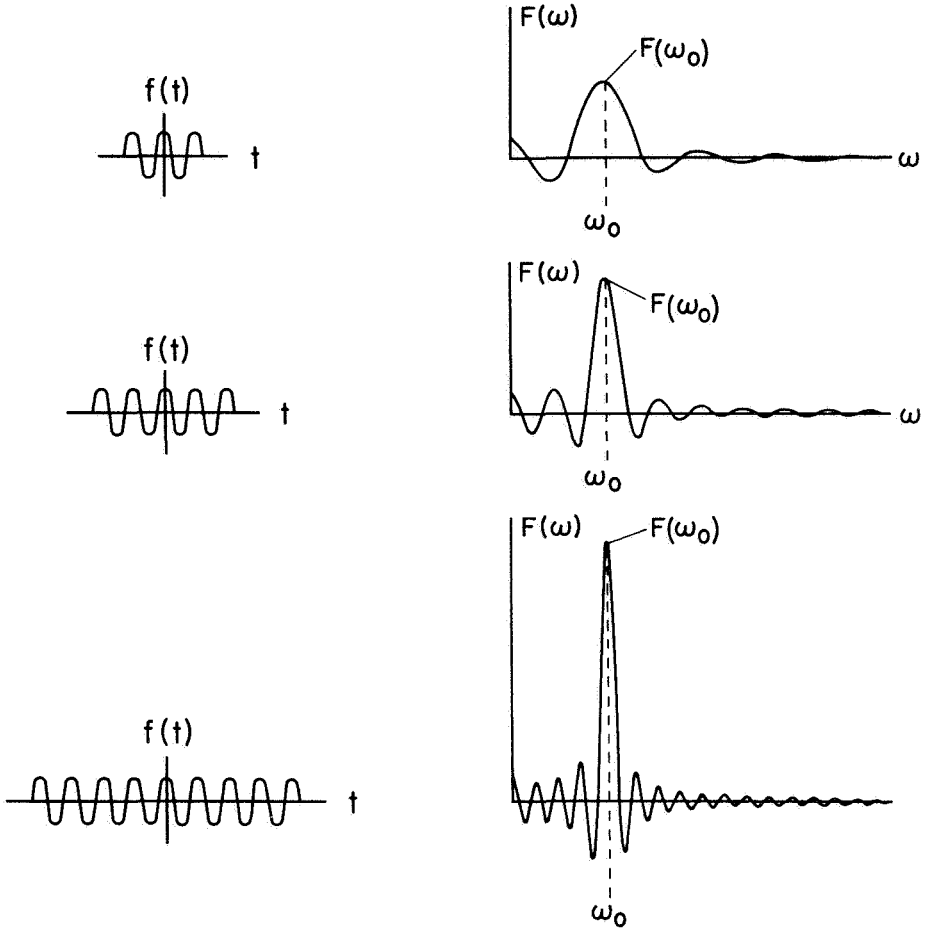

$$f(t) = \frac{1}{2\pi} \int_{-\infty}^{\infty} F(\omega)\, e^{i\omega t}\, d\omega \qquad F(\omega) = \int_{-\infty}^{\infty} f(t)\, e^{-i\omega t}\, dt$$

$$f(t) = \begin{cases} \cos(\omega_0 t), & |t| < \frac{\tau}{2} \\ 0, & |t| > \frac{\tau}{2} \end{cases} \qquad F(\omega) = \frac{\tau}{2}\left[\frac{\sin\left(\frac{\omega-\omega_0}{2}\right)\tau}{\left(\frac{\omega-\omega_0}{2}\right)\tau} + \frac{\sin\left(\frac{\omega+\omega_0}{2}\right)\tau}{\left(\frac{\omega+\omega_0}{2}\right)\tau}\right]$$

Figure 38. Fourier transform of finite trains of sine waves.

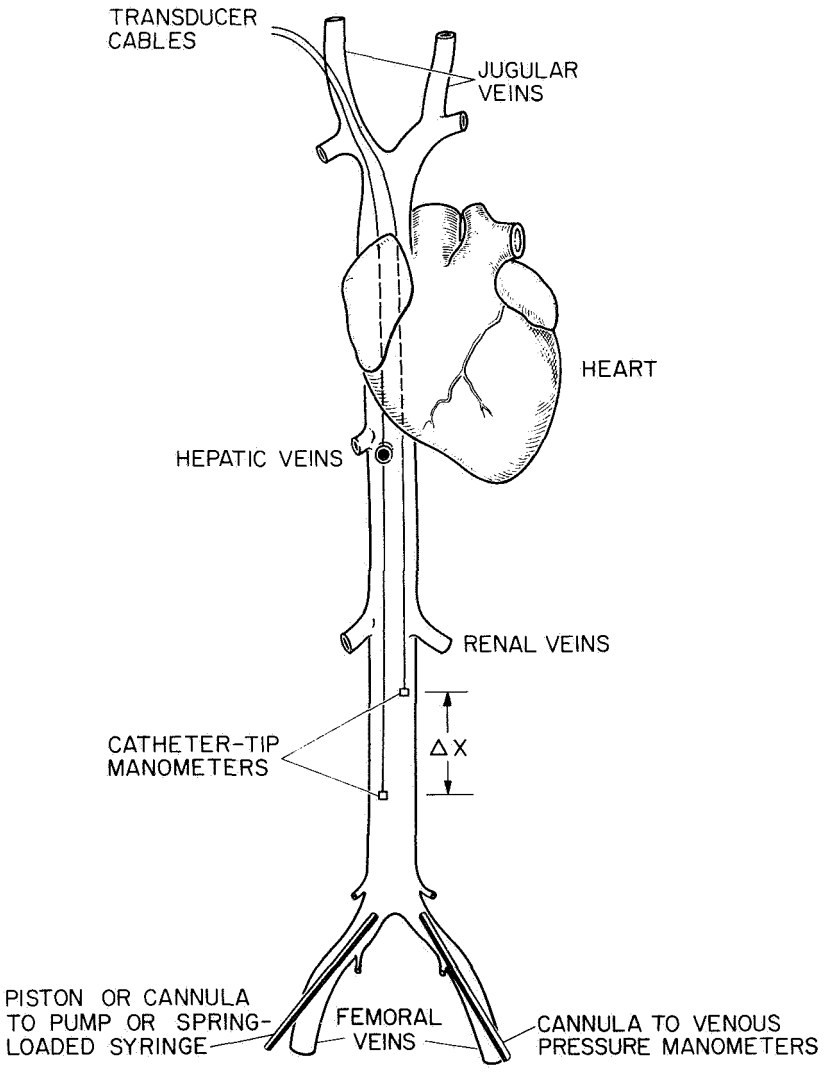

Figure 39. General experimental arrangement for studying the transmission characteristics of artificially induced pressure waves in the abdominal vena cava of anesthetized dogs.

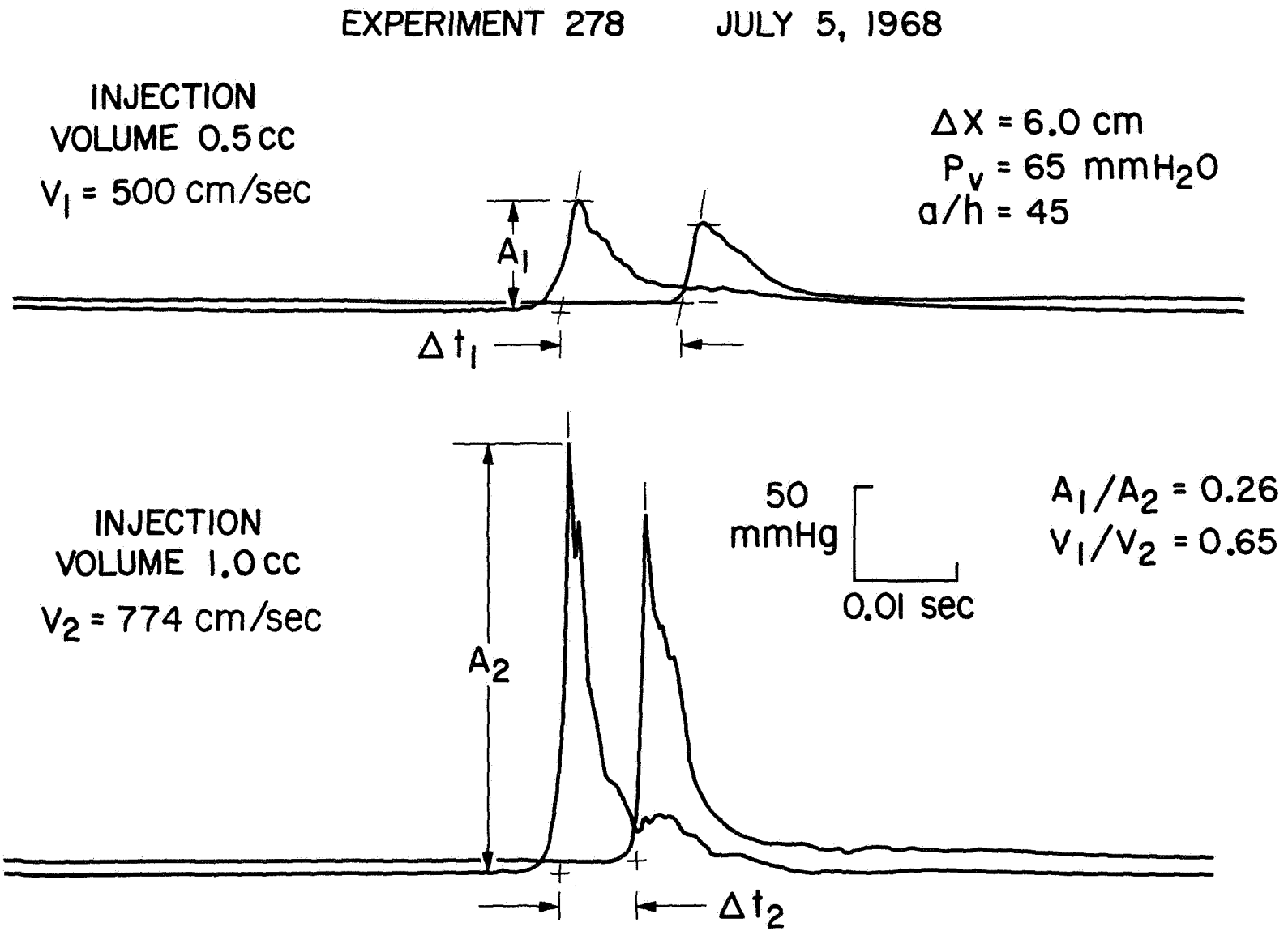

Figure 40. Variation in wave speed with signal amplitude for pulses produced in the abdominal vena cava by a spring-loaded syringe.

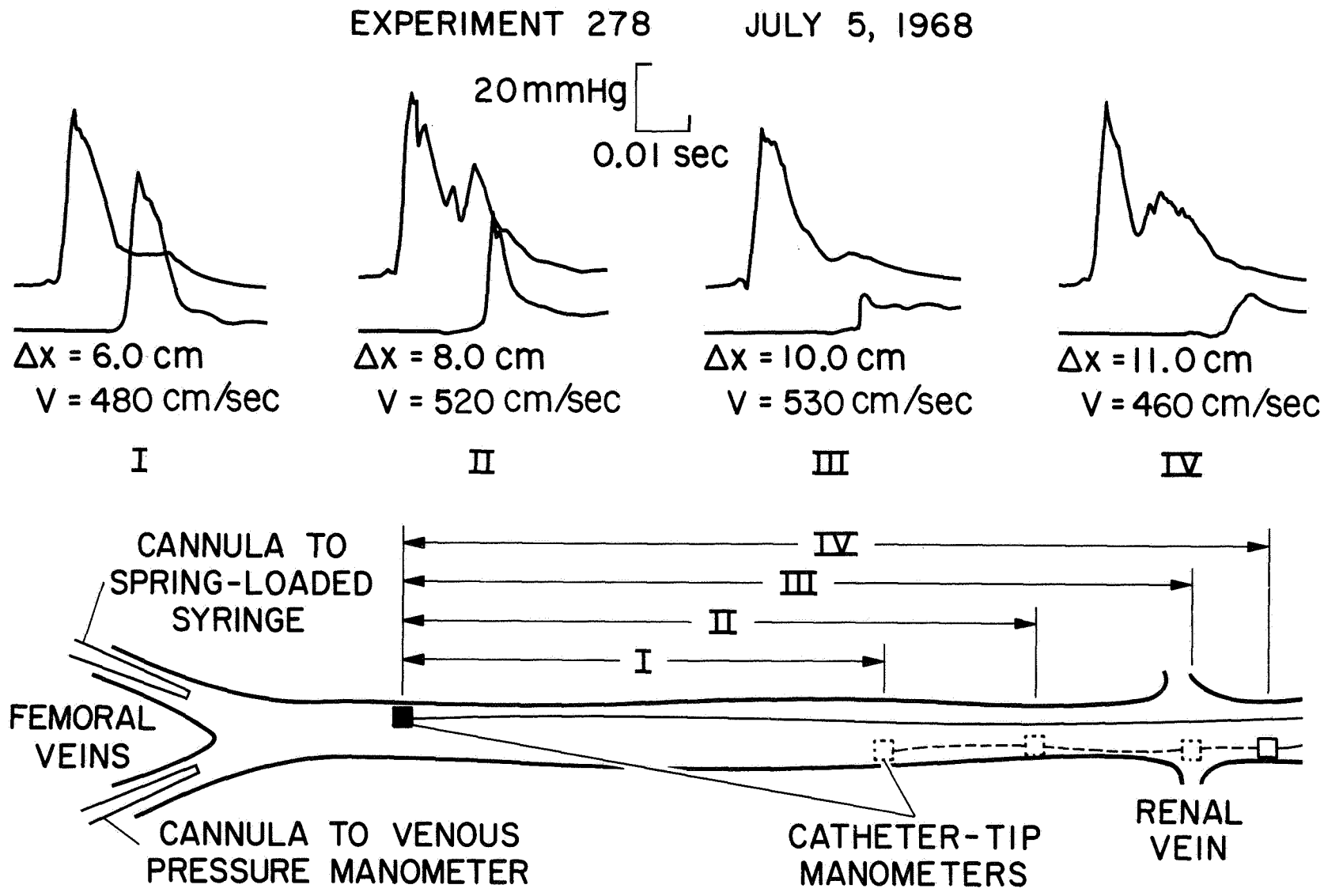

Figure 41. Variations in the shape and speed of pressure pulses at different locations in the abdominal vena cava.

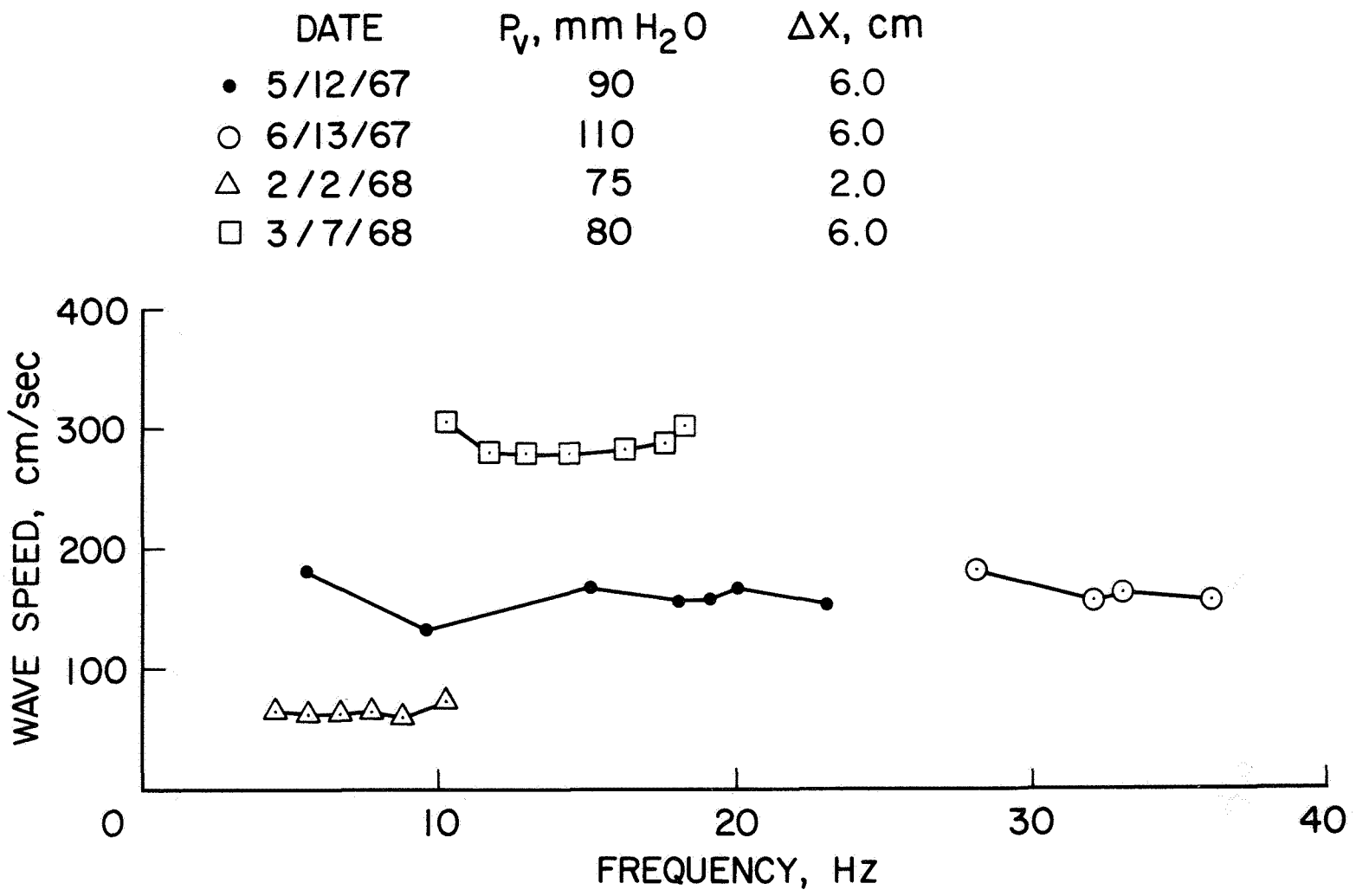

Figure 42. Representative dispersion curves for continuous pressure waves produced by the pump.

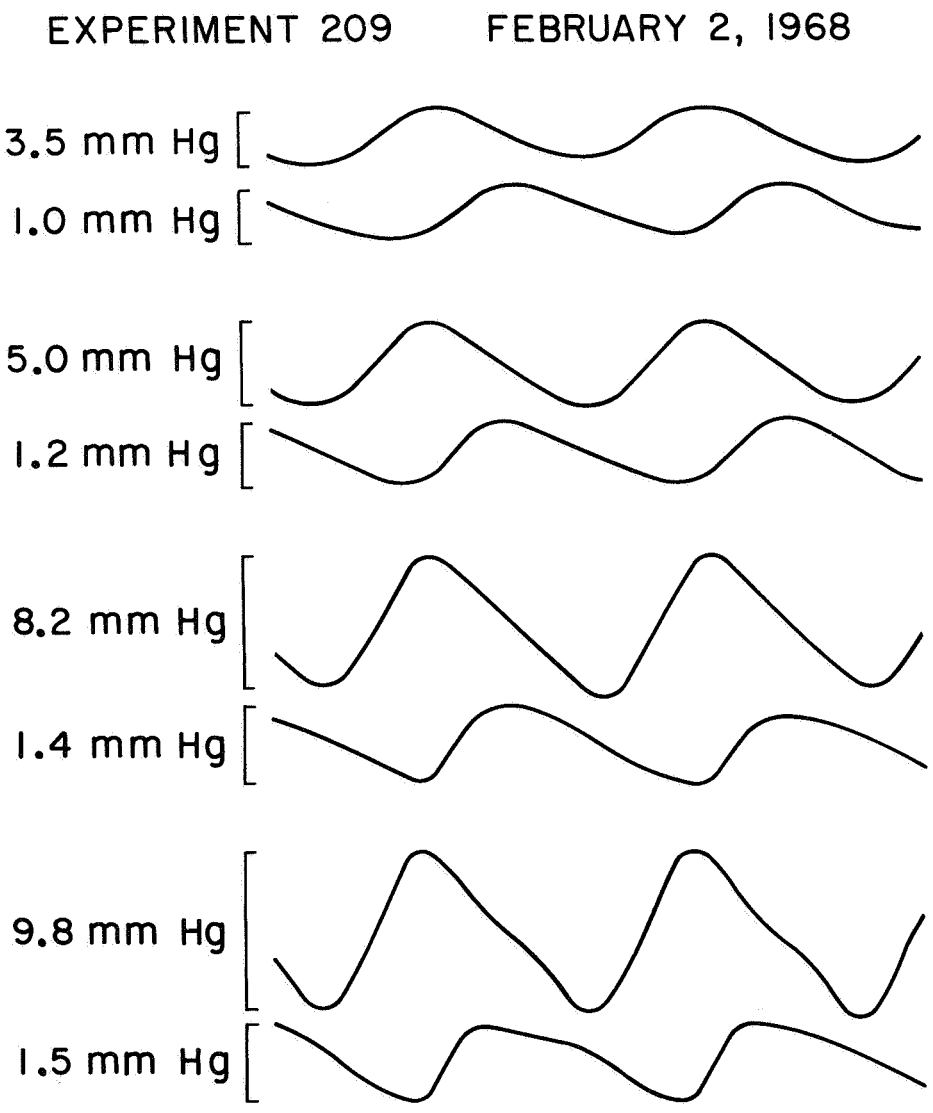

Figure 43. Changes in wave shape due to increasing signal amplitude.

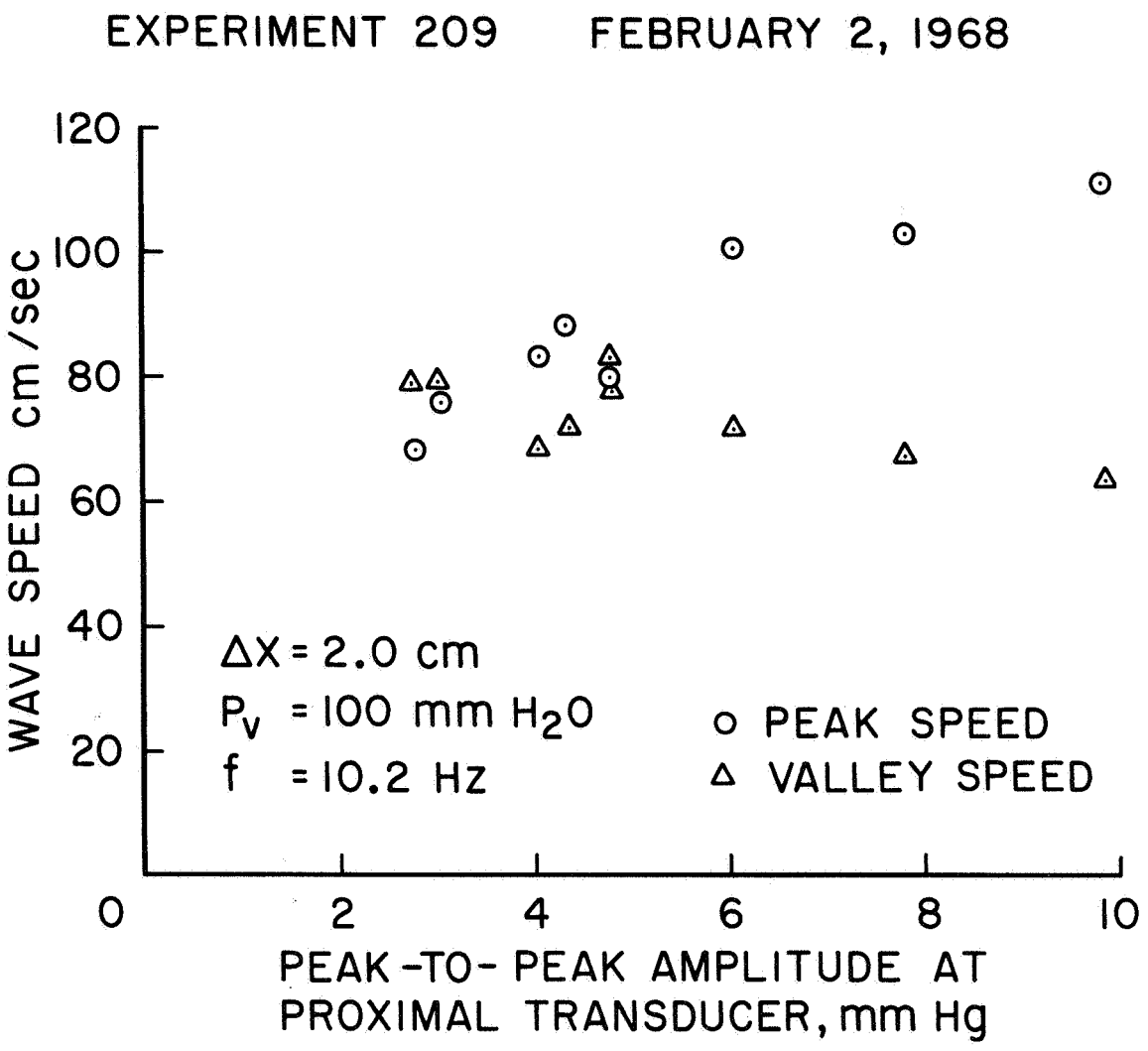

Figure 44. The effect of a large signal amplitude on the speed of the peaks and valleys of near sinusoidal pressure waves produced by the pump.

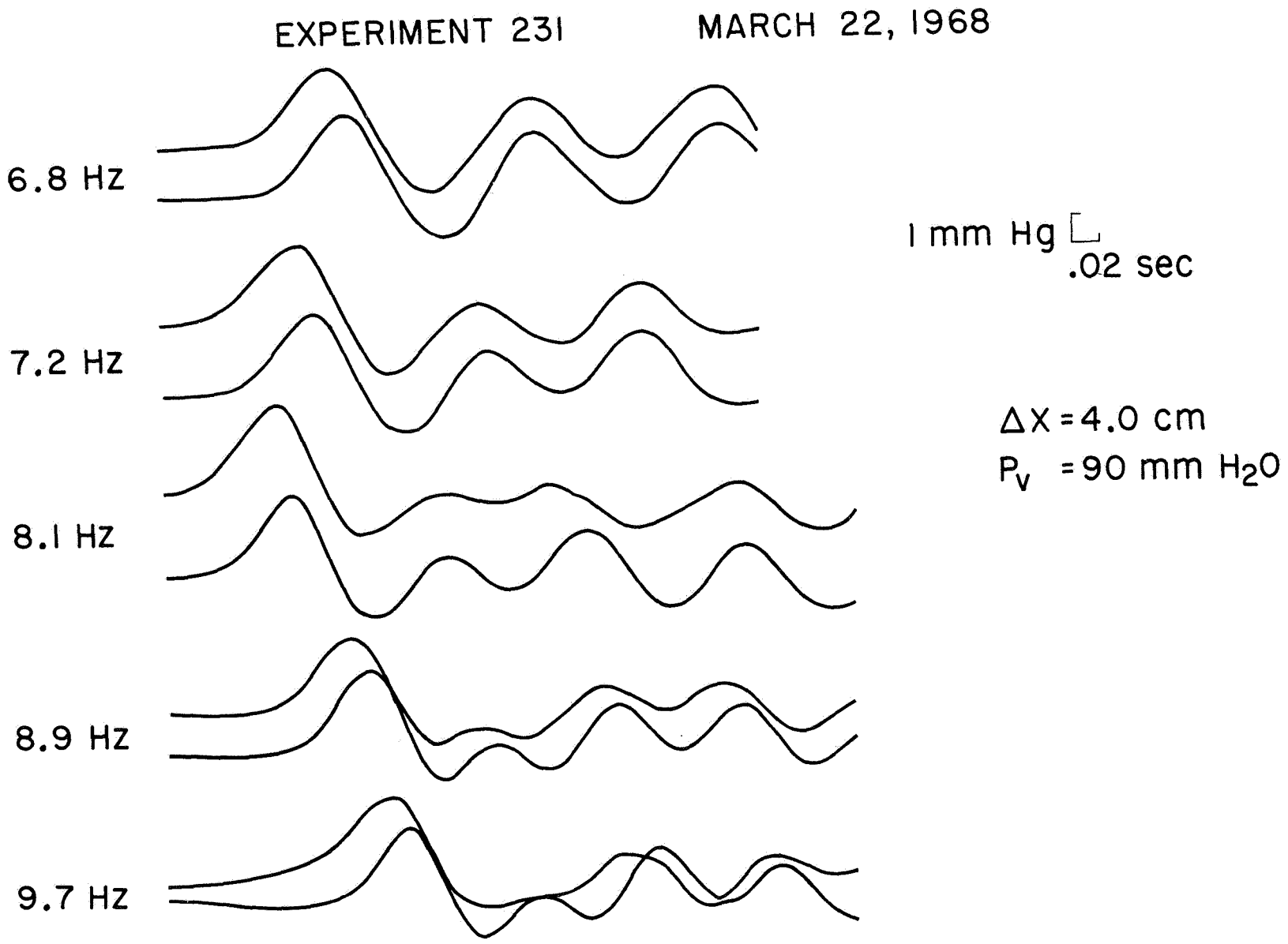

Figure 45. Indication of reflection interference associated with the propagation of large amplitude pressure waves produced by the pump.

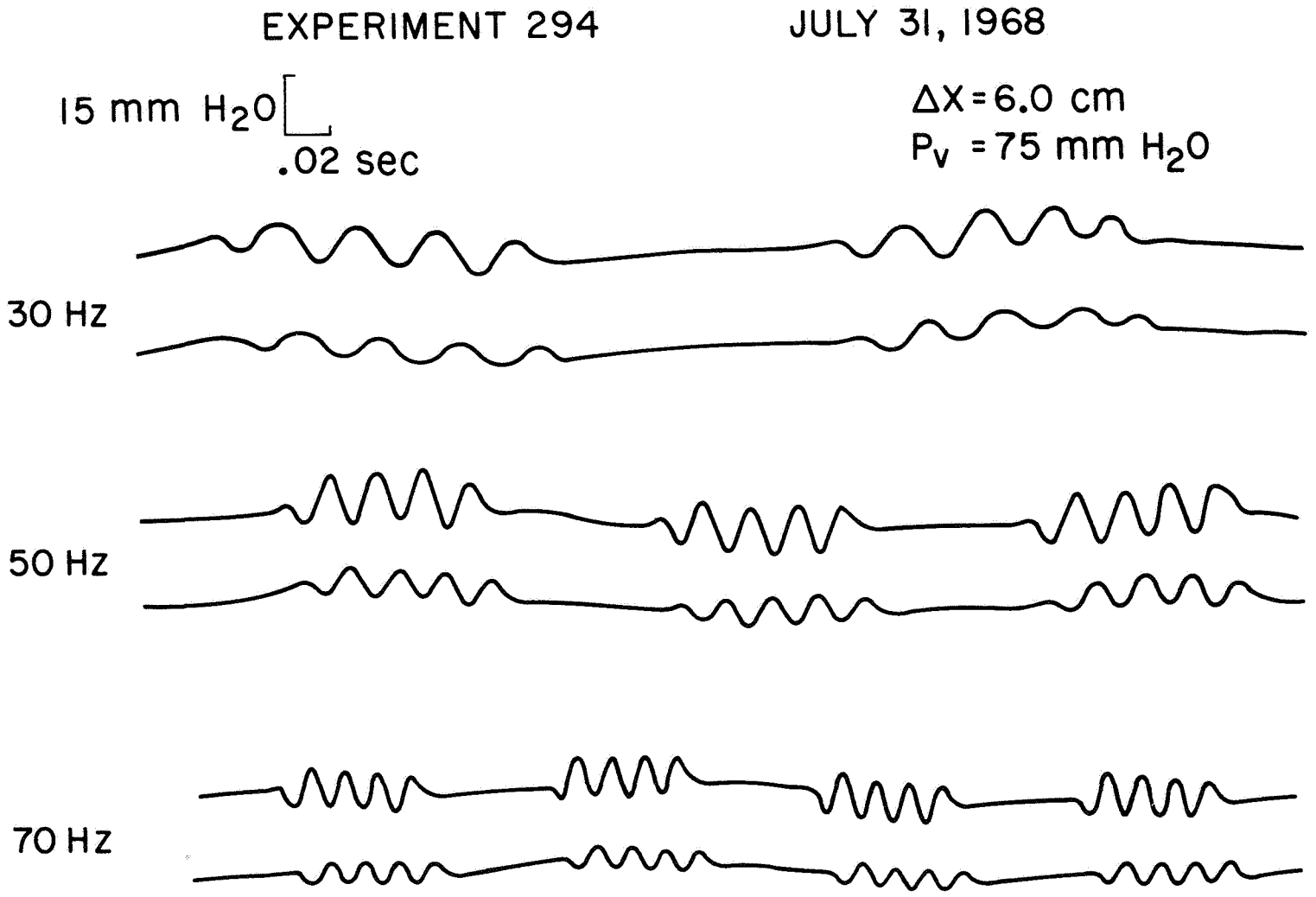

Figure 46. Sample tracings of finite trains of sinusoidal pressure waves of different frequencies generated by a vibrating piston and recorded in the vena cava.

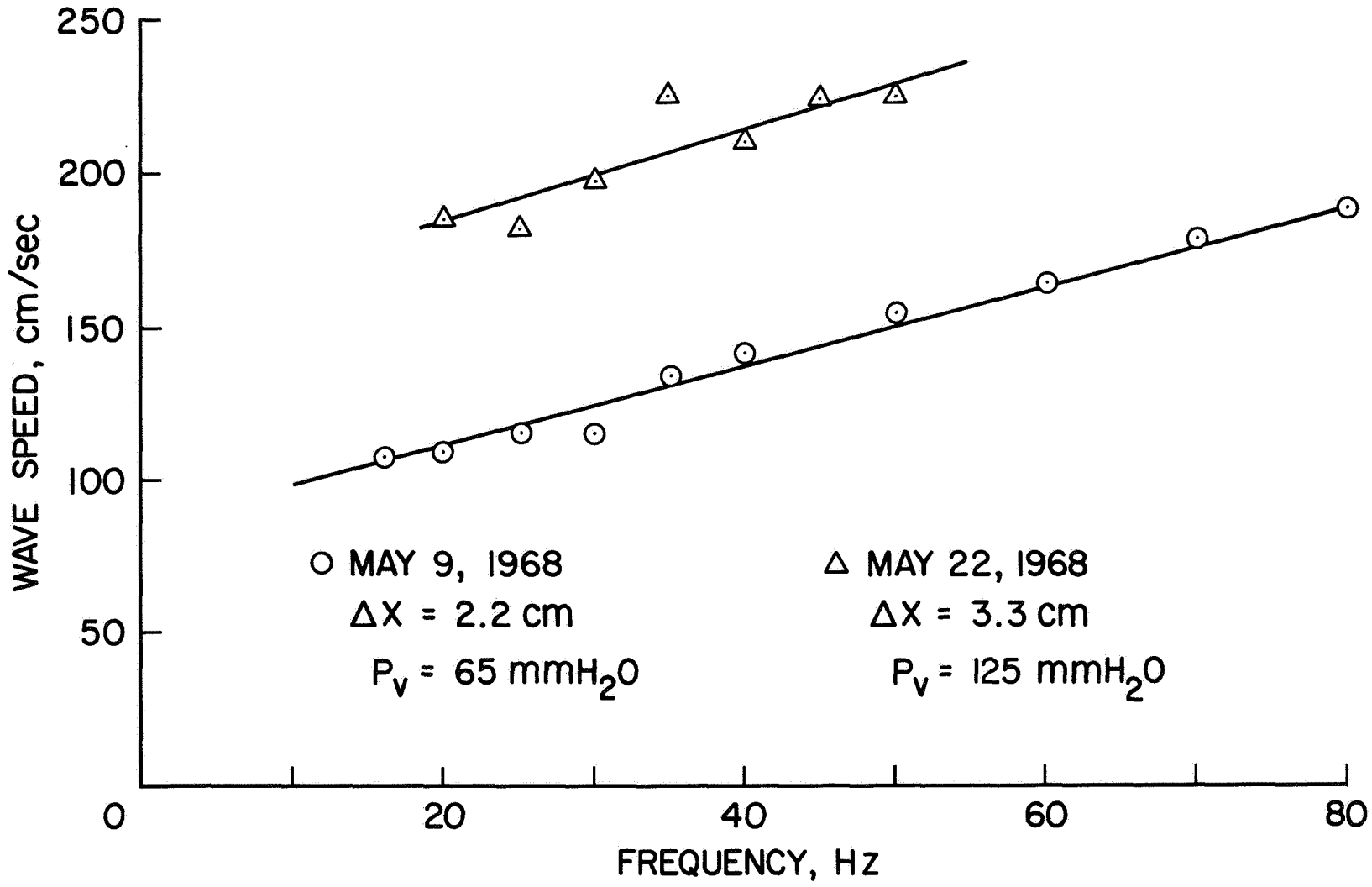

Figure 47. Representative dispersion curves for small pressure waves produced by the vibrating piston during the resting phase of the respiratory cycle.

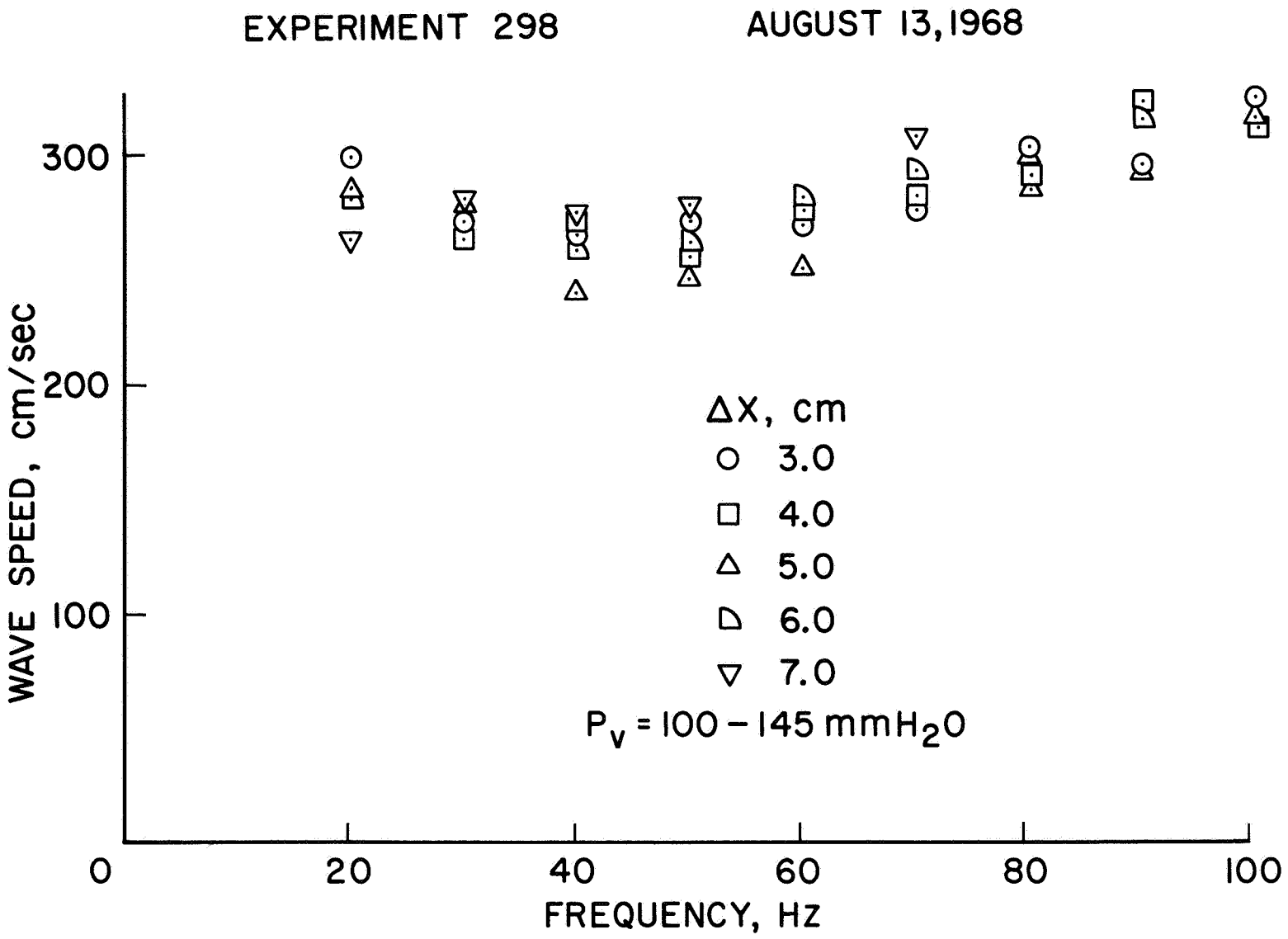

Figure 48. Dispersion of small pressure waves produced by the vibrating piston for various locations of the distal transducer and fixed position of the proximal transducer.

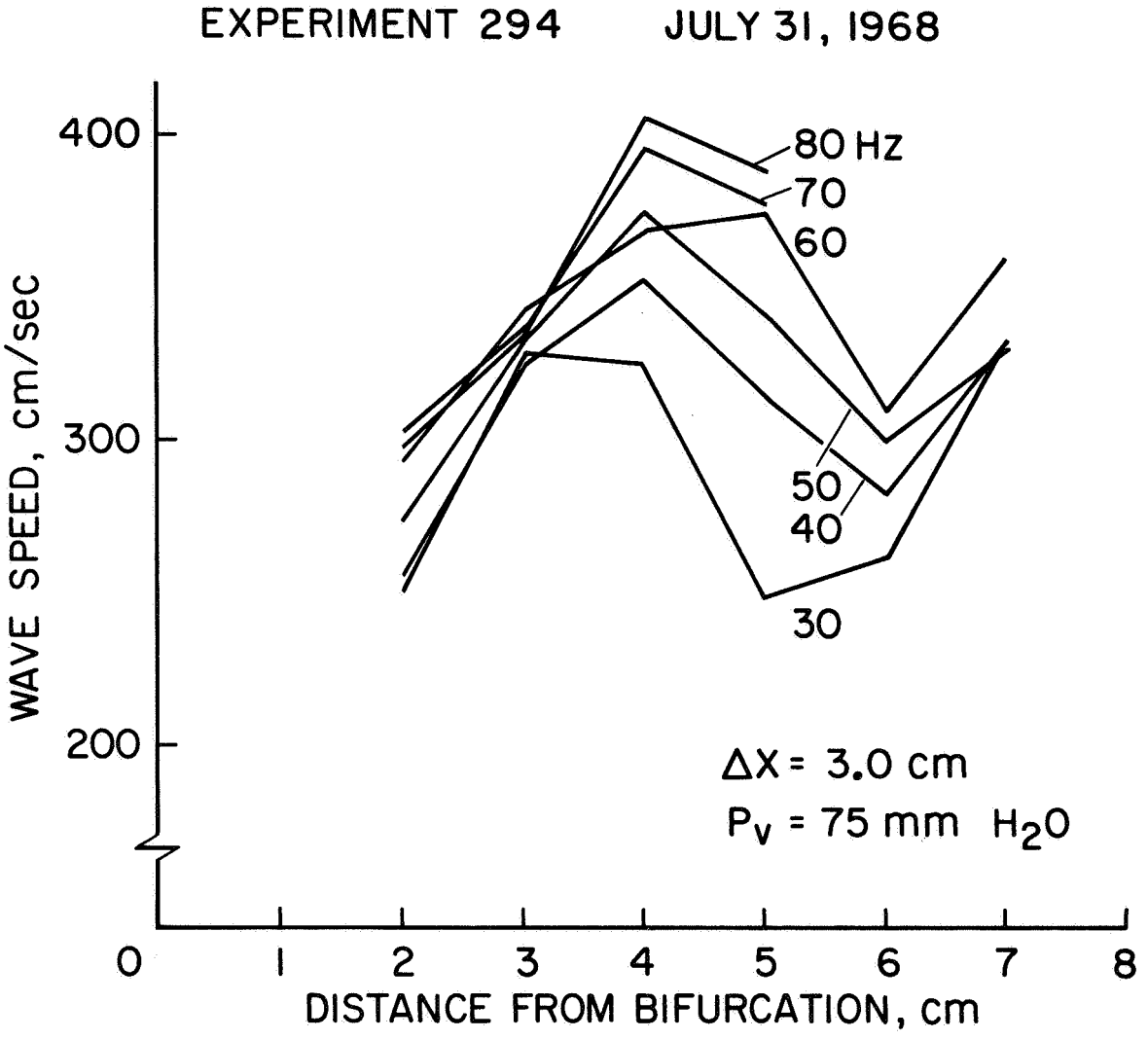

Figure 49. Variation in the speed of small pressure waves with frequency and transducer location.

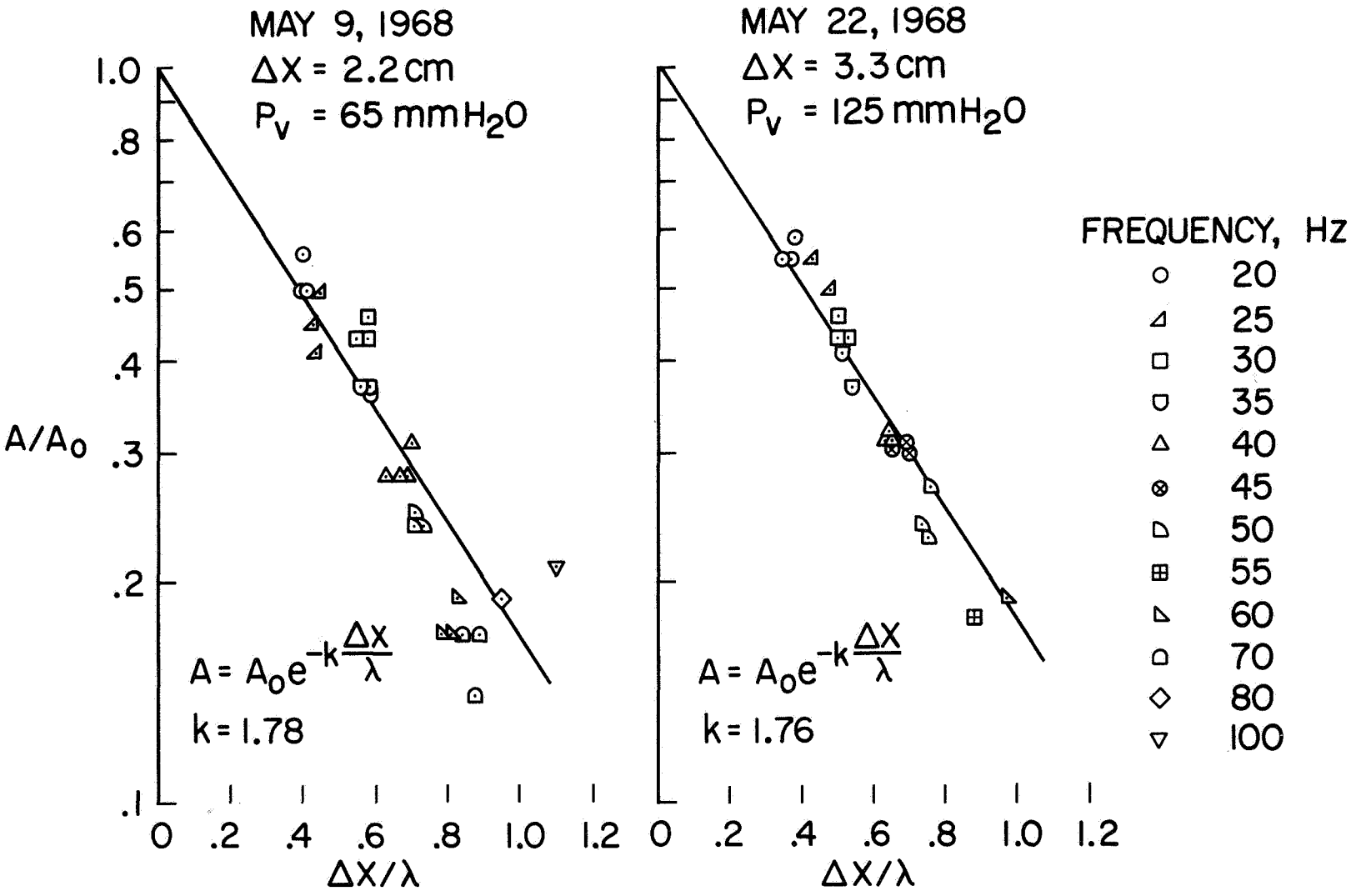

Figure 50. Attenuation curves corresponding to the dispersion data given in Figure 47.

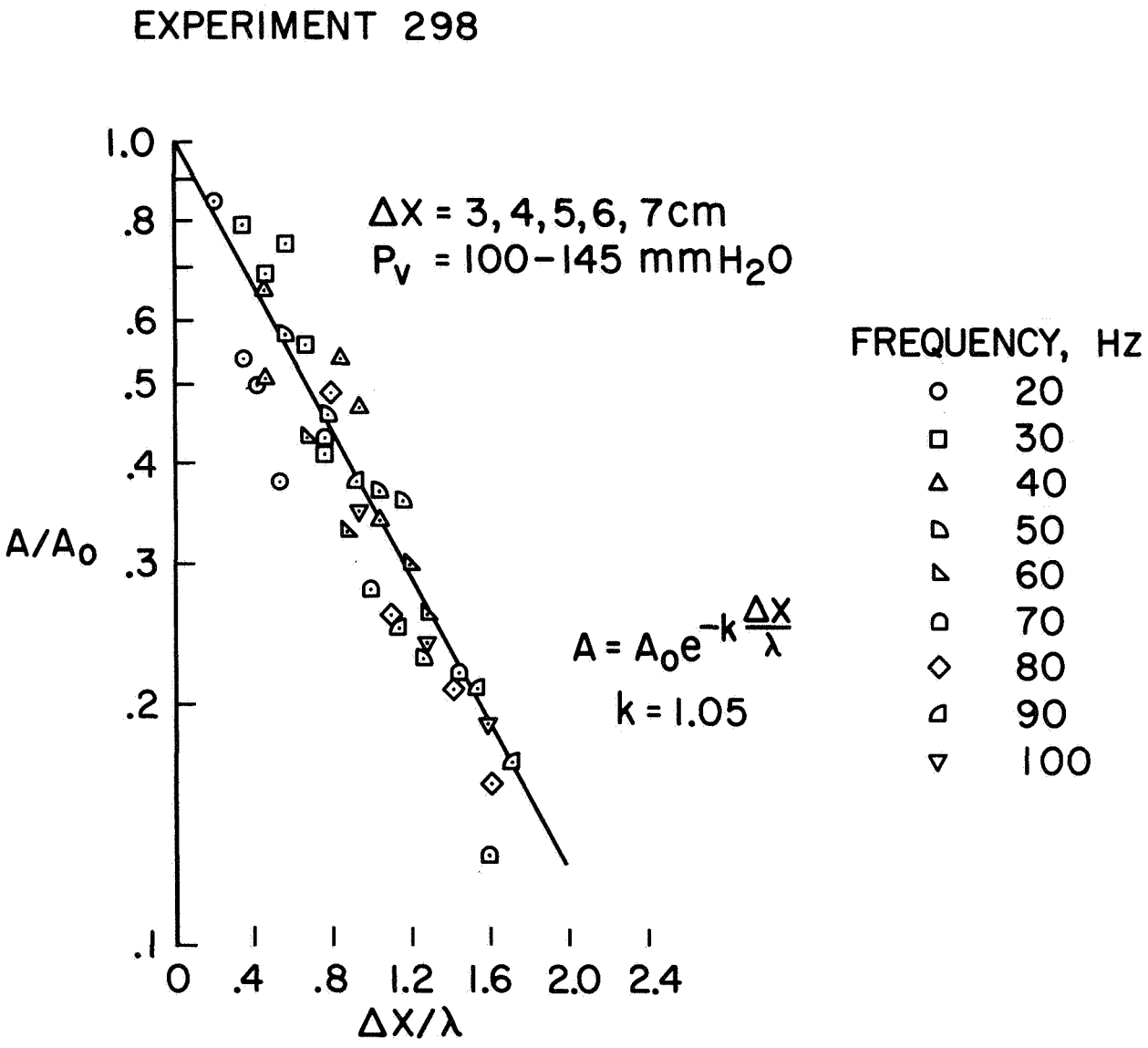

Figure 51. Attenuation curve corresponding to the dispersion data given in Figure 48.

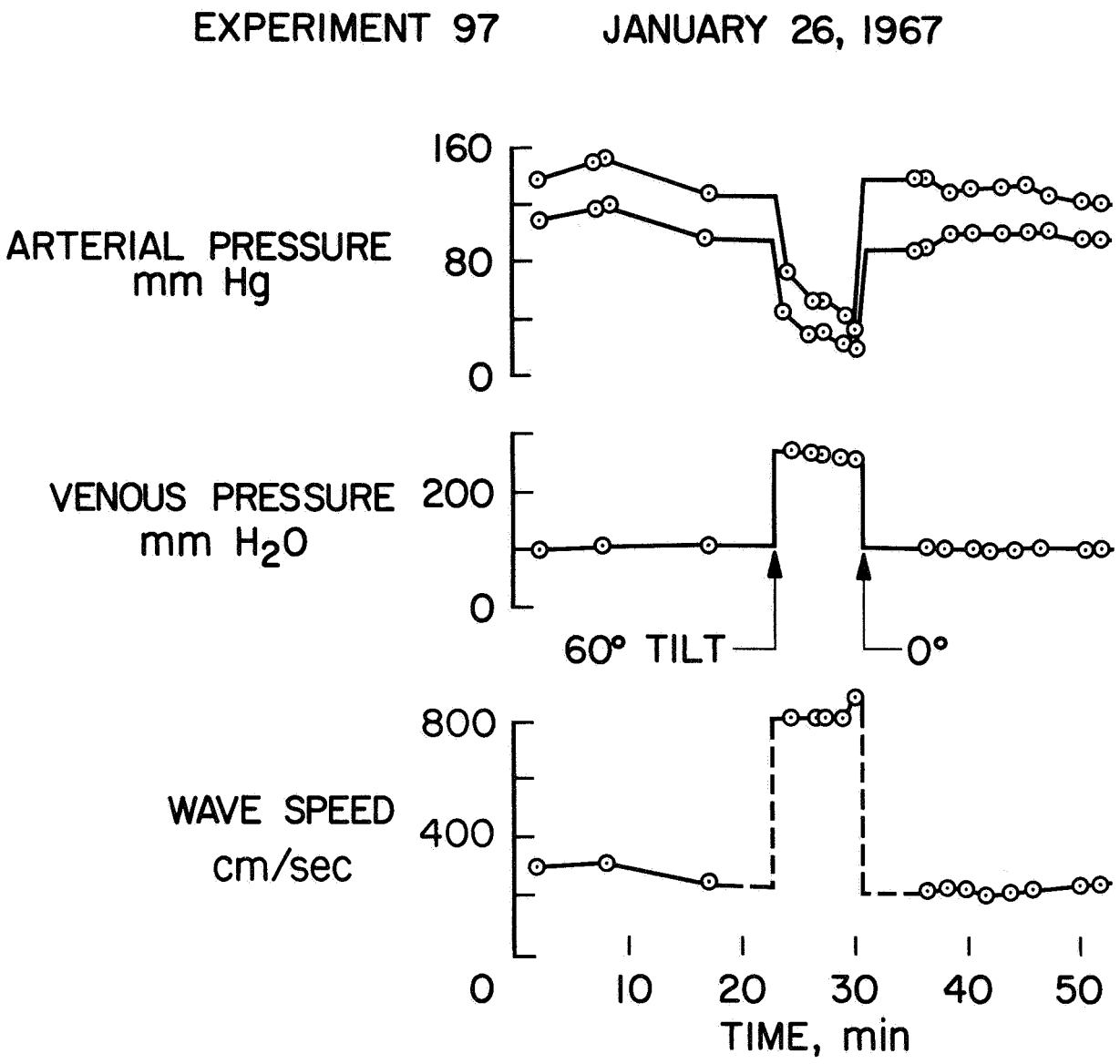

Figure 52. Typical example of the effects of tilting on the arterial and venous pressures and the speed of large amplitude pressure waves in the abdominal vena cava.

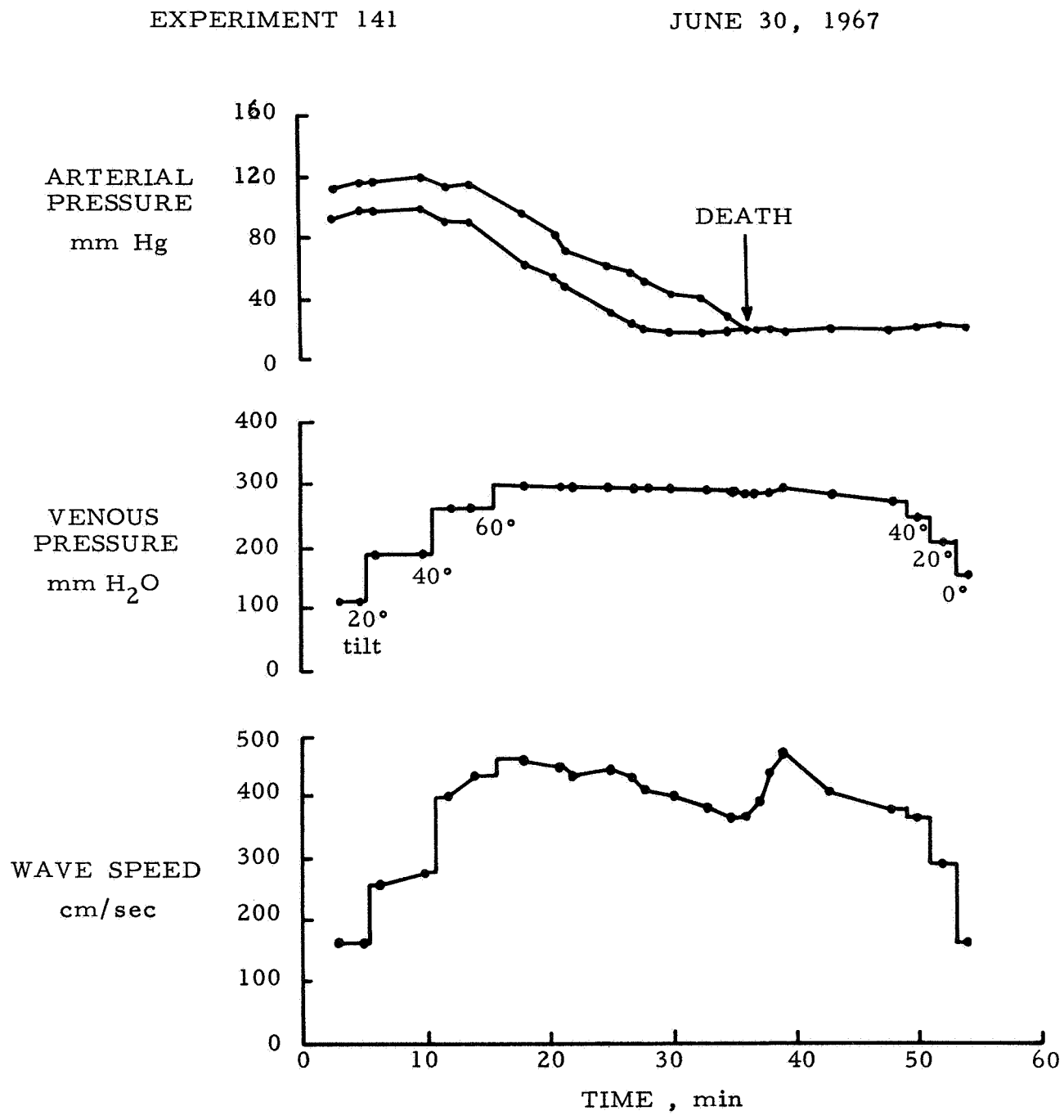

Figure 53. Effects of long duration tilt on arterial blood pressure and wave speed and transmural pressure in the vena cava.

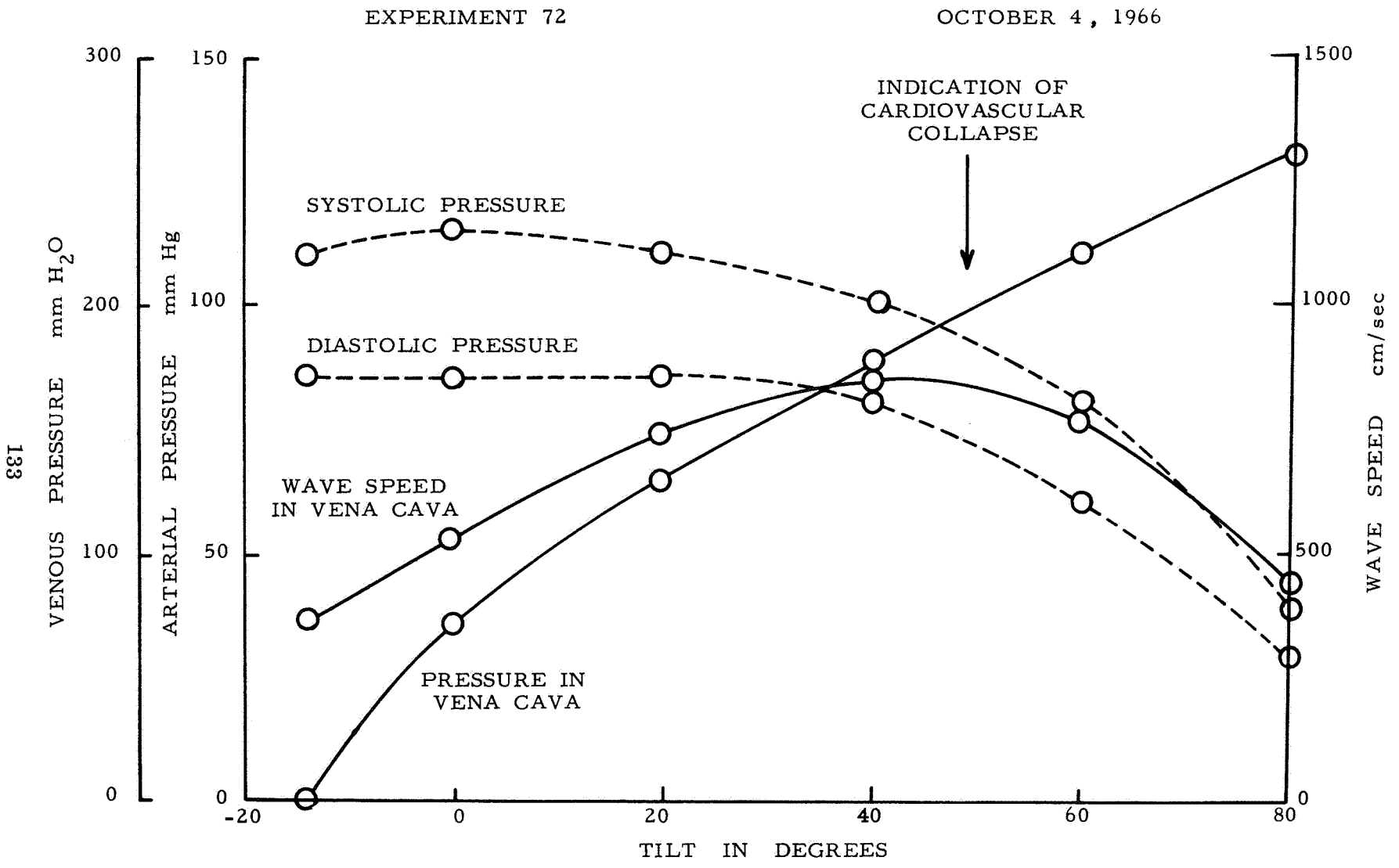

Figure 54. Effects of tilt on various cardiovascular parameters.

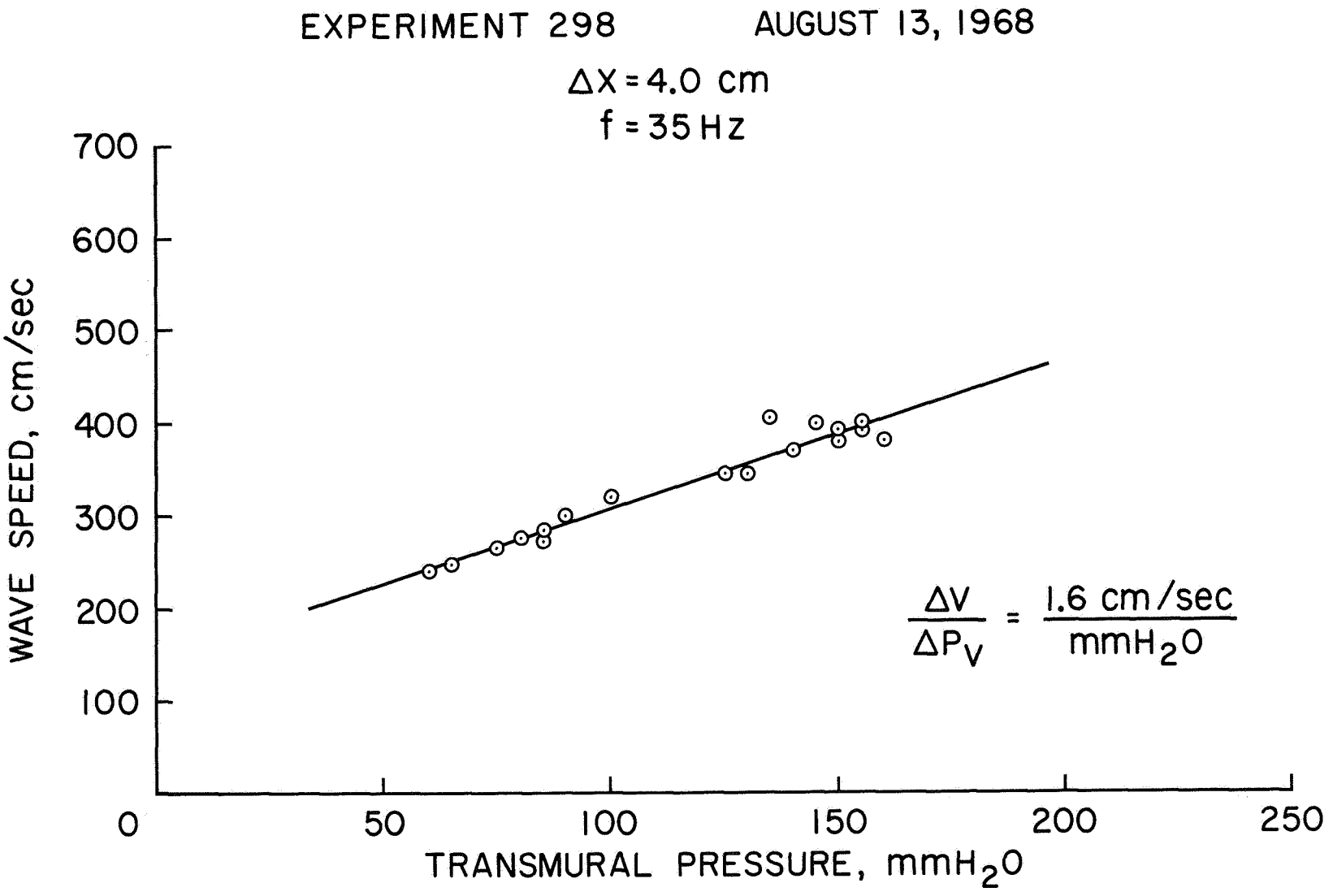

Figure 55. Variation in the speed of small amplitude pressure waves with transmural pressure in the vena cava.

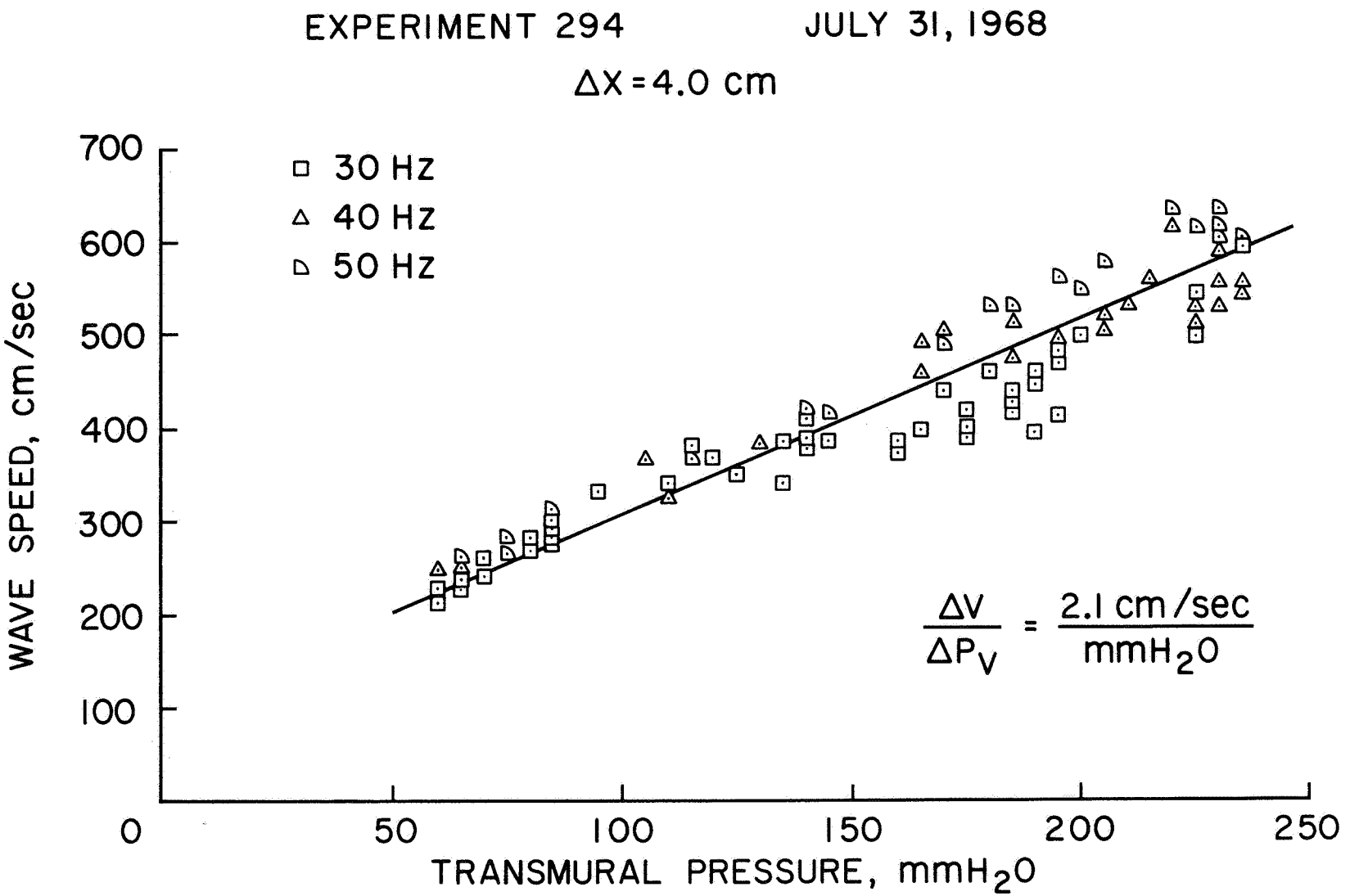

Figure 56. Variation in wave speed with transmural pressure for small amplitude sine waves of different frequencies.